

Modeling and Nonlinear Adaptive Control  
of an Aerial Manipulation System

by

Emre Yılmaz

Submitted to  
the Graduate School of Engineering and Natural Sciences  
in partial fulfillment of  
the requirements for the degree of  
Master of Science

Sabanci University

July, 2019

Modeling and Nonlinear Adaptive Control of an Aerial Manipulation System

Emre Yılmaz

APPROVED BY


Prof. Dr. Mustafa Ünel  
(Thesis Advisor)

.....

Assoc. Prof. Dr. Kemalettin Erbatur

.....

Asst. Prof. Dr. Ertuğrul Çetinsoy

.....

DATE OF APPROVAL: 16/7/2019.....

© Emre Yılmaz 2019  
All Rights Reserved



# Modeling and Nonlinear Adaptive Control of an Aerial Manipulation System

Emre Yılmaz

ME, Master's Thesis, 2019

Thesis Advisor: Prof. Dr. Mustafa Ünel

**Keywords:** Aerial Robots, Unmanned Aerial Vehicles, Robotic Arms, Aerial Manipulation, MRAC, Nonlinear Adaptive Control

## Abstract

Autonomous aerial robots have become an essential part of many civilian and military applications. The workspace and agility of these vehicles motivated great research interest resulting in various studies addressing their control architectures and mechanical configurations. Increasing autonomy enabled them to perform tasks such as surveillance, inspection and remote sensing in hazardous and challenging environments. The ongoing research promises further contributions to the society, in both theory and practice. To furthermore extend their vast applications, aerial robots are equipped with the tools to enable physical interaction with the environment. These tasks represent a great challenge due to the technological limitations as well as the lack of sophisticated methods necessary for the control of the system to perform desired operations in an efficient and stable manner. Modeling and control problem of an aerial manipulation is still an open research topic with many studies addressing these issues from different perspectives.

This thesis deals with the nonlinear adaptive control of an aerial manipulation system (AMS). The system consists of a quadrotor equipped with a 2 degrees of freedom (DOF) manipulator. The complete modeling of the system is done using the Euler-Lagrange method. A hierarchical nonlinear control structure which consists of outer and inner control loops has been utilized. Model Reference Adaptive Controller (MRAC) is designed for the outer loop where the required command signals are generated to force the quadrotor to move on a reference trajectory in the presence of mass uncertainties and reaction forces coming from the manipulator. For the inner loop, the attitude dynamics of the quadrotor and the joint dynamics of the 2-DOF robotic arm are considered as a fully actuated 5-DOF

unified part of the AMS. Nonlinear adaptive control has been utilized for the low-level controller where the changes in inertias have been considered. The proposed controller is tested on a high fidelity AMS model in the presence of uncertainties, wind disturbances and measurement noise, and satisfactory trajectory tracking performance with improved robustness is achieved.



# Bir Havada Manipulasyon Sisteminin Modellenmesi ve Doğrusal Olmayan Uyarlamalı Denetimi

Emre Yılmaz

ME, Master Tezi, 2019

Tez Danışmanı: Prof. Dr. Mustafa Ünel

**Anahtar kelimeler:** Hava Robotları, İnsansız Hava Araçları, Robotik Kollar, Havada Manipülasyon, MRAC, Doğrusal Olmayan Uyarlamalı Kontrol

## Özet

Otonom hava araçları birçok sivil ve askeri uygulamanın önemli bir parçası haline gelmiştir. Bu araçların çalışma alanı ve çevikliği, kontrol mimarilerini ve mekanik yapılandırmalarını ele alan çeşitli çalışmalarla sonuçlanan büyük araştırma ilgisini motive etti. Artan özerklik, tehlikeli ve zorlu ortamlarda gözetleme, denetim ve uzaktan algılama gibi görevleri gerçekleştirmelerini sağladı. Devam eden araştırmalar, hem teoride hem de pratikte topluma daha fazla katkı vaad etmektedir. Geniş uygulamalarını daha da genişletmek için, hava robotları çevre ile fiziksel etkileşimi sağlayan araçlarla donatılmaktadır. Bu görevler, teknolojik kısıtlamaların yanı sıra, sistemin kontrolü istenen işlemleri verimli ve istikrarlı bir şekilde yapması için gerekli karmaşık yöntemlerin bulunmamasından dolayı büyük bir zorluk teşkil etmektedir. Havada manipülasyonun modelleme ve kontrol sorunu, hala bu konuları farklı bakış açılarından ele alan birçok çalışmanın yer aldığı açık bir araştırma konusudur.

Bu tez, bir havada manipülasyon sisteminin (AMS) doğrusal olmayan uyarlanabilir kontrolü ile ilgilidir. Bu sistem, 2 serbestlik dereceli (DOF) manipülatör ile donatılmış bir quadrotordan oluşur. Sistemin tam modellenmesi Euler-Lagrange yöntemi kullanılarak yapılmıştır. Dış ve iç kontrol döngülerinden oluşan hiyerarşik bir doğrusal olmayan kontrol şeması kullanılmıştır. Model Referans Uyarlamalı Kontrolcü (MRAC), quadrotoru manipülatörden gelen belirsizlikler ve reaksiyon kuvvetleri varlığında referans yörünge üzerinde hareket etmeye zorlamak için gerekli komut sinyallerinin üretildiği dış döngü için tasarlanmıştır. İç döngü için, quadrotorun açısız dinamikleri ve 2-DOF robot kolunun eklem dinamikleri, AMS'nin tamamen harekete geçirilmiş 5-DOF bütünleşik parçası olarak dikkate

almaktadır. Ataletlerdeki deęişikliklerin dikkate alındığı düşük seviye kontrolcüsü için doğrusal olmayan uyarlamalı kontrol kullanılmıştır. Önerilen kontrolcü belirsizlikler, rüzgar bozucu etkisi ve ölçüm gürültüsü varlığında yüksek sadakatli bir AMS modelinde test edilmiş ve tatmin edici yörünge izleme performansının yanı sıra sistemin gürbüzlüğü iyileştirilmiştir.



# *Acknowledgements*

I would like to express my sincere gratitude and appreciation to my thesis advisor Prof. Dr. Mustafa Ünel for his precious guidance, teaching and continuous support. I have greatly benefited from his genuine enthusiasm for research and teaching, and willingness to always devote a great amount of time for fruitful discussions about my research directions. I would like to gratefully thank him for providing me with extended lab facilities and the opportunity to develop my research environment. His support and invaluable advices made my M.Sc. one of the greatest experience that I will benefit from throughout my life. I am really thankful to him for introducing me to this beautiful synergy of robotics, vision and control in the best possible manner I could have ever imagined. His inspiring and motivational personality, his trust in me strengthened my decision to follow my dream of pursuing a Ph.D. in these fields.

I would like to acknowledge Assoc. Prof. Dr. Kemalettin Erbatur and Assist. Prof. Dr. Ertuğrul Çetinsoy for reviewing my thesis and for their constructive comments and suggestions.

I would like to gratefully acknowledge the financial support provided by Ford Otosan of Turkey through the project “System Identification Methods for Diesel Engine Calibration Process” during my master studies. I acknowledge fruitful interactions and collaborations with Volkan Aran, Metin Yılmaz, Çetin Gürel, and Kerem Köprübaşı from the Ford Otosan’s Powertrain Controls and Calibration Department.

Last but not the least I would like to greatly thank my fellow colleagues Gökhan Alcan, Naida Fetic, Diyar Khalis Bilal, Hammad Zaki and Mehmet Emin Mumcuoğlu in our CVR research group, and Umut Çalışkan, Uğur Mengilli, Zeynep Özge Orhan and all remaining mechatronics laboratory members for their friendship and collaboration.

Finally, I would like to thank my sister and my dear parents for all their love and endless support throughout my life.



# Contents

<b>Abstract</b>	<b>iii</b>
<b>Özet</b>	<b>v</b>
<b>Acknowledgements</b>	<b>vii</b>
<b>Contents</b>	<b>viii</b>
<b>List of Figures</b>	<b>xii</b>
<b>List of Tables</b>	<b>xvi</b>
<b>1 Introduction</b>	<b>1</b>
1.1 Motivation . . . . .	3
1.2 Contributions of the Thesis . . . . .	4
1.3 Outline of the Thesis . . . . .	5
1.4 Publications . . . . .	6
<b>2 Literature Survey and Background</b>	<b>7</b>
2.1 Unmanned Aerial Vehicles . . . . .	7

---

2.2	Interaction/Manipulation Mechanisms . . . . .	9
2.3	Aerial Manipulation Missions . . . . .	12
2.4	Controllers . . . . .	13
2.4.1	Decentralized Approach . . . . .	14
2.4.1.1	Linear Controllers . . . . .	14
2.4.1.2	Nonlinear Model-Based Controllers . . . . .	14
2.4.2	Centralized Approach . . . . .	15
2.4.2.1	Linear Controllers . . . . .	15
2.4.2.2	Nonlinear Model-Based Controllers . . . . .	15
<b>3</b>	<b>Design and Construction of an Aerial Manipulation System</b>	<b>18</b>
3.1	Hardware Design and Integration . . . . .	19
3.1.1	Mechanical Platform . . . . .	19
3.1.1.1	UAV Base . . . . .	19
3.1.1.2	Manipulation Mechanicm . . . . .	20
3.1.2	Actuator Integration . . . . .	21
3.1.2.1	Rotor and Rotor Driver . . . . .	21
3.1.2.2	Propeller . . . . .	22
3.1.2.3	Servos . . . . .	22
3.1.2.4	Battery . . . . .	23
3.1.3	Sensor and Microcontroller Integration . . . . .	23
3.1.3.1	Myrio Data Acquisition Card . . . . .	23
3.1.3.2	Positioning System . . . . .	24
3.1.3.3	IMU . . . . .	25

---

3.1.4	Overall Hardware Architecture . . . . .	25
3.2	Software Architecture . . . . .	27
3.2.1	Real-Time Control . . . . .	27
3.2.2	Monitoring System . . . . .	27
<b>4</b>	<b>Modeling of the Aerial Manipulation System</b>	<b>28</b>
4.1	Model Description . . . . .	28
4.2	Kinematics for the Aerial Manipulation System . . . . .	29
4.3	Dynamics for the Aerial Manipulation System . . . . .	34
4.3.1	Newton-Euler Dynamic Model . . . . .	34
4.3.1.1	UAV-Quadrotor Dynamics . . . . .	35
4.3.1.2	Robotic Arm Dynamics with a Floating Base . . . . .	38
4.3.1.3	Coupled Dynamics of the Quadrotor with Robotic Arm . . . . .	40
4.3.2	Euler-Lagrange Dynamic Model . . . . .	41
<b>5</b>	<b>Nonlinear Adaptive Control of the Aerial Manipulation System</b>	<b>44</b>
5.1	Model Reference Adaptive Control (MRAC) Design . . . . .	45
5.2	Reference Model Design . . . . .	46
5.3	Adaptive Control . . . . .	47
5.4	Attitude Reference Calculation . . . . .	48
5.5	Nonlinear Adaptive Control Design . . . . .	49
5.6	An Example Flight Scenario . . . . .	50

---

<b>6</b>	<b>Simulation Results</b>	<b>52</b>
6.1	Free Motion Scenarios with the Robotic Arm during Hovering . . .	54
6.1.1	Drawing a Rectangular Shape . . . . .	54
6.1.2	Drawing a Circular Shape . . . . .	62
6.2	Motion of the Quadrotor with the Robotic Arm in a Fixed Position	70
6.3	A Manipulation Scenario Under Varying Disturbances . . . . .	77
<b>7</b>	<b>Conclusion and Future Works</b>	<b>85</b>
	<b>Bibliography</b>	<b>87</b>



# List of Figures

2.1	(a) Tai Anka Fixed-Wing UAV [1], (b) A Rotary-Wing UAV, DJI Quadrotor [2], (c) SUAVI tilt-wing UAV [3] . . . . .	8
2.2	Simple gripper configurations directly attachable under a UAV, (a) a gripper able to penetrate surfaces using its opposed microspines, (b) a gripper having pulleys, cables and elastic bands to provide compliance, (c) four fingers with elastic joints and actuated by a tendon mechanism . . . . .	9
2.3	Robotic arm configurations, (a-b) 2-DOF, (c) 6-DOF, (d) 5-DOF, (e-f) 7-DOF . . . . .	10
2.4	10-DOF lightweight dual-arm manipulator [4] . . . . .	10
3.1	CAD model of the UAV base . . . . .	19
3.2	CAD model of the robotic arm . . . . .	20
3.3	The hardware components of the robotic arm . . . . .	20
3.4	Rotor and rotor driver . . . . .	21
3.5	10x4.5 carbon fiber propeller . . . . .	22
3.6	Dynamixel XL-320 digital servo . . . . .	22
3.7	Leoparde 4S 5200Mah 30C lipo battery . . . . .	23
3.8	myRIO-1900 Data Acquisition Board . . . . .	24
3.9	Pozyx accurate positioning system . . . . .	24

---

3.10	x-IMU Inertial Measurement Unit . . . . .	25
3.11	Schematic of the hardware setup . . . . .	25
3.12	CAD Model of the Aerial Manipulation System . . . . .	26
3.13	Graphical User Interface . . . . .	27
4.1	Coordinate frames of the system . . . . .	29
4.2	Sketch of the two-link manipulator . . . . .	31
5.1	Overall Control System Architecture . . . . .	45
5.2	A model-reference adaptive control system [5] . . . . .	45
5.3	An Example Flight Scenario . . . . .	50
6.1	Simulink Model of the AMS . . . . .	53
6.2	The flight mode visualization from different views . . . . .	54
6.3	3D trajectory of the end-effector . . . . .	55
6.4	X position of the quadrotor (top), position error (bottom) vs Time	55
6.5	Y position of the quadrotor (top), position error (bottom) vs Time	56
6.6	Z position of the quadrotor (top), position error (bottom) vs Time .	56
6.7	Roll angle ( $\phi$ ) (top), tracking error (bottom) vs Time . . . . .	57
6.8	Pitch angle ( $\theta$ ) (top), tracking error (bottom) vs Time . . . . .	58
6.9	Yaw angle ( $\psi$ ) (top), tracking error (bottom) vs Time . . . . .	58
6.10	$\zeta_1$ tracking of the arm (top), tracking error (bottom) vs Time . . .	59
6.11	$\zeta_2$ tracking of the arm (top), tracking error (bottom) vs Time . . .	59
6.12	Control inputs . . . . .	60
6.13	Wind forces during the rectangle drawing task of the arm . . . . .	61
6.14	Wind moments during the rectangle drawing task of the arm . . . . .	61

---

6.15	The flight mode visualization from different views . . . . .	62
6.16	Trajectory of the end-effector . . . . .	63
6.17	X position of the quadrotor (top), position error (bottom) vs Time	63
6.18	Y position of the quadrotor (top), position error (bottom) vs Time	64
6.19	Z position of the quadrotor (top), position error (bottom) vs Time .	64
6.20	Roll angle ( $\phi$ ) (top), tracking error (bottom) vs Time . . . . .	65
6.21	Pitch angle ( $\theta$ ) (top), tracking error (bottom) vs Time . . . . .	65
6.22	Yaw angle ( $\psi$ ) (top), tracking error (bottom) vs Time . . . . .	66
6.23	$\zeta_1$ tracking of the arm (top), tracking error (bottom) vs Time . . .	66
6.24	$\zeta_2$ tracking of the arm (top), tracking error (bottom) vs Time . . .	67
6.25	Control inputs . . . . .	68
6.26	Wind forces during the circle drawing task of the arm . . . . .	69
6.27	Wind moments during the circle drawing task of the arm . . . . .	69
6.28	The flight mode visualization from different views . . . . .	70
6.29	X position of the quadrotor (top), position error (bottom) vs Time	71
6.30	Y position of the quadrotor (top), position error (bottom) vs Time	71
6.31	Z position of the quadrotor (top), position error (bottom) vs Time .	72
6.32	Roll angle ( $\phi$ ) (top), tracking error (bottom) vs Time . . . . .	72
6.33	Pitch angle ( $\theta$ ) (top), tracking error (bottom) vs Time . . . . .	73
6.34	Yaw angle ( $\psi$ ) (top), tracking error (bottom) vs Time . . . . .	73
6.35	$\zeta_1$ tracking of the arm (top), tracking error (bottom) vs Time . . .	74
6.36	$\zeta_2$ tracking of the arm (top), tracking error (bottom) vs Time . . .	74
6.37	Control inputs . . . . .	75
6.38	Wind forces during the circle drawing task of the quadrotor . . . . .	76

---

6.39	Wind moments during the circle drawing task of the quadrotor . . .	76
6.40	X position of the quadrotor (top), position error (bottom) vs Time	78
6.41	Y position of the quadrotor (top), position error (bottom) vs Time	78
6.42	Z position of the quadrotor (top), position error (bottom) vs Time .	79
6.43	Roll angle ( $\phi$ ) (top), tracking error (bottom) vs Time . . . . .	79
6.44	Pitch angle ( $\theta$ ) (top), tracking error (bottom) vs Time . . . . .	80
6.45	Yaw angle ( $\psi$ ) (top), tracking error (bottom) vs Time . . . . .	80
6.46	$\zeta_1$ tracking of the arm (top), tracking error (bottom) vs Time . . .	81
6.47	$\zeta_2$ tracking of the arm (top), tracking error (bottom) vs Time . . .	81
6.48	Control inputs . . . . .	82
6.49	Interaction forces and moments during the manipulation task . . . .	83
6.50	Wind forces during the manipulation task . . . . .	83
6.51	Wind moments during the manipulation task . . . . .	84



# List of Tables

3.1	The design specifications of the robotic arm [6] . . . . .	20
3.2	Dynamixel XL-320 specifications . . . . .	22
3.3	Hardware specifications of the AMS . . . . .	26
4.1	DH table for the two-link manipulator . . . . .	31
6.1	Simulation Parameters . . . . .	53
6.2	Tracking errors of the AMS for the task of rectangle drawing . . . . .	60
6.3	Tracking errors of the AMS for the task of circle drawing . . . . .	67
6.4	Tracking errors of the AMS for the scenario . . . . .	75
6.5	Tracking errors of the AMS for the task of pulling object . . . . .	84

# Chapter 1

## Introduction

Today, we are surrounded by various types of robots in daily life. Industrial, military to medical, robots are involved in diverse application fields [7]. Based on their operational environments, robots can be classified as *fixed robots* and *mobile robots*. Fixed robots are working in well-defined environments and are often referred to robotic manipulators. These are extensively used in industrial manufacturing for repetitive tasks such as soldering, welding, painting and drilling [7, 8]. Mobile robots, in contrast to the fixed robots, have the ability to move in an environment and are categorized as ground robots, underwater and aerial robots. Mobility of these robots introduces a great advantage of their increased workspaces [8]. However, most of them still operate while in contact with the ground which are called *ground robots*, i.e. wheeled robots (Google's self-driving car [9]) and legged robots (Big dog [10]).

Unmanned aerial vehicles which include rotary-wing (e.g. quadrotors, hexacopters, helicopters), fixed-wing (e.g. airplanes) and hybrid (e.g. tilt-wing, tilt-rotor) aircrafts are capable of operating in the atmosphere and do not require any human operator on-board. The history of UAVs dates back to 1917s when A.M. Low Rouston launched Aerial Torpedo using compressed air. The year after, Curtis Sperry under military patronage developed 'Flying Bomb' that was capable of flying in a straight line to a distance preset by the operator, and then automatically

ground itself. The remote-controlled flight technology advanced very fast during the First World War, the aerial target machines started being known as drones and machines as Sperry's 'Flying Bomb' are referred as guided missiles. Military continued advancing UAVs and expanding their applications to surveillance, exploration, target-acquisition and furthermore. The first non-military usage of UAVs is recorded in 1937 when Ross Hull and Clinton B. DeSoto developed remote-controlled model plane [11, 12]. However, recently UAVs gained their popularity and commercial values for civil purposes. The main reason for this is the advancement in other technologies (sensors, telemetry, computation and materials) that made UAVs accessible and more user-friendly. This motivated many other usages of UAVs in everyday applications. Some of the applications are listed below:

- Search and rescue [13]
- Border monitoring [14]
- Transmission line inspection [15]
- Remote sensing of agricultural products [16]
- Forest fire monitoring [17]

All the above examples reveal that industries benefit extensively from these achievements of aerial vehicles. However, they do not include active tasks which require physical interaction with the environment. Examples to such applications can be simply grasping and manipulation of equipment in an industrial operation area. This means that for manipulation skills of a UAV, it has to be equipped with an interaction/manipulation mechanism (i.e a robotic arm) which is so called *an Aerial Manipulation System*. Eventually, it can be employed as a robotic worker to perform assembling and disassembling of mechanical parts, transporting, positioning, etc.

## 1.1 Motivation

Attaching a robotic arm to a controllable aerial vehicle (i.e. a UAV) is an existing research field of study. From a broad point of view, attaching robotic arms to moving platforms is a well-known study area of mobile manipulation. Ground vehicles (i.e. differential drive robots [18], ships [19]) are already involved as mobile manipulators, however using aerial vehicles as mobile manipulators is a relatively new field of study that has the potential to grow.

Aerial vehicles bring a great workspace to mobile manipulation. It offers the ability to reach high elevations, difficult or inaccessible areas for humans and ground vehicles. Without any need of scaffolds and ladders, they can be used for window cleaning, power line inspection, painting, replacement of light bulbs and so on. Functional grippers and tools can be designed for the aerial manipulation systems to furthermore extend their applications for more complicated tasks. For example, by using specialized tools, assembling, welding and drilling tasks on a construction site can be done. Without any human intervention, they can be used in dangerous places such as nuclear power plants and skyscrapers. In case of a disaster (e.g. earthquake, explosion), these vehicles can deliver water, food and medical supplies to the people to be rescued.

Aerial vehicles can pass over a rough terrain faster than ground vehicles. This reduces operation time and cost. This capability makes them applicable for tasks in distant regions, such as fire monitoring and extinguishing in forestries, determining harvest diseases in agricultural fields, and water and soil sampling in seas and on the ground. Furthermore, an aerial manipulation system can work like a human operator in inspection sites to operate a machinery (i.e. turning valves), which can decrease human intervention in certain applications.

Despite the above mentioned benefits, aerial manipulation is a non-trivial task

from the control point of view. The highly coupled and nonlinear system dynamics of the UAV and the attached manipulator as a whole creates a control challenge. As arm operates, it produces reacting forces and moments on the UAV base. This makes the position of the UAV is difficult to maintain. Similarly, a change in UAV's position and orientation yields reactive forces and moments on the arm, which makes it hard to perform a reliable manipulation. Therefore, the system requires a combined and synchronized control structure for stable interaction with the environment.

When the manipulation mechanism (i.e. robotic arm) interacts with the environment, the unmodelled ground/surface dynamics creates another challenge for the aerial manipulation. The grasped object's mass and inertia introduce external disturbances on the overall system dynamics.

Although there are robust control schemes addressing the control problems of the quadrotor and the manipulator individually, they fail to provide an overall solution for the aerial manipulators. Therefore, the demand for a more sophisticated controller arises.

## 1.2 Contributions of the Thesis

The contributions of the thesis are summarized as follows:

- An experimental setup for the Aerial Manipulation System (AMS) is designed and constructed.
- A mathematical model of the AMS is developed using Euler-Lagrange formulation where
  - forces and moments which result from interaction with the environment and the coupling between the UAV and the robotic arm are considered.

- A nonlinear hierarchical adaptive controller is proposed where
  - uncertainties in the mass and reaction forces are handled by the model reference adaptive controller;
  - the change in the moments of inertia is handled by the nonlinear adaptive controller which is designed for the unified attitude and joint dynamics;
  - no linearization is needed in plant dynamics.
- A flight simulator with 3D visualization toolbox is developed in Simulink/MATLAB.
- Simulation results are presented where
  - Dryden wind model and measurement noise are included to emulate real-world conditions.

### 1.3 Outline of the Thesis

This thesis is organized into seven chapters. These chapters provide the following information:

Chapter 2 includes a literature survey about UAVs, interaction/manipulation mechanisms, aerial manipulation missions and controllers are provided.

Chapter 3 details the design and construction procedure of the aerial manipulation system.

Chapter 4 explains the entire kinematics and dynamics of the aerial manipulation system.

In Chapter 5, a hierarchical control approach is developed. In the proposed control approach, a Model Reference Adaptive Controller stands for the high level control where positional dynamics are controlled and reference attitudes are generated. As a low level control, nonlinear adaptive control is utilized where the rotational dynamics of the UAV and joints angles of the manipulator are controlled.

Chapter 6 presents a detailed discussion of simulation results.

Finally, Chapter 7 gives concluding remarks and indicates possible future work.

## 1.4 Publications

The following publications have been produced during the MSc studies:

- **Emre Yilmaz**, Hammad Zaki, Mustafa Unel, “Nonlinear Adaptive Control of an Aerial Manipulation System”, European Control Conference (ECC 2019), Napoli, Italy, 25-28 June 2019.
- Gokhan Alcan, **Emre Yilmaz**, Mustafa Unel, Volkan Aran, Metin Yilmaz, Cetin Gurel, Kerem Koprubasi, Estimating Soot Emission in Diesel Engines using Gated Recurrent Unit Networks, 9th IFAC International Symposium on Advances in Automotive Control (AAC 2019), Orléans, France, 24-27 June 2019.

# Chapter 2

## Literature Survey and Background

Aerial Manipulation System (AMS) is a flying robot system, composed of an unmanned aerial vehicle platform and a manipulation mechanism. This chapter presents the literature survey about unmanned aerial vehicles, manipulation mechanisms, aerial manipulation missions and controllers.

### 2.1 Unmanned Aerial Vehicles

An Unmanned Aerial Vehicle (UAV) is an aerial mobile robot that operates autonomously or through the remote control from a ground station. In order to perform the desired operation, UAV platforms include various sensors such as Inertial Measurement Units (IMUs), GPS sensors, altimeters, ultrasonic distance sensors for state estimations. In indoor environments, they can utilize visual sensors alternative to GPS. An example of such sensors can be a motion capture system (i.e. VICON) that provides position and velocity information.

UAVs can be categorized into three main configurations: fixed-wing, rotary-wing and hybrid designs (see Fig. 2.1 for examples of such configurations). Fixed



wings have long endurance but require a runway for take-off and landing which makes them inapplicable for indoor operations [20]. Rotary-wing UAVs, on the other hand, are suitable for both indoor and outdoor applications thanks to their vertical take-off and landing (VTOL) capabilities. Hybrid designs which include tilt-rotor and tilt-wing UAVs, utilize the advantages of both fixed-wing and rotary-wing configurations.

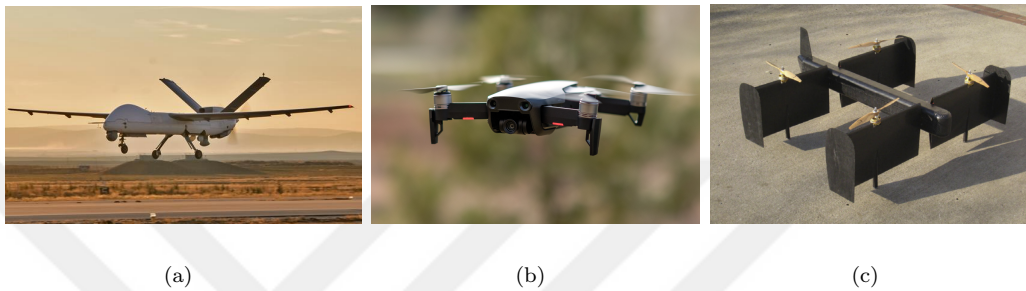


FIGURE 2.1: (a) Tai Anka Fixed-Wing UAV [1], (b) A Rotary-Wing UAV, DJI Quadrotor [2], (c) SUAVI tilt-wing UAV [3]

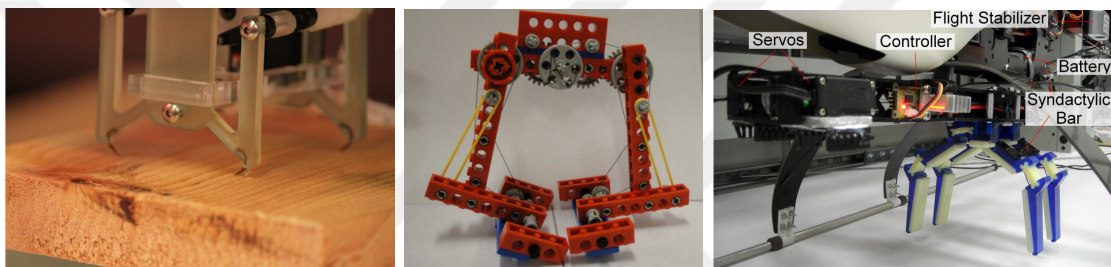
Fixed-wing UAVs do not have a hovering capability which makes their application in aerial manipulation problems limited to tasks such as aerial refueling [21]. On the other hand, rotary-wing UAVs are widely utilized due to their hovering capability. Some of the popular rotary-wing UAVs are octoquads, tri-rotors, hexarotors, conventional helicopters and vehicles with ducted fans. Among those, helicopters are primary platforms that were considered in aerial manipulation missions such as aerial grasping and transportation [22]. Different from conventional helicopters, ducted fans were preferred for applications where static thrusts are required and size limitation is a problem in the system design [23].

Among rotary-wing UAVs, quadrotors are the most common platforms used for aerial manipulation as they are easily accessible and affordable for a wide range of people, and they have well-studied dynamics and control schemes [24]. Among hybrid design UAVs, tilt-rotor UAVs are applied in aerial manipulation tasks to increase the efficiency of the interaction with the environment, while the vehicle

maintains its position at a hover position [25–27]. Tilt-rotor configurations require a well-designed swashplate mechanism for proper tilting actions.

## 2.2 Interaction/Manipulation Mechanisms

A physical mechanism is essential to interact with the environment for an aerial manipulation system. The interaction mechanisms can be classified into four categories: (1) grippers, (2) robotic arms, (3) cables or tethers, (4) a rigid tool.



(a) Mellinger et.al.[28]

(b) Ghadiok et.al.[29]

(c) Pounds et.al.[30]

FIGURE 2.2: Simple gripper configurations directly attachable under a UAV, (a) a gripper able to penetrate surfaces using its opposed microspines, (b) a gripper having pulleys, cables and elastic bands to provide compliance, (c) four fingers with elastic joints and actuated by a tendon mechanism

Grippers, depicted in Fig. 2.2 are directly attached under an aerial vehicle. These simple grippers offer a grasping ability to the attached vehicle and enable the object transportation. Since they do not bring too much dexterity and do not allow operations more than pick-and-place, they are mostly used in early applications of aerial manipulation systems in the literature [31].

Robotic arms are the most relevant branch of the interaction mechanisms for an aerial manipulation system. Configurations of robotics arms differ by degrees of freedom ranging from 1-DOF [32] to 2-DOF [33–35] and several DOFs [36, 37]. Sample configurations are presented in Figs. 2.3 and 2.4.

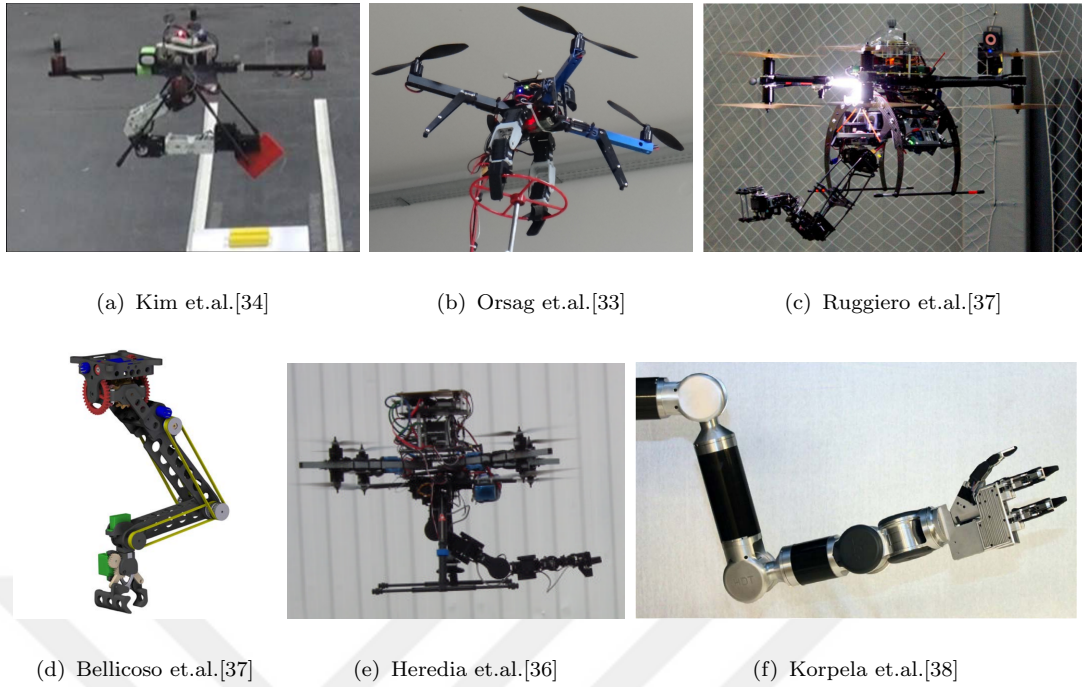


FIGURE 2.3: Robotic arm configurations, (a-b) 2-DOF, (c) 6-DOF, (d) 5-DOF, (e-f) 7-DOF

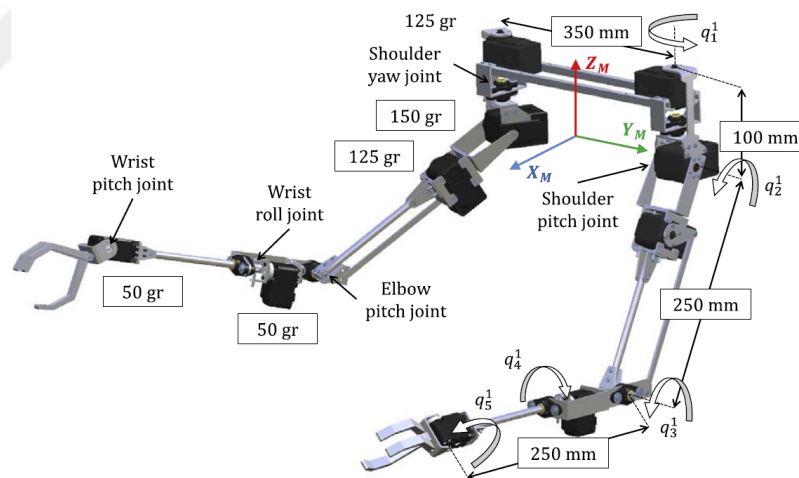


FIGURE 2.4: 10-DOF lightweight dual-arm manipulator [4]

In the work by [39], a self-folding 5-DOF arm with a compact design was developed to accomplish manipulation tasks of an AMS, which featured low variations in AMS's center of gravity during the flight. In [36], an octocopter was equipped with a dexterous 7-DOF arm having a 1.5 kg payload capacity was developed. They demonstrated that in outdoor environments as the arm operates, the attitude of the AMS could be maintained reasonably well. In [40] an AscTec Pelican

quadcopter was fitted with a 6-DOF arm. Using the redundancy in the developed arm, the control of the arm joints and AMS's center of gravity was realized with minimum joint velocities while performing its main goal of tracking the trajectory of the end effector. Similarly, in [41] subtasks such as controlling the AMS's center of gravity, joint-limit avoidance, camera view and gripper's pose were prioritized using a hierarchical-task approach. In the works of [42, 43], three different methods were utilized for determination of the inverse kinematics of a hyper-redundant manipulator. These methods were weighted pseudo-inverse Jacobian, regular pseudo-inverse Jacobian, and heuristic approach. By exploiting the highly redundant DOFs the destabilizing effects on the manipulator base were minimized, while the end-effector's pose was accurately controlled in a highly reachable workspace. It should be noted that prismatic joints were rarely used for the construction of manipulators in literature such as in [44, 45], while most of the works used servo-driven revolute joints [32, 35, 46–48].

As for interaction in environments which require only tensile forces, tethers or cables have proven to be very useful [49, 50]. However, the usage of tethers and cables is very limited and can not be applied for more general tasks such as pick and place missions and force exertion.

Another category of manipulation systems include the usage of a rigid body attached to the aerial vehicle or using its body [51–55] for performing the task [56–60]. For example in the work by [51], a VTOL vehicle was developed which is able to track its trajectory, while having direct contact with vertical surfaces. In the works of [52, 53], a line/surface contact was established using the structure of the propeller protection. Moreover, in [55] the body of a UAV was utilized for opening a door. Besides these, a quadrotor was equipped with a rigid tool for applying force to an environment in [56]. In their work, it was suggested that a counterweight should be mounted to balance the attached rigid tool. This seems a viable solution but it has the drawback of the addition of the extra weight to the

AMS system which is undesired. The authors of [61] used a marker for performing aerial writing which was rigidly attached to a quadrotor. Their work proved to be successful in interaction with the environment and showed that inspection through contact is also possible using AMS. Moreover, in the work of [58] thrust vectoring was shown to be very useful way for exerting large forces to objects. More importantly, in [60] it was analytically concluded that in order to maintain stability, the tooltip has to be strictly above the vehicle's center of mass.

### 2.3 Aerial Manipulation Missions

Aerial manipulation systems are used for a wide variety of missions and operations. Manipulation tasks are mainly focused on the load transportation, with a recent extension to the applications that involve transportation of automatic barrel, retrieval and transportation of ground robots as well as their cooperative load transportation. In the literature load transportation approaches can be classified into three main categories. The first approach considers tethered UAV. In this approach, automation of the picking process along with the stability of UAV constitutes a great challenge due to the load swinging affected by system motion and the environment. In the other two approaches, the load is picked by a gripper or manipulator. Attachment of the additional mechanism to the platform is challenging since additional tool increases payload of the AMS that is of limited capability.

The second class of the manipulation tasks considers aerial systems capable of actively modifying its environment. These tasks require the exertion of the forces and moments to the environment. Some of the applications of such aerial systems are infrastructure inspection, manipulation of movable objects such as doors, valve turning and more. In the literature, different architectures and applications are investigated to obtain the most efficient aerial manipulation capable of modifying the environment. Most common architecture involves AMS with manipulator attached underneath it used for the opening of the door with unknown mechanical

properties [62]. These tasks in indoor environments represent a great challenge that requires different force exertion schemes. In [63], author presents a scheme where quadcopter first approaches to the door, changes its attitude, perches on the door using suction cups, and then by means of soft bag actuators and its thrust force opens the door. The authors of [64] propose an aerial manipulator consisted of two 2-DOF robotic manipulators. The system is capable of grasping and opening the valve by means of its manipulators and yaw motion.

The assembly and construction of different structures represent the another manipulation missions of aerial manipulation systems. The first example of these applications is found in [65] where a team of quadcopters was used to build a 6m long tower. Afterwards they were utilized for building of truss structures [66, 67] which are used in tower cranes, power transmission towers and scaffolds.

Some of the applications that do not fall into the mentioned categories are autonomous water sampling [68], in-situ oil-spill cleanup operations [21], forest canopy sampling [69] and more. Usage of aerial manipulation systems in these applications is cheaper and more efficient compared to the existing approaches [21]. One of the ongoing challenges is autonomous air refueling using AMS [70–74]. In [74], authors use GPS and vision-based sensory data to fuel the tanker using receiver UAV and refueling boom. Furthermore, vision based drogue estimation algorithm was shown to be successful in air refueling of receiver UAVs by tanker UAV in [75].

## 2.4 Controllers

During aerial manipulation, the manipulation mechanism and/or a grasped object create coupling effects on the UAV base platform. A quadrotor platform, for example, is already underactuated and has intrinsically unstable dynamics. The additional coupling effects on the quadrotor create more challenge on the control of the overall system. Hence, in the literature, this problem is tackled in two different ways: (1) Decentralized approach or (2) Centralized approach.

## 2.4.1 Decentralized Approach

In the decentralized control approach, the control problem of the aerial manipulation system is evaluated by considering the unmanned aerial vehicle and the manipulation mechanism as two independent systems. During the aerial vehicle flight mission, the undesired coupling effect coming from the manipulation mechanism is taken as an external disturbance.

### 2.4.1.1 Linear Controllers

A PID controller was utilized for a quadrotor endowed with a gripper where the change in the center of mass had been tackled. The quadrotor and the gripper were taken as two independent units in system control. The mass of the overall system including payload was considered as unknown. The change in the mass was estimated using the least-squares method [76]. Similar studies with PID controllers considering the change in the center of mass are addressed in [29, 77, 78]. The PID techniques which utilize simplified dynamics can cause instabilities during a manipulation task in a flight scenario. Simple PD and PID control approaches are utilized separately for a UAV and a manipulator in [35]. The proposed controllers may not perform well during a flight scenario where the center of mass and inertia of the system changes.

### 2.4.1.2 Nonlinear Model-Based Controllers

Das et. al. [79] utilized a hierarchical control structure for the quadrotor, which consists of an outer proportional derivative loop and dynamic inversion for the inner loop. Another study, done by Achtelik et. al. [80], presented a hierarchical control scheme where an outer control loop based on dynamic inversion, a proportional controller is in the inner loop.

In addition, a Direct Adaptive Feedback Linearization for a Quadrotor is suggested in [81]. It is found robust to external disturbances and parameter changes during

a flight. Based on Lyapunov theory, it is ensured to be asymptotically stable. In [82], a Model Reference Adaptive Control, which is designed for a lightweight quadrotor, introduced robustness to parametric uncertainties. Nonlinear Model Predictive Control approach for aerial robots were addressed in [83].

## 2.4.2 Centralized Approach

The quadrotor and the robotic arm are considered as a unified entity, and its control scheme is derived from the complete model of the system. There are numerous different control approaches proposed to enable these systems to perform a stable flight mission. These control approaches can be reviewed under two branches: Linear Controllers and Nonlinear Model-Based Controllers.

### 2.4.2.1 Linear Controllers

Vast variety of previous studies show that it is possible to control the quadrotor equipped with a robotic arm using linear control methods by linearizing the system dynamics around a flight operation point (i.e. hover condition).

Linear-quadratic regulator (LQR) is an optimal control method which is used for the control of aerial vehicles in the literature [32, 84–86]. In [32], a standard LQR method was utilized near the equilibrium point of the entire dynamics of an unmanned helicopter equipped with a 1 DOF robotic arm. The controller shows a stable performance only in a close vicinity to the equilibrium point.

### 2.4.2.2 Nonlinear Model-Based Controllers

Nonlinear control techniques, that covers a broad range of dynamics of a vehicle for all flight operation scenarios, give better performance for the quadrotor equipped with a robotic arm.



Feedback linearization is a common method where the complex nonlinear system is algebraically transformed into its equivalent linear dynamics. Rather than a Jacobian linearization which includes a linear approximation of dynamics, feedback linearization is formed by an exact state transformation [87]. Aerial manipulation controller design based on output feedback linearization and stable zero dynamics is performed in [88, 89]. Dynamic inversion is another version of the feedback linearization where the nonlinear dynamics are inverted and taken as a feedback [90, 91].

Feedback linearization approaches are quite sensitive to modeling uncertainties and errors. Adaptive control techniques, on the other hand, are robust to those issues as they have adaptation mechanisms updating the unknown system parameters changing in time [92]. An adaptive sliding mode controller was proposed to overcome the modeling uncertainties of an aerial manipulation system. The controller handled the uncertainties caused by the unmodeled dynamics of an object picked up and delivered during a mission scenario [34]. The proposed adaptive sliding mode control methods have advantages over traditional sliding mode controllers, the adaptive ones yield smaller control inputs and chattering phenomena are avoided [93, 94]. In [95], an augmented passivity based controller is utilized to estimate the unknown parameters of a payload using a parameter estimator derived based on the parametrization of system dynamics. It is stated that the proposed controller outperforms the adaptive sliding mode controller.

The backstepping control is a recursive procedure which defines a number of the state variables as pseudo controls. Input-output does not required to be linear in this approach. The complexity of the approach is diminished without canceling any nonlinear dynamics [96]. For a hexarotor with a 2-DOF robotic arm, the nonlinear backstepping control is utilized for a simultaneous trajectory control. The system was able to perform the desired missions of the manipulator end-effector [97].

Model Predictive Control (MPC) predicts forthcoming response of the plant and generates control inputs using an explicit model [98]. In [61], MPC was designed for a variety of missions of an aerial manipulation system interacting with the environment, i.e. aerial writing. In this work, while in contact with a surface, stable trajectory control of the system and secure interaction with the environment were achieved by the MPC.



## Chapter 3

# Design and Construction of an Aerial Manipulation System

The design of the Aerial Manipulation System (AMS) is shaped based on the missions that it will accomplish. The system has a quadrotor base platform equipped with a two-DoF robotic arm. It is desired to perform simple aerial manipulation tasks i.e. pick-and-place of an object. Twenty minutes is set as the desired flight endurance for a manipulation scenario. The physical characteristics of the aerial vehicle are defined as below:

- maximum total weight of 2.5 kg
- payload capacity of 500 g

The design procedure includes

- **Hardware design and integration:** mechanical designs of the UAV and robotic arm, selection of their actuators, sensors and microcontrollers.
- **Software architecture:** real-time control and monitoring system.

## 3.1 Hardware Design and Integration

The hardware design stage of the vehicle is a crucial part of the development phase. For an excellent performance of the system, the aerial vehicle should have a small size, low weight, high thrust to weight ratio, high payload capacity and extended flight time. However, there is an inherent tradeoff between those parameters.

This section details the mechanical subparts of the AMS such as the UAV base and robotic arm and their actuators and sensors integrated into the design.

### 3.1.1 Mechanical Platform

The mechanical structure of the platforms should be capable of withstanding to interaction forces and moments. The main structure of the AMS is composed of a UAV base and a manipulation mechanism. Design properties of those subparts are given in the following sections.

#### 3.1.1.1 UAV Base

The base structure of the platform is chosen to be off-the-shelf DJI F450 quadrotor frame. It has an overall diagonal dimension of 450 mm and weighs 282 g. It carries a computational unit, a battery, sensors, and actuators. The CAD Model of the design is depicted in Fig. 3.1.



FIGURE 3.1: CAD model of the UAV base

### 3.1.1.2 Manipulation Mechanisms

The robotic arm was designed in Solidworks software. The two-finger gripper used in the design is an open-source commercial product [6]. The specifications of the arm are listed in Table 3.1.

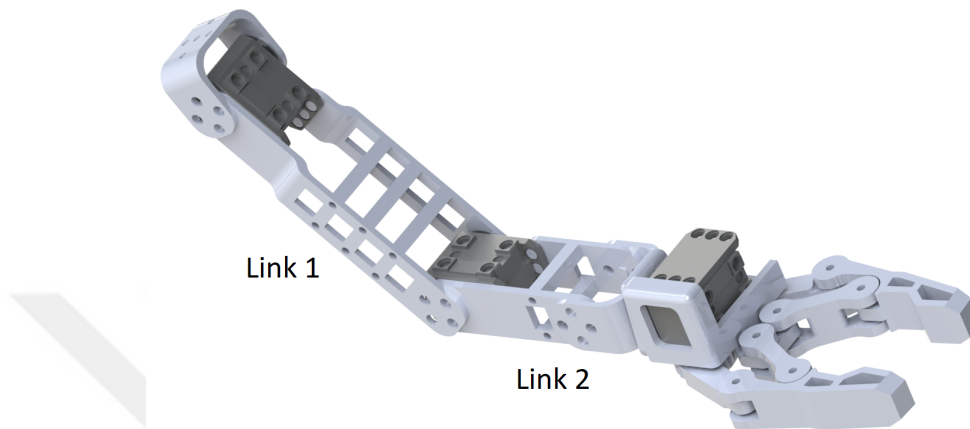


FIGURE 3.2: CAD model of the robotic arm

TABLE 3.1: The design specifications of the robotic arm [6]

Specification	Value
Link 1 length	100 mm
Link 2 length	100 mm
Weight	150 g
Gripper max opening width	59 mm

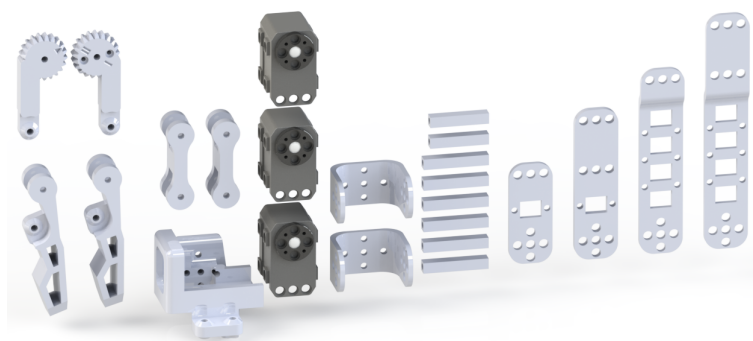


FIGURE 3.3: The hardware components of the robotic arm

The hardware components of the robotic arm are depicted in Fig. 3.3. The gripper is composed of 7 components and they were 3D printed with resin material. As for the arm links, its 14 components were 3D printed with PLA material.

### 3.1.2 Actuator Integration

The actuation system of AMS consists of rotors, rotor drivers, propellers, servos and batteries.

#### 3.1.2.1 Rotor and Rotor Driver

The total mass of the quadrotor and the attached manipulator arm was measured to be 2.5 kg. Since a maximum of 0.5 kg payload was specified as a design criterion, the minimum thrust to be produced was estimated as 4 kg by selecting a thrust to weight ratio of 4/3. The total thrust was distributed to each rotor assuming 0.625 kg of nominal thrust, 0.125 kg payload and a 0.25 kg of control margin summing up to 1 kg. Based on the thrust requirement, EMAX-MT3110 rotor (Fig. 3.4) was considered an adequate selection due to its 1.2 kg thrust output and low weight (78 gr).

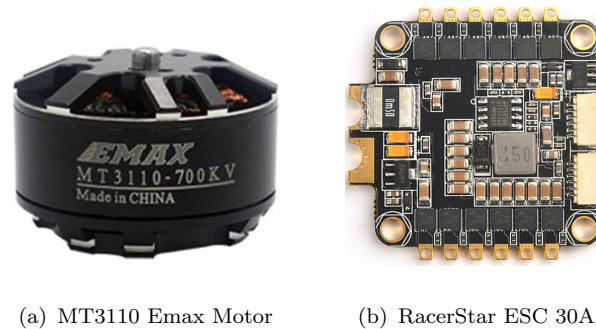


FIGURE 3.4: Rotor and rotor driver

Racerstar BLHeli-S 4in1 Series are chosen as electronic speed controllers (ESC) to drive the EMAX rotors. The 10 gr weighting driver can supply up to 30A constant current simultaneously to four rotors with a constant frequency of 50 Hz. It has 36x36mm dimensions.

### 3.1.2.2 Propeller

As the length of a blade increases, its efficiency enhances by providing larger thrust. However, its mass and inertia also grow, which degrades the output response time and increases the power requirement. Based on the frame length of the UAV base, propellers set to a maximum of 10 inches (254 mm) was selected considering some clearance between the central structure and blade tip. The selected 10x4.5 carbon fiber propeller is shown in Fig. 3.5.



FIGURE 3.5: 10x4.5 carbon fiber propeller

### 3.1.2.3 Servos

Dynamixel XL320 digital servos are used in the robotic arm mechanism. These servos have a maximum 0.39 Nm stall torque (at 7.4V, 1.1A) and 114 rpm no load speed (at 7.4V, 0.18A). Fig. 3.6 shows the XL-320 digital servo. It communicates with half-duplex asynchronous serial communication. It has the functionality to provide position, temperature, load, and input voltage feedback signals.



FIGURE 3.6: Dynamixel XL-320 digital servo

TABLE 3.2: Dynamixel XL-320 specifications

Weight [g]	Dimension [mm]	Resolution [°]
16.7	24 x 36 x 27	0.29

### 3.1.2.4 Battery

Although high energy capacity and lightweight Li-Po batteries were used as the power source of actuation, the greatest percentage of the AMS's weight was due to the batteries. In order to ensure twenty minutes flight time, a 5200 mAh 4S 30C battery with a mass of 512 g (Fig. 3.7) was used to power the onboard electronics and actuators of the AMS.



FIGURE 3.7: Leopard 4S 5200Mah 30C lipo battery

## 3.1.3 Sensor and Microcontroller Integration

In this section, the sensors used to realize the developed AMS's flight and manipulation tasks are detailed. The sensors used were x-IMU, Pozyx positioning system, sonar and optical flow cameras. The data acquisition from these sensors and communication with the actuators were realized using myRIO and Arduino microcontrollers.

### 3.1.3.1 Myrio Data Acquisition Card

In this work, NI myRIO-1900 data acquisition card shown in Fig. 3.8 was utilized as the central micro controller of the system. This board is developed by National Instruments and has multiple input/output (I/O) channels. Some of these are:

- 40 bidirectional digital IO channels
- 8 single-ended 12-bit analog input channels
- 8 16-bit PWM output channels
- 2 I2C ports



- 2 UART ports

The device features a dual-core ARM Cortex-A9 processor clocked at 667 MHz and a Xilinx Z-7010 FPGA. It can be programmed using both LabVIEW and C languages and it has an on-board 2.4 Ghz wifi module for wireless communication.



FIGURE 3.8: myRIO-1900 Data Acquisition Board

### 3.1.3.2 Positioning System

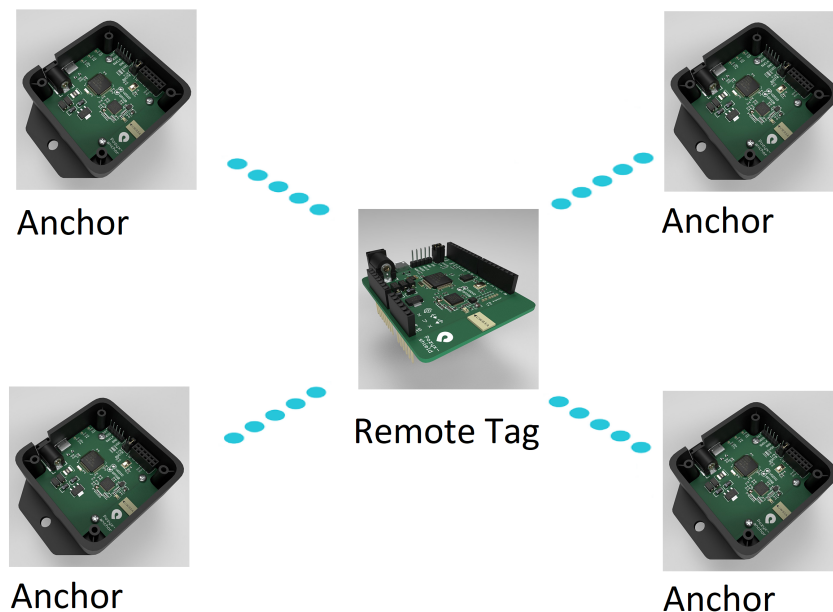


FIGURE 3.9: Pozyx accurate positioning system

In this work, Pozyx positioning system was used for tracking the pose of the quadrotor. Pozyx is an ultra wideband based 3D positioning system for indoor and outdoors. It consists of a remote tag which is attached to the tracked target and it can estimate its pose through the measurements obtained from at least 4

stationary anchors which must be placed at various locations in the flight area. The Pozyx system is able to track multiple targets at the same time with an accuracy of 10 cm and a single tag supports update rates up to 60 Hz.

### 3.1.3.3 IMU

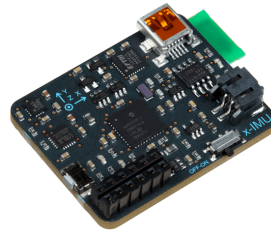


FIGURE 3.10: x-IMU Inertial Measurement Unit

The x-IMU, produced by x-IO technologies, is an Inertial Measurement Unit (IMU) which has 3-axis gyroscope, 3-axis accelerometer, and 3 axis magnetometer. Its onboard Attitude Heading Reference System (AHRS) provides Euler angle estimates. The internal states are updated up to 512Hz. Real-time communication of the module can be done through UART, bluetooth or USB.

### 3.1.4 Overall Hardware Architecture

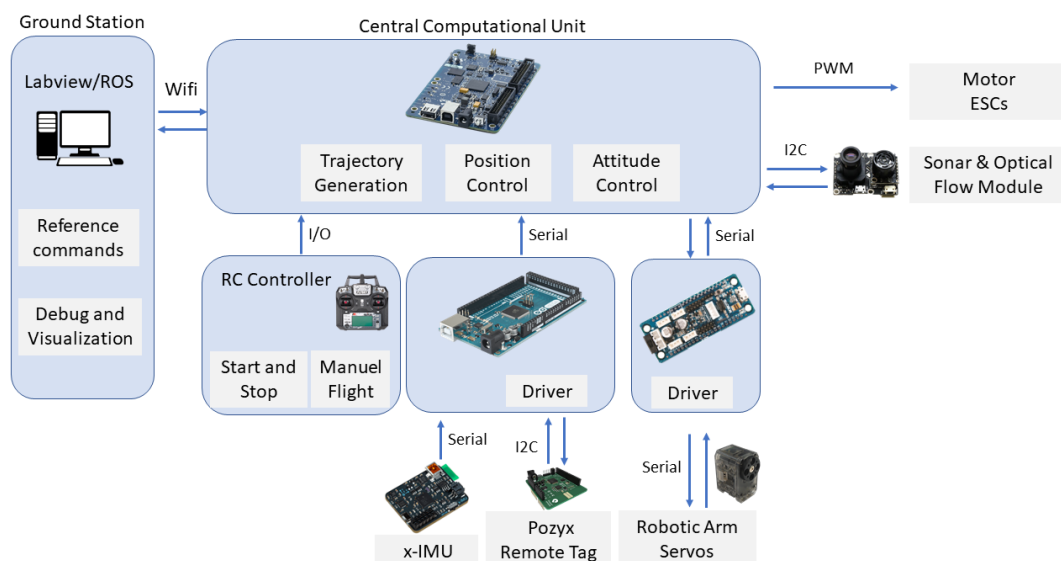


FIGURE 3.11: Schematic of the hardware setup

Fig. 3.11 depicts the overall hardware architecture of the system. In the figure, the on-board central computational unit takes the position estimates from the Pozyx, reference commands from the ground station and attitude estimates from the x-IMU module. The robotic arm servos supply the joint angle and velocity measurements. Altitude and optical flow measurements come from the Sonar and optical flow module. The computational unit utilizes all received information and calculates the required control efforts to operate the system. Once the control efforts are generated, they were mapped to the PWM signals to drive the Motor ESCs. The RC controller is used for the manual flight, start and stop purposes.

CAD Model of the overall system has been depicted in Fig. 3.12. Hardware specifications of the system has been presented in Table 3.3.



FIGURE 3.12: CAD Model of the Aerial Manipulation System

TABLE 3.3: Hardware specifications of the AMS

Parameters	Value
Hub-to-hub diameter	45 cm
Overall diameter (with 10inch propellers)	69 cm
Weight of the AMS (without battery)	1778 g
Weight of robotic arm (with microcontroller)	190 g
Battery weight (4S 5200Mah)	516 g
Takeoff gross weight	2484 g
Max. thrust per arm	1210 g

## 3.2 Software Architecture

As stated before, myRIO acts as the central unit and all of the data flows through it. In this work, the 32 bit version of LabVIEW myRIO 2018 software was used to program the myRIO-1900 microcontroller. Whereas, C language was used to program the Pozyx, x-IMU, sonar and optical flow modules.

### 3.2.1 Real-Time Control

FPGA module of the myRIO-1900 was utilized for the real time control of the system. All sensor information flows into the FPGA module to get the required the control efforts to make the AMS follow its desired trajectory. The data flow was published in real-time over the 2.4 Ghz local network for the monitoring purposes.

### 3.2.2 Monitoring System

The developed graphical user interface for trajectory input and monitoring of all the AMS's sensors is shown in Fig. 3.13. This interface was developed in LabVIEW and it was used for providing reference commands and monitoring the position, attitude, voltage levels and joint angles of the AMS.

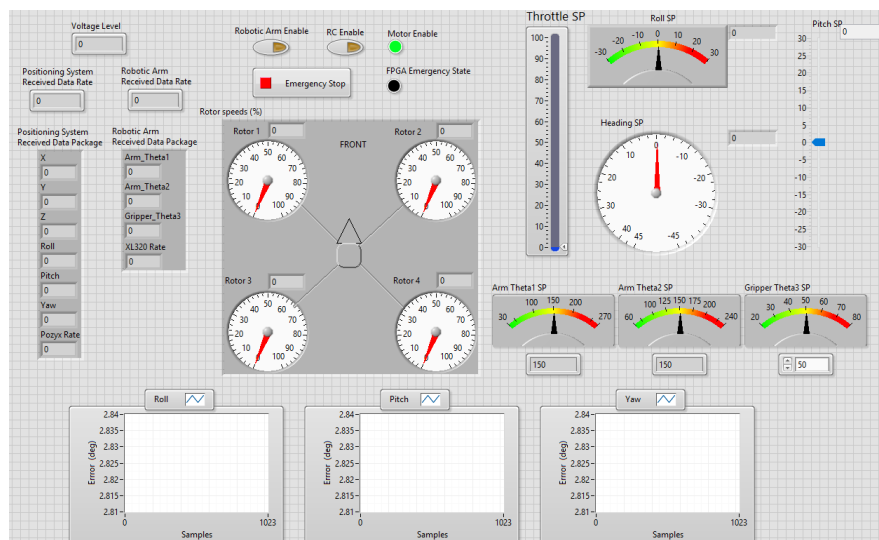


FIGURE 3.13: Graphical User Interface

# Chapter 4

## Modeling of the Aerial Manipulation System

“All models are wrong, but some are useful”

—George E.P.Box

A mathematical model is required to describe the system designed in Chapter 3. The model is used to design all control architectures and tune them in simulations before experimentation on the hardware setup.

In this chapter, the kinematics and nonlinear dynamics of the system are described. All coupling effects coming from the robotic arm are considered in the mathematical model of the system.

### 4.1 Model Description

There are six inputs to the Aerial Manipulation System (AMS). Four inputs represent the quadrotor actuators ( $U_1, U_2, U_3, U_4$ ) and two are the manipulator actuators ( $\tau_{\zeta_1}, \tau_{\zeta_2}$ ).  $U_1$  is the total thrust,  $U_2, U_3$  and  $U_4$  are rolling, pitching, and yawing moments of the quadrotor respectively.  $\tau_{\zeta_1}, \tau_{\zeta_2}$  are the manipulator joint torques.

The system has sixteen outputs, eight of which are the positions of quadrotor  $X = [X, Y, Z]^T$ ,  $\Phi = [\phi, \theta, \psi]^T$ , and the manipulator joints  $\zeta = [\zeta_1, \zeta_2]^T$ . The other eight outputs are the velocities of the quadrotor  $\dot{X} = [\dot{X}, \dot{Y}, \dot{Z}]^T$ ,  $\dot{\Phi} = [\dot{\phi}, \dot{\theta}, \dot{\psi}]^T$ , and manipulator joints  $\dot{\zeta} = [\dot{\zeta}_1, \dot{\zeta}_2]^T$ .

With its numerous inputs and outputs, the system can be considered as a Multiple Input, Multiple Output (MIMO) system.

## 4.2 Kinematics for the Aerial Manipulation System

Coordinate frames are required to describe the position and orientation of the system.

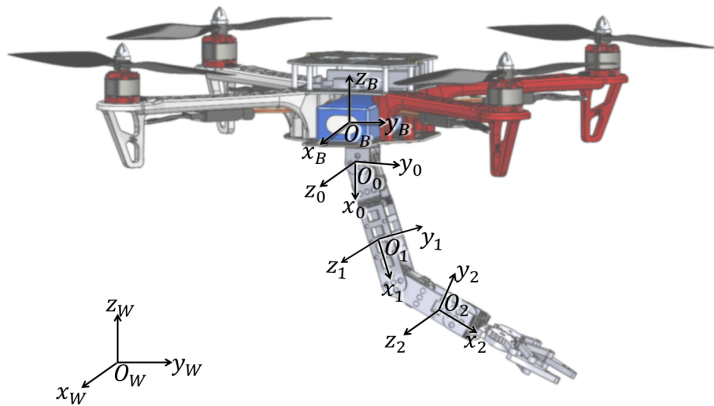


FIGURE 4.1: Coordinate frames of the system

Considering the sketch of the system depicted in Fig. 4.1,  $O_W$ ,  $O_B$ ,  $O_0$ ,  $O_1$  and  $O_2$  denote the world (inertial) frame, the body (base) frame of the quadrotor, base link, link 1 and link 2 respectively. The Earth-North-Up (ENU) convention is used for the quadrotor and world reference frames. The link coordinate frames are assigned based on the Denavith-Hanterberg (DH) convention.

The rotation matrix  $R_b^w$  denotes the transformation from  $O_B$  to  $O_W$  and it is defined as follows:

$$\begin{aligned}
 R_b^w &= R_{z,\psi} R_{y,\theta} R_{x,\phi} \\
 &= \begin{bmatrix} c_\psi & -s_\psi & 0 \\ s_\psi & c_\psi & 0 \\ 0 & 0 & 1 \end{bmatrix} \begin{bmatrix} c_\theta & 0 & s_\theta \\ 0 & 1 & 0 \\ -s_\theta & 0 & c_\theta \end{bmatrix} \begin{bmatrix} 1 & 0 & 0 \\ 0 & c_\phi & -s_\phi \\ 0 & s_\phi & c_\phi \end{bmatrix} \\
 &= \begin{bmatrix} c_\theta c_\psi & s_\phi s_\theta c_\psi - c_\phi s_\psi & s_\phi s_\theta c_\psi - c_\phi s_\psi \\ c_\theta s_\psi & s_\phi s_\theta s_\psi + c_\phi s_\psi & c_\phi s_\theta s_\psi - s_\phi c_\psi \\ -s_\theta & s_\phi c_\theta & c_\phi c_\theta \end{bmatrix} \tag{4.1}
 \end{aligned}$$

where  $s_{(\cdot)}$  and  $c_{(\cdot)}$  represent trigonometric sine and cosine functions respectively.

Similarly,  $R_i^b$  defines a transformation from  $O_i$  to  $O_B$ . The subscript  $i = 0, 1, 2$  denotes the link number.

The relationship between the joint variables and the position, and orientation of the manipulator end-effector is derived by the Denavith-Hanterberg (DH) method. DH notation attaches a coordinate frame at each joint and specifies four parameters for each link  $i$ . The four parameters are  $a_i, \alpha_i, d_i, \theta_i$ , which are namely link length, link twist, link offset, and joint angle. In this convention, the homogenous transformation  $A_i$  is defined as follows [99]:

$$\begin{aligned}
 A_i &= Rot_{z,\theta_i} \cdot Trans_{z,d_i} \cdot Trans_{x,a_i} \cdot Rot_{x,\alpha_i} \\
 &= \begin{bmatrix} c_{\theta_i} & -s_{\theta_i} & 0 & 0 \\ s_{\theta_i} & c_{\theta_i} & 0 & 0 \\ 0 & 0 & 1 & 0 \\ 0 & 0 & 0 & 1 \end{bmatrix} \begin{bmatrix} 1 & 0 & 0 & 0 \\ 0 & 1 & 0 & 0 \\ 0 & 0 & 1 & d_i \\ 0 & 0 & 0 & 1 \end{bmatrix} \begin{bmatrix} 1 & 0 & 0 & a_i \\ 0 & 1 & 0 & 0 \\ 0 & 0 & 1 & 0 \\ 0 & 0 & 0 & 1 \end{bmatrix} \begin{bmatrix} 1 & 0 & 0 & 0 \\ 0 & c_{\alpha_i} & -s_{\alpha_i} & 0 \\ 0 & s_{\alpha_i} & c_{\alpha_i} & 0 \\ 0 & 0 & 0 & 1 \end{bmatrix} \\
 &= \begin{bmatrix} c_{\theta_i} & -s_{\theta_i} c_{\alpha_i} & s_{\theta_i} s_{\alpha_i} & a_i c_{\theta_i} \\ s_{\theta_i} & c_{\theta_i} c_{\alpha_i} & -c_{\theta_i} s_{\alpha_i} & a_i s_{\theta_i} \\ 0 & s_{\alpha_i} & c_{\alpha_i} & d_i \\ 0 & 0 & 0 & 1 \end{bmatrix} \tag{4.2}
 \end{aligned}$$

The Denavit-Hartenberg (DH) table for the two-link manipulator (Fig. 4.2), of which joint coordinates are defined in Fig. 4.1, can be formed as below:

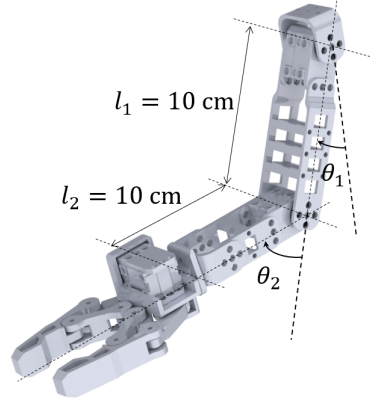


FIGURE 4.2: Sketch of the two-link manipulator

TABLE 4.1: DH table for the two-link manipulator

Link	a	$\alpha$	d	$\theta$
1	$l_1$	0	0	$\theta_1$
2	$l_2$	0	0	$\theta_2$

The transformation from the end-effector to the base of the manipulator can be defined as:

$$T_n^0 = T_n^{n-1} \dots T_2^1 T_1^0 \quad (4.3)$$

where the link number of the end-effector is  $n$  and for the base it is 0.

Based on the equation (4.1), the homogenous transformation from the link1 to the base ( $T_1^0$ ), and from the link2 to the link1 ( $T_2^1$ ) can be written as follows:

$$T_1^0 = A_1 = \begin{bmatrix} c_{\theta_1} & -s_{\theta_1} & 0 & l_1 c_{\theta_1} \\ s_{\theta_1} & c_{\theta_1} & 0 & l_1 s_{\theta_1} \\ 0 & 0 & 1 & 0 \\ 0 & 0 & 0 & 1 \end{bmatrix} \quad T_2^1 = A_2 = \begin{bmatrix} c_{\theta_2} & -s_{\theta_2} & 0 & l_2 c_{\theta_2} \\ s_{\theta_2} & c_{\theta_2} & 0 & l_2 s_{\theta_2} \\ 0 & 0 & 1 & 0 \\ 0 & 0 & 0 & 1 \end{bmatrix}$$

For a two-link manipulator, the transformation matrix of the end-effector with



respect to the base link is obtained as follows:

$$T_2^0 = \begin{bmatrix} c(\theta_1+\theta_2) & -s(\theta_1+\theta_2) & 0 & l_1c\theta_1 + l_2c(\theta_1+\theta_2) \\ s(\theta_1+\theta_2) & c(\theta_1+\theta_2) & 0 & l_1s\theta_1 + l_2s(\theta_1+\theta_2) \\ 0 & 0 & 1 & 0 \\ 0 & 0 & 0 & 1 \end{bmatrix} \quad (4.4)$$

Rewriting the equation (4.5) in this form,

$$T_2^0 = \begin{bmatrix} R_2^0 & t_2^0 \\ 0 & 1 \end{bmatrix} \quad (4.5)$$

The rotation matrix and the translation vector of the end-effector can be extracted as follows:

$$R_2^0 = \begin{bmatrix} c(\theta_1+\theta_2) & -s(\theta_1+\theta_2) & 0 \\ s(\theta_1+\theta_2) & c(\theta_1+\theta_2) & 0 \\ 0 & 0 & 1 \end{bmatrix} \quad (4.6)$$

$$t_2^0 = \begin{bmatrix} l_1c\theta_1 + l_2c(\theta_1+\theta_2) \\ l_1s\theta_1 + l_2s(\theta_1+\theta_2) \\ 0 \end{bmatrix} \quad (4.7)$$

The x and y positions of the end-effector with respect to  $O_o$ :

$$x = l_1c\theta_1 + l_2c(\theta_1+\theta_2) \quad (4.8)$$

$$y = l_1s\theta_1 + l_2s(\theta_1+\theta_2) \quad (4.9)$$

The joint angles of the link2 and link1:

$$\theta_2 = \cos^{-1} \frac{x^2 + y^2 - l_1^2 - l_2^2}{2l_1l_2} \quad (4.10)$$

$$\theta_1 = \tan^{-1} \frac{y}{x} - \tan^{-1} \frac{l_2s\theta_2}{l_1 + l_2c\theta_2} \quad (4.11)$$

For the combined system, which includes the quadrotor and a two-link manipulator, the generalized coordinate variables are defined as

$$q = [p \ \Phi \ \zeta]^T \quad (4.12)$$

where  $p = [X, Y, Z]$  stands for the position of the quadrotor in inertial frame,  $\Phi = [\phi, \theta, \psi]$  denotes the attitudes of the quadrotor and  $\zeta = [\zeta_1, \zeta_2]$  represents the joint angles of the manipulator.

For the quadrotor, the translational and angular velocities in the inertial frame are represented as  $\dot{p}$  and  $\omega$ .

$$\dot{p} = R_b^w \dot{p}^b \quad (4.13)$$

$$\omega = R_b^w \omega^b = T \dot{\Phi} \quad (4.14)$$

where  $\omega^b$  is the angular velocities in the body frame of the quadrotor. The transformation from Euler rates ( $\dot{\Phi}$ ) to angular velocities ( $\omega$ ) is represented with  $T$  and defined as below:

$$T = \begin{bmatrix} 1 & 0 & -s_\theta \\ 0 & c_\phi & s_\phi c_\theta \\ 0 & -s_\phi & c_\phi c_\theta \end{bmatrix} \quad (4.15)$$

The position  $p_i$  of the center of mass of each link  $i$  in the inertial frame are associated as

$$p_i = p + R_b^w p_i^b \quad (4.16)$$

where  $p_i^b$  is the position of center of mass in body frame of each link  $i$ .

For each link  $i$ , the translational and angular velocities in the inertial frame are represented as  $\dot{p}_i$  and  $\omega_i$ .

$$\dot{p}_i = \dot{p} + \dot{R}_b^w p_i^b + R_b^w \dot{p}_i^b \quad (4.17)$$

$$\omega_i = \omega + R_b^w J_t \dot{\zeta} \quad (4.18)$$

where  $\dot{R}_b^w = S(\omega_b) R_b^w$ ,  $\dot{p}_i^b = J_t \dot{\zeta}$  and  $\omega_i^b = J_r \dot{\zeta}$ . The Jacobian matrices of the translations and rotations of links are represented with  $J_t$  and  $J_r$  respectively.

$S(w)$  is the skew-symmetric matrix and defined as below:

$$S(\omega) = \begin{bmatrix} 0 & -\omega_3 & \omega_2 \\ \omega_3 & 0 & -\omega_1 \\ -\omega_2 & \omega_1 & 0 \end{bmatrix}, \quad \text{where } \omega = \begin{bmatrix} \omega_1 \\ \omega_2 \\ \omega_3 \end{bmatrix} \quad (4.19)$$

The relations above are collected into the following matrix forms:

$$\dot{p} = \begin{bmatrix} I_{3 \times 3} & 0_{3 \times 3} & 0_{3 \times 2} \end{bmatrix} \dot{q} \triangleq \mathcal{A}_1 \dot{q} \quad (4.20)$$

$$\omega = \begin{bmatrix} 0_{3 \times 3} & T & 0_{3 \times 2} \end{bmatrix} \dot{q} \triangleq \mathcal{A}_2 \dot{q} \quad (4.21)$$

$$\dot{p}_i = \begin{bmatrix} I_{3 \times 3} & -S(R_b^w p_i^b)T & R_b^w J_{t,i} \end{bmatrix} \dot{q} \triangleq \mathcal{A}_3 \dot{q} \quad (4.22)$$

$$\omega_i = \begin{bmatrix} 0_{3 \times 3} & T & R_b^w J_{r,i} \end{bmatrix} \dot{q} \triangleq \mathcal{A}_4 \dot{q} \quad (4.23)$$

### 4.3 Dynamics for the Aerial Manipulation System

An aerial manipulation vehicle has highly coupled dynamics due to the interaction between the quadrotor and manipulator. The nonlinear coupling brings up reaction forces and moments on the quadrotor which makes a precise control difficult. The forces and moments change dramatically in case of an interaction with the environment.

There are mainly two approaches to represent the mathematical model of the aerial vehicle dynamics: Newton-Euler and Lagrange-Euler. This chapter covers the dynamical model of the system by these two different approaches.

#### 4.3.1 Newton-Euler Dynamic Model

In this section, the aerial manipulation system is decoupled into two individual systems: UAV and robotic arm. UAV dynamics are extracted in terms of the

Newton-Euler formulation while the robotic arm dynamics are derived through the recursive Newton-Euler formulation. Once the coupling effects coming from the robotic arm is derived, coupled dynamics of the entire system is obtained.

#### 4.3.1.1 UAV-Quadrotor Dynamics

Considering the quadrotor as a rigid body, the dynamics of the vehicle can be obtained as

$$\begin{bmatrix} mI_{3x3} & 0_{3x3} \\ 0_{3x3} & I_b \end{bmatrix} \begin{bmatrix} \dot{V}_w \\ \dot{\Omega}_b \end{bmatrix} + \begin{bmatrix} 0 \\ \Omega_b \times (I_b \Omega_b) \end{bmatrix} = \begin{bmatrix} F \\ \tau \end{bmatrix} \quad (4.24)$$

where  $m$  is the mass and  $I_b$  is the moment of inertia matrix in the body frame of the vehicle.  $I_{3x3}$  and  $0_{3x3}$  are 3x3 identity and zero matrices respectively.  $V_w = [\dot{X}, \dot{Y}, \dot{Z}]^T$  is the linear velocity in the world frame, and  $\Omega_b = [p, q, r]^T$  is the angular velocity in the body frame of the vehicle. Total forces and moments applied on the UAV are represented with  $F$  and  $\tau$  respectively.

Motor thrusts are modeled as

$$F_i = kw_i^2 \quad (4.25)$$

where  $w_i$  is the rotor speed and  $k$  is the thrust coefficient.

Motor torques are modeled as

$$T_i = \lambda_i kw_i^2 \quad (4.26)$$

where  $\lambda_i$  is the torque/force ratio. For the counterclockwise rotors  $\lambda_{1,4} = \lambda$ , although for the clockwise rotors  $\lambda_{2,3} = -\lambda$ .

The dynamics of the vehicle can be rewritten in a more compact form as follows:

$$M\dot{\lambda} + C(\lambda)\lambda = G + O(\lambda)\omega + E(\zeta)\omega^2 + W(\lambda) + D(\lambda, \zeta) \quad (4.27)$$

where  $\lambda = [\dot{X}, \dot{Y}, \dot{Z}, p, q, r]^T$  defines the generalized velocity vector.  $\dot{X}, \dot{Y}, \dot{Z}$  are the linear velocities in the world frame,  $p, q, r$  are the angular velocities in the body

frame of the vehicle.  $\zeta = [X, Y, Z, \phi, \theta, \psi]^T$  denotes the position and orientation of the vehicle with respect to the world frame.

The transformation between  $\lambda$  and  $\zeta$  is defined by the following relation,

$$\dot{\zeta} = J\lambda \Rightarrow \begin{bmatrix} \dot{X} \\ \dot{Y} \\ \dot{Z} \\ \dot{\phi} \\ \dot{\theta} \\ \dot{\psi} \end{bmatrix} = \begin{bmatrix} I_{3 \times 3} & 0_{3 \times 3} \\ 0_{3 \times 3} & \begin{bmatrix} 1 & s_\phi t_\theta & c_\phi t_\theta \\ 1 & c_\phi & -s_\phi \\ 1 & s_\phi/c_\theta & c_\phi/c_\theta \end{bmatrix} \end{bmatrix} \begin{bmatrix} \dot{X} \\ \dot{Y} \\ \dot{Z} \\ p \\ q \\ r \end{bmatrix} \quad (4.28)$$

The inertia matrix  $M$ , the gravity vector  $G$ , the system actuator  $E(\zeta)\omega^2$ , the gyroscopic term, Coriolis-centripetal matrix  $C(\lambda)$ , and  $O(\lambda)\omega$  are defined as follows:

$$M = \begin{bmatrix} mI_{3 \times 3} & 0_{3 \times 3} \\ 0_{3 \times 3} & \text{diag}(I_{xx}, I_{yy}, I_{zz}) \end{bmatrix} \quad (4.29)$$

where  $I_{xx}$ ,  $I_{yy}$  and  $I_{zz}$  are the vehicle moment of inertias around x, y and z axis in the body frame.

$$G = [0, 0, -mg, 0, 0, 0]^T \quad (4.30)$$

$$E(\zeta)\omega^2 = \begin{bmatrix} (c_\phi s_\theta c_\psi + s_\phi s_\psi)U_1 \\ (c_\phi s_\theta s_\psi - s_\phi c_\psi)U_1 \\ (c_\phi c_\theta)U_1 \\ U_2 \\ U_3 \\ U_4 \end{bmatrix} \quad (4.31)$$

where  $U_1$  is the thrust force,  $U_2$ ,  $U_3$  and  $U_4$  are the rolling, pitching and yawing moments respectively.

$$C(\lambda) = \begin{bmatrix} 0_{3 \times 3} & & & & 0_{3 \times 3} & & & & \\ & & & & & & & & \\ & & & 0 & I_{zz}r & -I_{yy}q & & & \\ 0_{3 \times 3} & & -I_{zz}r & & 0 & I_{xx}p & & & \\ & & I_{yy}q & -I_{xx}p & & 0 & & & \end{bmatrix} \quad (4.32)$$

$$O(\lambda)\omega = \begin{bmatrix} 0_{3 \times 1} \\ -J_{prop}(q \sum_{i=1}^4 \eta_i \omega_i) \\ J_{prop}(p \sum_{i=1}^4 \eta_i \omega_i) \\ 0 \end{bmatrix} = \begin{bmatrix} 0_{3 \times 1} \\ -J_{prop}q\omega_p \\ J_{prop}p\omega_p \\ 0 \end{bmatrix} \quad (4.33)$$

where  $J_{prop}$  is the moment of inertial of a propeller.

$$U_1 = k(\omega_1^2 + \omega_2^2 + \omega_4^2 + \omega_4^2) \quad (4.34)$$

$$U_2 = kl_s(\omega_1^2 - \omega_2^2 + \omega_3^2 - \omega_4^2) \quad (4.35)$$

$$U_3 = kl_l(-\omega_1^2 - \omega_2^2 + \omega_3^2 + \omega_4^2) \quad (4.36)$$

$$U_4 = k\lambda(\omega_1^2 - \omega_2^2 - \omega_3^2 + \omega_4^2) \quad (4.37)$$

$D(\lambda, \zeta)$  term represents the external disturbances acting on the UAV.

As a result, the position and attitude dynamics of the UAV can be expressed as below:

$$\begin{aligned} \ddot{X} &= (c_\phi s_\theta c_\psi + s_\phi s_\psi) \frac{U_1}{m} \\ \ddot{Y} &= (c_\phi s_\theta s_\psi - s_\phi c_\psi) \frac{U_1}{m} \\ \ddot{Z} &= -g + (c_\phi c_\theta) \frac{U_1}{m} \\ \ddot{\phi} &= \frac{I_{yy} - I_{zz}}{I_{xx}} qr + \frac{U_2}{I_{xx}} - \frac{J_{prop}}{I_{xx}} q\omega_p \\ \ddot{\theta} &= \frac{I_{zz} - I_{xx}}{I_{yy}} pr + \frac{U_3}{I_{yy}} + \frac{J_{prop}}{I_{yy}} p\omega_p \\ \ddot{\psi} &= \frac{I_{xx} - I_{yy}}{I_{zz}} pq + \frac{U_4}{I_{zz}} + \frac{J_{prop}}{I_{zz}} r\omega_p \end{aligned} \quad (4.38)$$

### 4.3.1.2 Robotic Arm Dynamics with a Floating Base

The method starts with the forward computation of angular and linear velocities of each link starting from the base link to the end effector of the robotic arm. Once the angular and linear velocities of the end-effector are obtained, the backward calculation of all forces and moments acting on each joints of the system starting from the end-effector to the base link can be extracted [100, 101].

(a) Forward Computation:

By assuming the manipulator base link is attached to the center of mass of the UAV base, then the following initial conditions can be considered for the base link:

$$\begin{aligned} v_o &= R_w^o V_w, & \dot{v}_o &= R_w^o (\dot{V}_w + [0, 0, g]^T) \\ \omega_o &= R_B^o \omega_B, & \dot{\omega}_o &= R_B^o \dot{\omega}_B \end{aligned}$$

where

$$R_w^o = R_B^o R_w^B \quad \text{and} \quad R_B^o = \begin{bmatrix} 0 & 0 & -1 \\ 0 & 1 & 0 \\ 1 & 0 & 0 \end{bmatrix} \quad (4.39)$$

For  $i = 1:n$

Angular and linear velocities of the link (i) relative to the link (i-1) can be expressed as follows:

$$\omega_i = R_{i-1}^i (\omega_{i-1} + z_o \dot{q}_i) \quad (4.40)$$

$$v_i = R_{i-1}^i (v_{i-1} + \omega_i \times r_i) \quad (4.41)$$

where  $\omega_i$  is the angular velocity,  $v_i$  is the linear velocity,  $r_i$  is the position of the center of mass and  $q_i$  is the joint angle of link (i) relative to link (i-1),  $z_o$  is the vector that represents the rotation direction of the joint (i) which is  $[0 \ 0 \ 1]^T$ .

By taking derivatives of equations (4.40)-(4.41), corresponding angular and linear accelerations can be found as follows:

$$\dot{\omega}_i = R_{i-1}^i(\dot{\omega}_{i-1} + z_o\ddot{q}_i + \omega_{i-1} \times z_o\dot{q}_i) \quad (4.42)$$

$$\dot{v}_i = R_{i-1}^i(\dot{v}_{i-1}) + \dot{\omega}_i \times r_i + \omega_i \times (\omega_i \times r_i) \quad (4.43)$$

Based on the equation (4.1),

the transformation from the link (i-1) to the link (i) is:

$$R_{i-1}^i = \begin{bmatrix} c_{\theta_i} & s_{\theta_i} & 0 \\ -s_{\theta_i} & c_{\theta_i} & 0 \\ 0 & 0 & 1 \end{bmatrix}$$

the transformation from the link (i+1) to the link (i) is:

$$R_{i+1}^i = \begin{bmatrix} c_{\theta_i} & -s_{\theta_i} & 0 \\ s_{\theta_i} & c_{\theta_i} & 0 \\ 0 & 0 & 1 \end{bmatrix}$$

(b) Backward Computation:

Backward computation starts with the following initials coming from the end-effector of the robotic arm:

$$f_{n+1} = F_C, \quad \tau_{n+1} = T_C$$

where  $F_C$  is the contact force, and  $T_C$  is the contact torque.

For each link i = n:1

$$f_i = R_{i+1}^i(f_{i+1}) + m_i(\dot{v}_i + \dot{\omega}_i \times r_{ci} + \omega_i \times (\omega_i \times r_{ci})) \quad (4.44)$$

$$\tau_i = R_{i+1}^i(\tau_{i+1}) - f_i \times (r_i + r_{ci}) + f_{i+1} \times r_{ci} + I_i\dot{\omega}_i + \omega_i \times (I_i\omega_i) \quad (4.45)$$



where  $r_i$  is the position vector of the origin of the  $(i)^{th}$  link frame with respect to the  $(i-1)^{th}$  link frame,  $r_{ci}$  is the position vector of the center of mass of the  $(i)^{th}$  link frame with respect to the  $(i-1)^{th}$  link frame.

where

$$\begin{aligned} r_1 &= [l_1, 0, 0]^T, & r_2 &= [l_2, 0, 0]^T \\ r_{1c} &= [l_1/2, 0, 0]^T, & r_{2c} &= [l_2/2, 0, 0]^T \end{aligned}$$

#### 4.3.1.3 Coupled Dynamics of the Quadrotor with Robotic Arm

Coupled dynamics of the quadrotor with robotic arm is derived by including the coupling forces and moments of the robotic arm on the quadrotor dynamics in (4.24). The coupled dynamics in a matrix form is as follows:

$$\begin{bmatrix} mI_{3 \times 3} & 0_{3 \times 3} \\ 0_{3 \times 3} & I_b \end{bmatrix} \begin{bmatrix} \dot{V}_w \\ \dot{\Omega}_b \end{bmatrix} + \begin{bmatrix} 0 \\ \Omega_b \times (I_b \Omega_b) \end{bmatrix} + \begin{bmatrix} F_m \\ \tau_m \end{bmatrix} = \begin{bmatrix} F \\ \tau \end{bmatrix} \quad (4.46)$$

where  $[F_m \ \tau_m]^T$  are the coupling force and moment exerted by the manipulator on the quadrotor.

The coupled dynamics can be expressed as below as well:

$$\begin{aligned} \ddot{X} &= (c_\phi s_\theta c_\psi + s_\phi s_\psi) \frac{U_1}{m} - \frac{F_{M,x}}{m} \\ \ddot{Y} &= (c_\phi s_\theta s_\psi - s_\phi c_\psi) \frac{U_1}{m} - \frac{F_{M,y}}{m} \\ \ddot{Z} &= -g + (c_\phi c_\theta) \frac{U_1}{m} - \frac{F_{M,z}}{m} \\ \ddot{\phi} &= \frac{I_{yy} - I_{zz}}{I_{xx}} qr + \frac{U_2}{I_{xx}} - \frac{J_{prop}}{I_{xx}} qw_p - \frac{\tau_{M,x}}{I_{xx}} \\ \ddot{\theta} &= \frac{I_{zz} - I_{xx}}{I_{yy}} pr + \frac{U_3}{I_{yy}} + \frac{J_{prop}}{I_{yy}} pw_p - \frac{\tau_{M,y}}{I_{yy}} \\ \ddot{\psi} &= \frac{I_{xx} - I_{yy}}{I_{zz}} pq + \frac{U_4}{I_{zz}} + \frac{J_{prop}}{I_{zz}} rw_p - \frac{\tau_{M,z}}{I_{zz}} \end{aligned} \quad (4.47)$$

where  $m$  is the mass of the quadrotor,  $I_{xx}$ ,  $I_{yy}$ ,  $I_{zz}$  are the quadrotor moment of inertia around  $x_B$ ,  $y_B$ ,  $z_B$  axes respectively.  $F_{M,x}$ ,  $F_{M,y}$  and  $F_{M,z}$  are the components of the manipulator coupling force  $F_M$ , similarly  $\tau_{M,x}$ ,  $\tau_{M,y}$  and  $\tau_{M,z}$  are the components of the manipulator coupling moment  $\tau_M$ .

### 4.3.2 Euler-Lagrange Dynamic Model

Dynamic modeling of the aerial manipulation system is performed based on the Euler-Lagrange formulation.

$$\frac{d}{dt} \frac{\partial \mathcal{L}}{\partial \dot{q}_i} - \frac{\partial \mathcal{L}}{\partial q_i} = \tau_i + \tau_{ext} \quad (4.48)$$

$$\mathcal{L} = \mathcal{K} - \mathcal{U} \quad (4.49)$$

where  $\mathcal{K}$  is the total kinetic energy,  $\mathcal{U}$  is the total potential energy of the aerial manipulation system,  $q_i$  states the  $i^{th}$  generalized coordinate of  $q$  and  $\tau_i$  is the associated  $i^{th}$  generalized force, for  $i=1, \dots, 8$ . The last term  $\tau_{ext}$  denotes the effect of external generalized forces.

The calculation of the total kinetic energy can be expressed as

$$\mathcal{K} = \mathcal{K}_b + \sum_{i=1}^2 \mathcal{K}_i \quad (4.50)$$

where

$$\mathcal{K}_b = \frac{1}{2} \dot{p}^T m_b \dot{p} + \frac{1}{2} \omega^T (R_b^w) I_b (R_b^w)^T \omega \quad (4.51)$$

$$\mathcal{K}_i = \frac{1}{2} \dot{p}_i^T m_i \dot{p}_i + \frac{1}{2} \omega_i^T (R_b^w R_i^b) I_i (R_b^w R_i^b)^T \omega_i \quad (4.52)$$

The total potential energy is calculated as

$$\mathcal{U} = m_b g e_3^T p + \sum_{i=1}^2 m_i g e_3^T (p + R_b^w p_i^b) \quad (4.53)$$

where the gravity acceleration value,  $g = 9.81 \text{ m/s}^2$  and the vector indicating the direction of the gravity that acts along z axis of the system,  $e_3 = [0 \ 0 \ 1]^T$ .

After all, the dynamic equation of the aerial manipulation system can be composed in a more compact form as

$$M(q)\ddot{q} + C(q, \dot{q})\dot{q} + G(q) = \tau \quad (4.54)$$

The total kinetic energy can be reformulated in terms of the inertia matrix  $M(q)$  as

$$\mathcal{K} = \frac{1}{2}\dot{q}^T M(q)\dot{q} \quad (4.55)$$

By utilizing equations (4.20)-(4.23),  $M(q)$  can be obtained as

$$M(q) = \mathcal{A}_1^T m_b \mathcal{A}_1 + \mathcal{A}_2^T (R_b^w) I_b (R_b^w)^T \mathcal{A}_2 + \sum_{i=1}^2 \mathcal{A}_3^T m_i \mathcal{A}_3 + \mathcal{A}_4^T (R_b^w R_i^b) I_i (R_b^w R_i^b)^T \mathcal{A}_4 \quad (4.56)$$

The elements of the Coriolis matrix are formulated as follows:

$$c_{kj} = \sum_{i=1}^8 \frac{1}{2} \left\{ \frac{\partial m_{kj}}{\partial q_i} + \frac{\partial m_{ki}}{\partial q_j} - \frac{\partial m_{ij}}{\partial q_k} \right\} \dot{q}_i \quad (4.57)$$

The gravity matrix  $G(q)$  is calculated as

$$G(q) = \frac{\partial \mathcal{U}}{\partial q} \quad (4.58)$$

When the manipulator is in contact with the environment, the dynamic equation (4.54) must be modified as

$$M(q)\ddot{q} + C(q, \dot{q})\dot{q} + G(q) + J^T(q)F_e = \tau \quad (4.59)$$

where  $J$  is the jacobian matrix of the AMS and  $F_e$  is the generalized forces at the end-effector.

The control inputs for the quadrotor ( $U_1, U_2, U_3, U_4$ ) and manipulator actuators ( $\tau_1, \tau_2$ ) are converted to the generalized force  $\tau$  in Eqn. (4.54) as follows

$$\begin{bmatrix} \tau(1) \\ \vdots \\ \tau(8) \end{bmatrix} = \begin{bmatrix} R_b^w & 0_{3 \times 3} & 0_{3 \times 2} \\ 0_{3 \times 3} & ((R_b^w)^T T)^{-1} & 0_{3 \times 2} \\ 0_{2 \times 3} & 0_{2 \times 3} & I_{2 \times 2} \end{bmatrix} \begin{bmatrix} 0_{2 \times 1} \\ U_1 \\ U_2 \\ U_3 \\ U_4 \\ \tau_{\zeta_1} \\ \tau_{\zeta_2} \end{bmatrix} \quad (4.60)$$

where  $U_1$  is the total thrust,  $U_2$ ,  $U_3$  and  $U_4$  are rolling, pitching, and yawing moments of the quadrotor respectively.  $\tau_{\zeta_1}$  and  $\tau_{\zeta_2}$  denote the manipulator joint torques.

## Chapter 5

# Nonlinear Adaptive Control of the Aerial Manipulation System

In order to design flight controllers, the aerial manipulation system which consists of a quadrotor endowed with a 2-DOF robotic arm is considered as a unified system. It means that it has 3-DOF positional and 5-DOF unified attitude and joint dynamics. A Model Reference Adaptive Controller (MRAC) is designed as the upper level controller for the position subsystem, whereas a Nonlinear Adaptive Controller is utilized for the rotational subsystem which includes the attitude and joint dynamics. This part is also referred as the lower level controller. In this hierarchical structure, MRAC generates the control signals required to control the position of the quadrotor in the presence of reaction forces acting on the positional dynamics and uncertainties in the mass of the aerial manipulation system. The desired attitude angles which are calculated based on these MRAC control inputs and the desired joint angles comes from the inverse kinematics of the desired end-effector positions are fed into the lower level controller. The Nonlinear Adaptive Controller outputs the attitude and joint control inputs by compensating the change in the inertias of the aerial manipulation system. Block diagram of the overall control system architecture is depicted in Fig. 5.1.

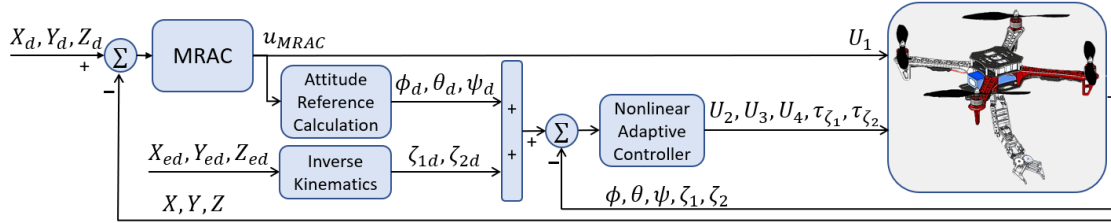


FIGURE 5.1: Overall Control System Architecture

## 5.1 Model Reference Adaptive Control (MRAC) Design

A Model Reference Adaptive Controller (MRAC) is designed to control the position of the AMS where its positional dynamics is assumed as a double integrator system. This controller generates the control inputs in X, Y and Z directions which are utilized in the calculations of the thrust force and the attitude references. Uncertainty in the mass of the aerial manipulation system is compensated by the online estimation of the control parameters based on the positional trajectory error. The overall structure of the MRAC is shown in Fig 5.2.

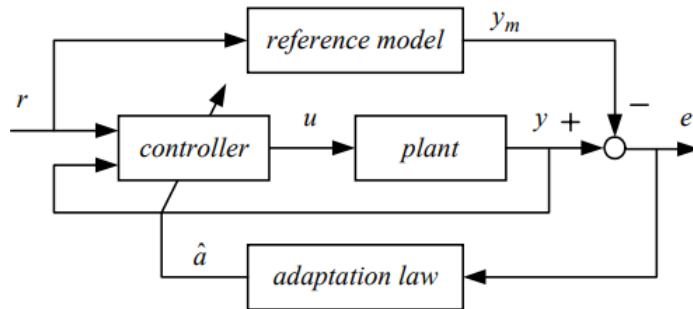


FIGURE 5.2: A model-reference adaptive control system [5]

Consider the following positional dynamics of the AMS as the plant model, [102, 103]

$$\begin{aligned}\dot{\mathcal{X}} &= F\mathcal{X} + G_n\Delta(u + D) \\ y &= H\mathcal{X}\end{aligned}\tag{5.1}$$

where  $\mathcal{X} = [X, Y, Z, \dot{X}, \dot{Y}, \dot{Z}]^T \in R^6$  is the state vector,  $y \in R^3$  is the plant output,

$$F = \begin{bmatrix} 0_{3 \times 3} & I_{3 \times 3} \\ 0_{3 \times 3} & 0_{3 \times 3} \end{bmatrix} \quad (5.2)$$

$$G_n = \begin{bmatrix} 0_{3 \times 3} \\ I_{3 \times 3} \end{bmatrix} \frac{1}{m_n} \quad (5.3)$$

$$D = \begin{bmatrix} 0_{2 \times 1} \\ mg \end{bmatrix} \quad (5.4)$$

$$H = \begin{bmatrix} I_{3 \times 3} & 0_{3 \times 3} \end{bmatrix}, \quad (5.5)$$

$$\Delta = \frac{m_n}{m} \quad (5.6)$$

where  $m_n$  and  $m$  are the nominal and actual masses of the AMS respectively.  $\Delta$  denotes the uncertainty in the AMS mass.  $g$  is the gravitational acceleration.

## 5.2 Reference Model Design

Reference model dynamics is derived based on the nominal system dynamics, where  $\Delta=1$ . Consider the following nominal control law,

$$u_n = K_x^T \mathcal{X} + K_r^T r - D_n \quad (5.7)$$

where  $r = [X_d, Y_d, Z_d]^T \in R^3$  is the reference input,  $K_x \in R^{6 \times 3}$  is the state gain matrix,  $K_r \in R^{3 \times 3}$  is the reference gain matrix and  $D_n = D = [0, 0, m_n g]^T \in R^3$ .

The nominal closed loop dynamics can be written as

$$\begin{aligned} \dot{\mathcal{X}}_n &= (F + G_n K_x^T) \mathcal{X}_n + G_n K_r^T r \\ y_n &= H \mathcal{X}_n \end{aligned} \quad (5.8)$$

By defining  $F_m = F + G_n K_x^T$ , the nominal plant output in s-domain can be written as,

$$y_n(s) = H(sI - F_m)^{-1} G_n K_r^T r(s) \quad (5.9)$$

By utilizing final value theorem, the steady-state output is calculated for a constant  $r$ ,

$$y_{ss} = -H F_m^{-1} G_n K_r^T r \quad (5.10)$$

using  $K_r^T = -(H F_m^{-1} G_n)^{-1}$ , it is found as

$$\lim_{t \rightarrow \infty} (y_n - r) = 0 \quad (5.11)$$

Finally, the reference model dynamics is determined as

$$\dot{\mathcal{X}}_m = F_m \mathcal{X}_m + G_m r \quad (5.12)$$

$$y_m = H \mathcal{X}_m$$

where

$$F_m = F + G_n K_x^T \quad (5.13)$$

$$G_m = G_n K_r^T \quad (5.14)$$

$K_x$  in the reference model can be determined using a linear quadratic regulator (LQR) and  $K_r$  is obtained as

$$K_r^T = -(H F_m^{-1} G_n)^{-1} \quad (5.15)$$

### 5.3 Adaptive Control

In the presence of uncertainties in the plant model (5.1), the constant gains in the control law (5.7) should be changed with their adaptive estimates.



Consider the following adaptive controller [103]:

$$u_{MRAC} = \hat{K}_x^T \mathcal{X} + \hat{K}_r^T r + \hat{D} \quad (5.16)$$

with the adaptive laws

$$\dot{\hat{K}}_x = -\Gamma_x (\mathcal{X} e^T P G_n - \sigma_x \|e\| \hat{K}_x) \quad (5.17)$$

$$\dot{\hat{K}}_r = -\Gamma_r (r e^T P G_n - \sigma_r \|e\| \hat{K}_r) \quad (5.18)$$

$$\dot{\hat{D}}^T = -\Gamma_D (e^T P G_n - \sigma_D \|e\| \hat{D}) \quad (5.19)$$

where  $e = \mathcal{X} - \mathcal{X}_m$ ,  $\Gamma_x$ ,  $\Gamma_r$ ,  $\Gamma_D$  are adaptive gains,  $\sigma_x$ ,  $\sigma_r$  and  $\sigma_D$  are positive scalar gains and  $P$  is the symmetric solution of the Lyapunov equation

$$F_m^T P + P F_m = -Q \quad (5.20)$$

where  $Q \in R^{6 \times 6}$  is a positive definite matrix.

## 5.4 Attitude Reference Calculation

From the equation (5.16), using the first two components of the  $u_{MRAC}$  and assuming small roll and pitch angles, one can derive the desired attitude angles of the quadrotor as

$$\begin{bmatrix} \phi_d \\ \theta_d \end{bmatrix} = \frac{1}{U_1} \begin{bmatrix} \sin \psi^* & -\cos \psi^* \\ \cos \psi^* & \sin \psi^* \end{bmatrix} \begin{bmatrix} u_{MRAC}^1 \\ u_{MRAC}^2 \end{bmatrix} \quad (5.21)$$

where  $U_1 = \|u_{MRAC}\|$ ,  $\psi_d = \psi^*$  is the desired fixed yaw angle and  $u_{MRAC}^i$  is the  $i^{th}$  component of the  $u_{MRAC}$ ,  $i = 1, 2, 3$ .

## 5.5 Nonlinear Adaptive Control Design

The nonlinear adaptive controller [5] is employed to force the AMS to follow its desired attitude angles, in the presence of uncertainties and change of inertias due to manipulator. Consider the attitude and manipulator dynamics as

$$M(\alpha_\omega)\dot{\Omega}_\omega + C(\alpha_\omega, \Omega_\omega)\Omega_\omega = u' \quad (5.22)$$

where  $\alpha_\omega = [\phi, \theta, \psi, \zeta_1, \zeta_2]^T$ . Through a long but tedious procedure, one can parameterize this equation linearly in terms of moments of inertia of the UAV and the manipulator; i.e.

$$Y(\alpha_\omega, \dot{\alpha}_\omega, \ddot{\alpha}_\omega)I_{AMS} = u' \quad (5.23)$$

where  $I_{AMS} = [I_{xx}, I_{yy}, I_{zz}, I_1, I_2]$ . In order to get rid of the acceleration term  $\ddot{\alpha}_\omega$  which is difficult to obtain, the following filtered error is defined;

$$s = \dot{\tilde{\alpha}}_\omega + \Lambda_s \tilde{\alpha}_\omega \quad (5.24)$$

where  $\tilde{\alpha}_\omega = \alpha_\omega - \alpha_{\omega d}$ ,  $\alpha_{\omega d}$  is the desired value of  $\alpha_\omega$  and  $\Lambda_s$  is a symmetric positive definite matrix. Eqn. (5.24) can be rewritten as

$$s = \dot{\alpha}_\omega - \dot{\alpha}_{\omega r} \quad (5.25)$$

where  $\dot{\alpha}_{\omega r} = \dot{\alpha}_{\omega d} - \Lambda_s \tilde{\alpha}_\omega$

A matrix  $Y' = Y'(\alpha_\omega, \dot{\alpha}_\omega, \dot{\alpha}_{\omega r}, \ddot{\alpha}_{\omega r})$  can be defined, to be used in linear parametrization, as in the case of equation (5.23) such that

$$M(\alpha_\omega)\dot{\Omega}_\omega + C(\alpha_\omega, \Omega_\omega) = Y'(\alpha_\omega, \dot{\alpha}_\omega, \dot{\alpha}_{\omega r}, \ddot{\alpha}_{\omega r})I_{AMS} \quad (5.26)$$

It can be shown that the following nonlinear controller

$$u_{AMS} = Y'\hat{I}_{AMS} - K_D s \quad (5.27)$$

where  $K_D$  is positive definite matrix and  $\hat{I}$  is an estimate of the uncertain parameter  $I$ , with an adaptive law

$$\dot{\hat{I}}_{AMS} = -\Gamma_I Y^T s \tag{5.28}$$

where  $\Gamma_I$  is the adaption rate, stabilizes the closed loop system and makes the error  $\tilde{\alpha}_\omega$  converge to zero.

## 5.6 An Example Flight Scenario

As an example flight scenario, the AMS is desired to pull an object from where it stuck. To analyze behaviour of the AMS during hover, task preparation and manipulation phases, the flight scenario is constructed in Figure 5.3.

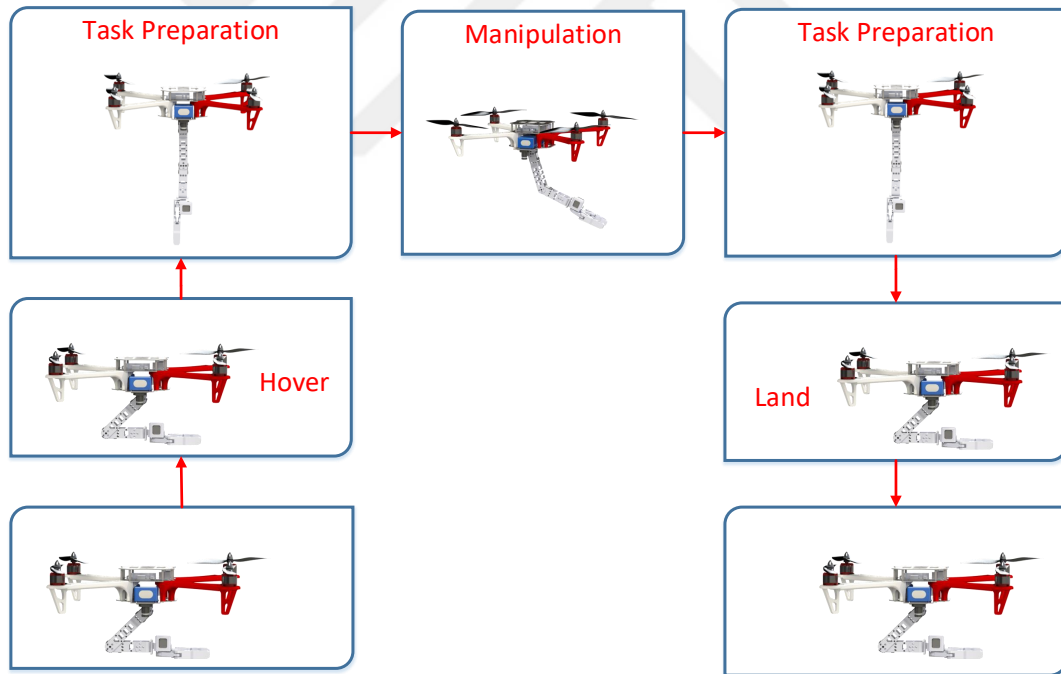


FIGURE 5.3: An Example Flight Scenario

During the flight scenario:

- The AMS takes-off from a start position with  $\zeta_1 = -22.33^\circ$ ,  $\zeta_2 = 112.33^\circ$  joint angles (0-5 sec).

- After reaching the desired hover position, it goes to the manipulation location (5-10 sec).
- Then, it extends the arm (10-15 sec).
- During the manipulation phase, the AMS interacts with the object (15-65 sec).
- It collects its arm (65-70 sec).
- After the manipulation phase, it collects its arm back to  $\zeta_1 = -22.33^\circ$ ,  $\zeta_2 = 112.33^\circ$  joint angles and goes back to its hover position (70-75 sec).
- Then it lands to its start position back (75-80 sec).

# Chapter 6

## Simulation Results

In this chapter, the performance of the proposed controllers is evaluated for different flight scenarios using the nonlinear dynamics of the AMS. These flight scenarios are investigated during hovering, task preparation, manipulation and landing as defined in Section 5.6. The scenarios include:

- **Free motion scenarios with the robotic arm during hovering:** Quadrotor maintains its position at a certain altitude, and the arm follows the desired trajectory.
- **Motion of the quadrotor with the robotic arm in a fixed position:** In this scenario, joint angles of the arm are fixed and the quadrotor follows the desired trajectory.
- **A manipulation scenario under varying disturbances:** An object is stuck to a location and is required to be pulled out. The AMS pulls out the object under the effects of varying interaction and wind forces.

The nonlinear dynamic model derived in Chapter 4 is constructed in Simulink/MATLAB environment (Fig. 6.1).

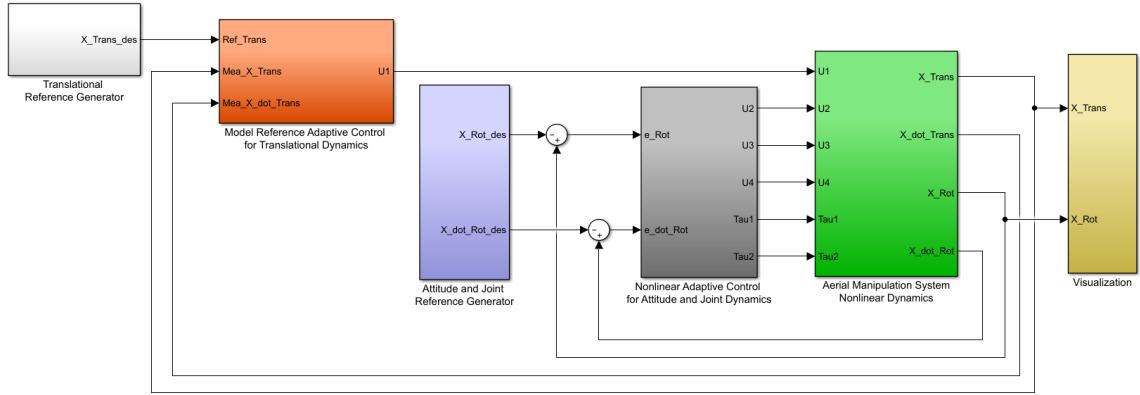


FIGURE 6.1: Simulink Model of the AMS

The reference model for the design of the outer loop controller is determined using a linear quadratic regulator (LQR). It is assumed that UAV mass is uncertain with a 20% uncertainty. Dryden Wind model and measurement noise are included in all of the flight scenarios mentioned above and simulation parameters are tabulated in Table 6.1.

TABLE 6.1: Simulation Parameters

Symbol	Description	Magnitude
$m_b$	Mass of the UAV	2.5 kg
$m_1$	Mass of the link 1	0.1 kg
$m_2$	Mass of the link 2	0.1 kg
$L_1$	Length of the link 1	0.15 m
$L_2$	Length of the link 2	0.15 m
$I_{xx}$	Moment of inertia of the UAV ( $x_B$ axis)	12e-3 kgm <sup>2</sup>
$I_{yy}$	Moment of inertia of the UAV ( $y_B$ axis)	12e-3 kgm <sup>2</sup>
$I_{zz}$	Moment of inertia of the UAV ( $z_B$ axis)	16e-3 kgm <sup>2</sup>
$I_1$	Moment of inertia of the link 1	1.875e-4 kgm <sup>2</sup>
$I_2$	Moment of inertia of the link 2	1.875e-4 kgm <sup>2</sup>

## 6.1 Free Motion Scenarios with the Robotic Arm during Hovering

Free motion flight scenarios include: (1) drawing a rectangular shape, and (2) a circular shape. Note that these scenarios utilize Eqn. (4.54) as the dynamics model of the AMS.

### 6.1.1 Drawing a Rectangular Shape

In this flight scenario, the robotic arm carries a 50-gram spray-box to draw a rectangular shape. The quadrotor hovers at a certain altitude, then the manipulator starts drawing the rectangular pattern. Fig. 6.2 visualizes the flight scenario in a Virtual Reality (VR) environment constructed in Simulink/MATLAB.

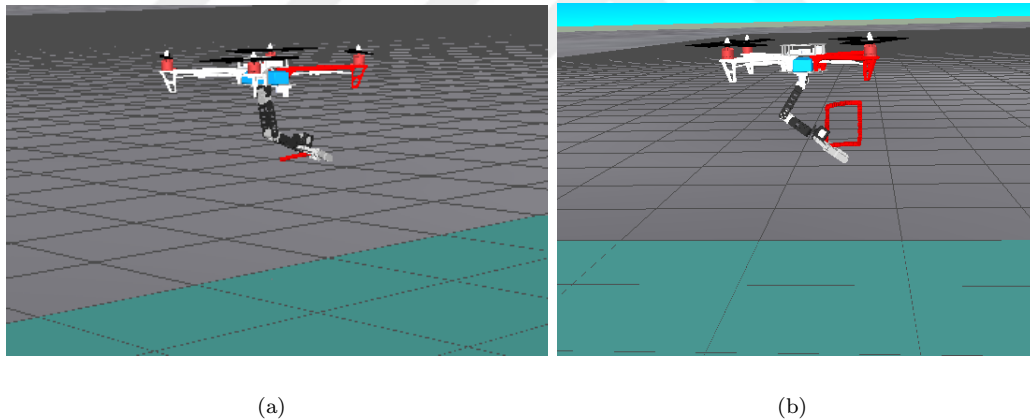


FIGURE 6.2: The flight mode visualization from different views

The end-effector trajectory of the manipulator has been depicted in Fig. 6.3. Cartesian position plots for this scenario have been shown in Figs. 6.4–6.6, where the quadrotor shows a stable hovering at the desired altitude under external disturbances varying from  $-1\text{N}$  to  $0.5\text{N}$  (Fig. 6.13).

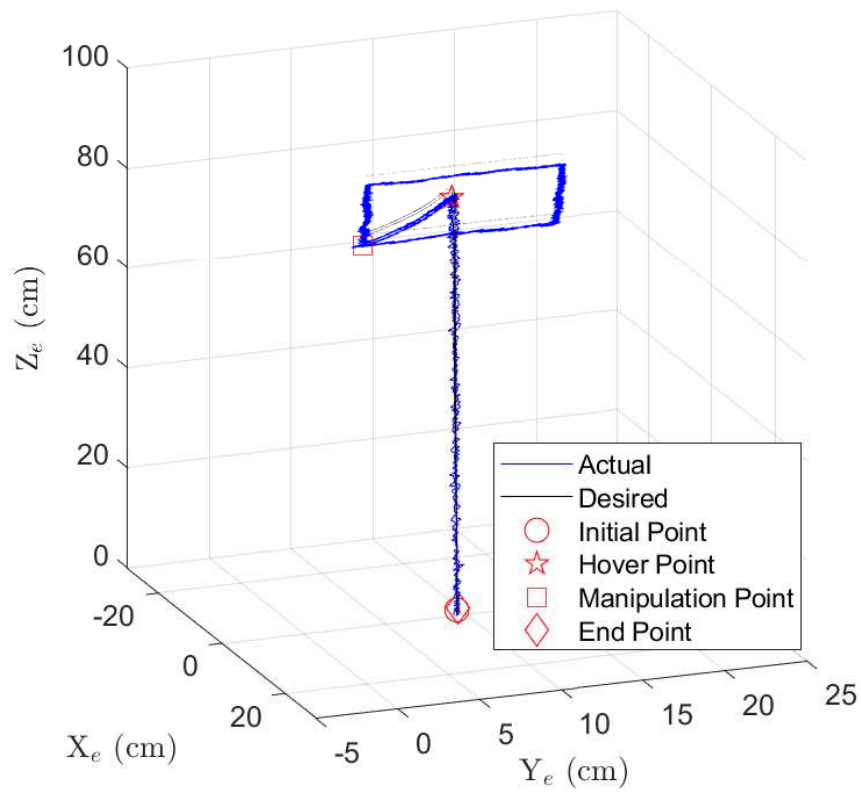


FIGURE 6.3: 3D trajectory of the end-effector

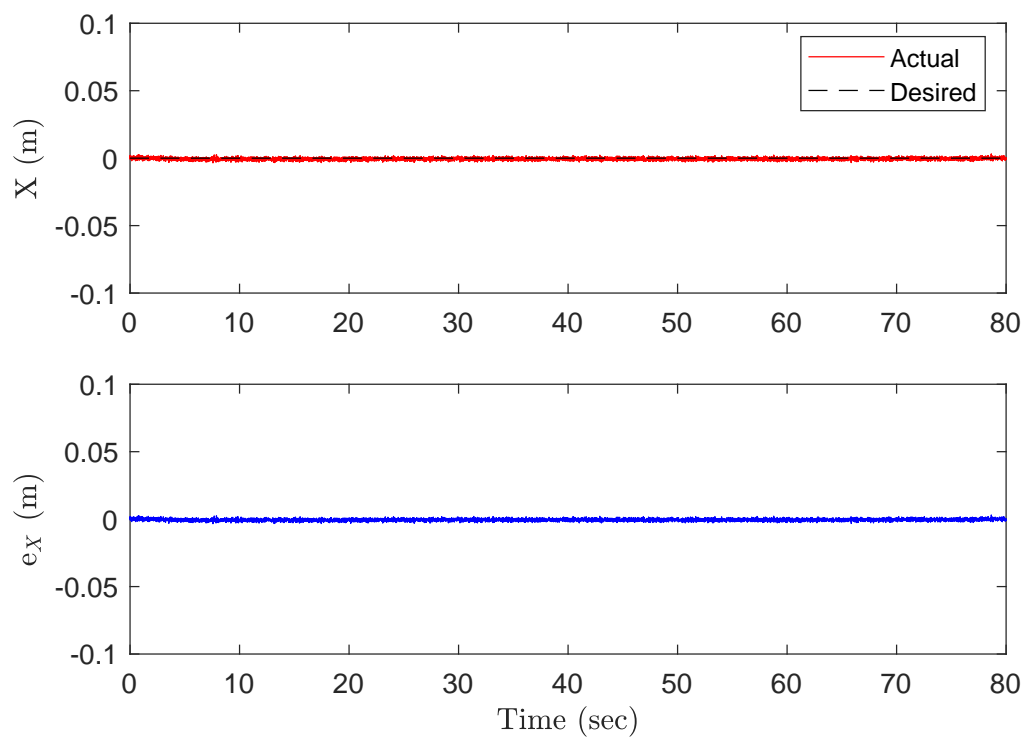


FIGURE 6.4: X position of the quadrotor (top), position error (bottom) vs Time



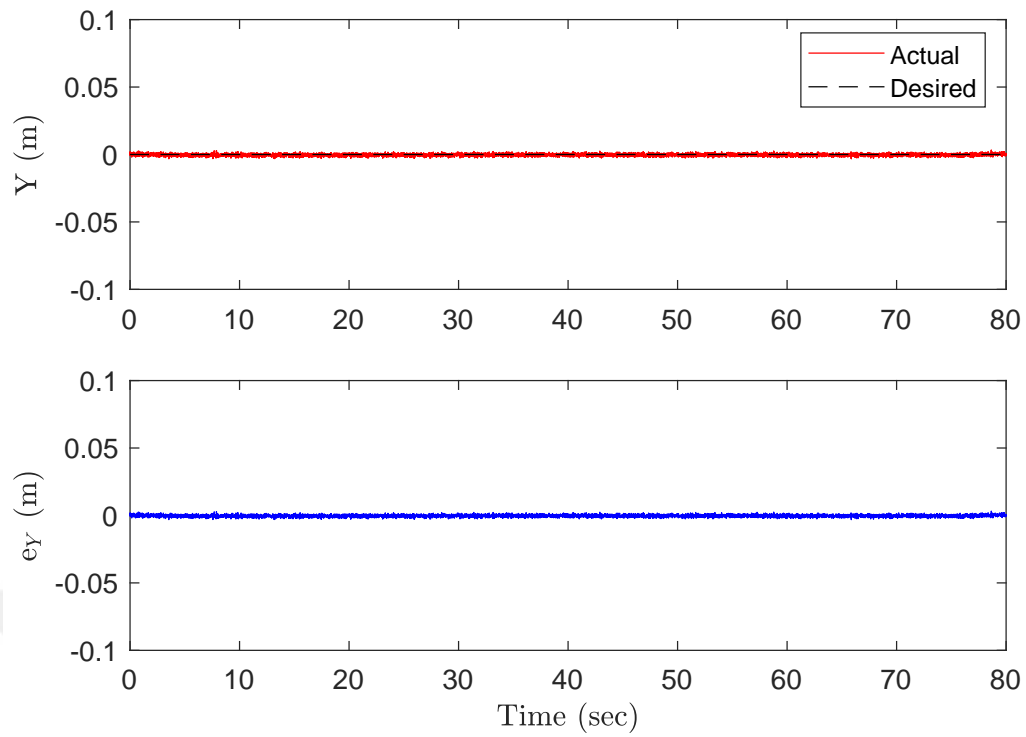


FIGURE 6.5: Y position of the quadrotor (top), position error (bottom) vs Time

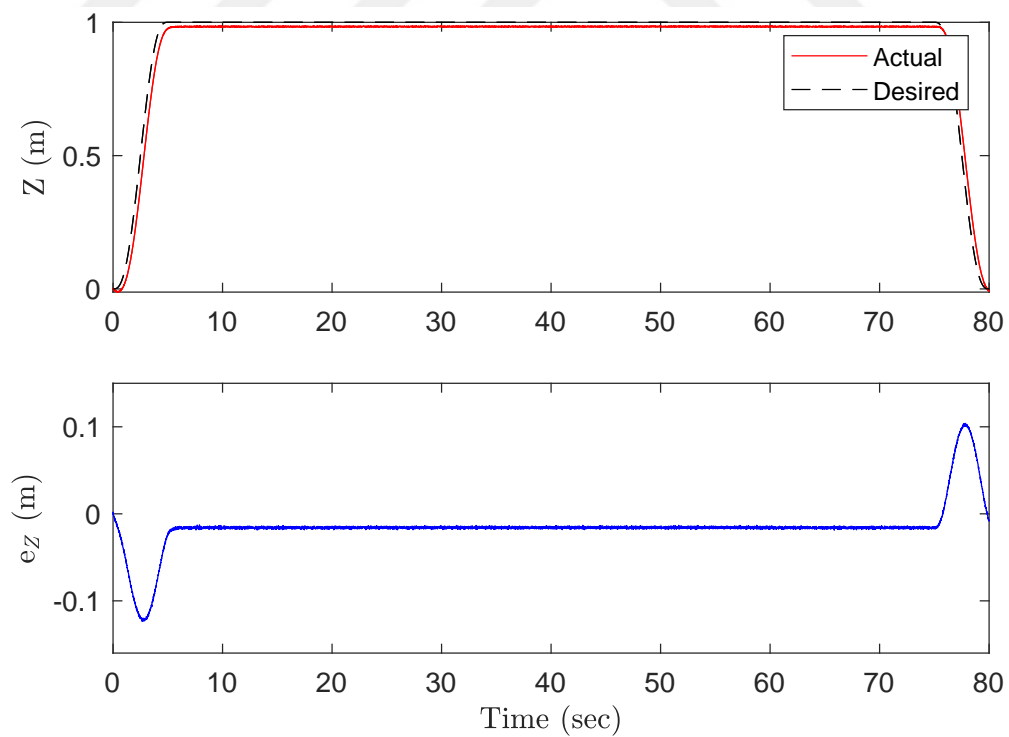


FIGURE 6.6: Z position of the quadrotor (top), position error (bottom) vs Time

According to the tracking errors given in Table 6.2, the position tracking of the quadrotor is quite accurate with RMSE in the range of 0.001m–0.030m. In Table 6.2,  $e_{X_e}$ ,  $e_{Y_e}$ , and  $e_{Z_e}$  denote the positional errors for the end-effector of the manipulator. Note that there is no significant difference between tracking performances of the quadrotor and the manipulator end-effector. Worst-case position errors are also very small, i.e around 0.13m, for both the quadrotor and the manipulator.

Attitude angles of the quadrotor and the manipulator joint angles are depicted in Figs. 6.7–6.11 where it can be noticed that the system follows the desired angles satisfactorily under external disturbances varying from -1Nm to 1Nm (Fig. 6.14).

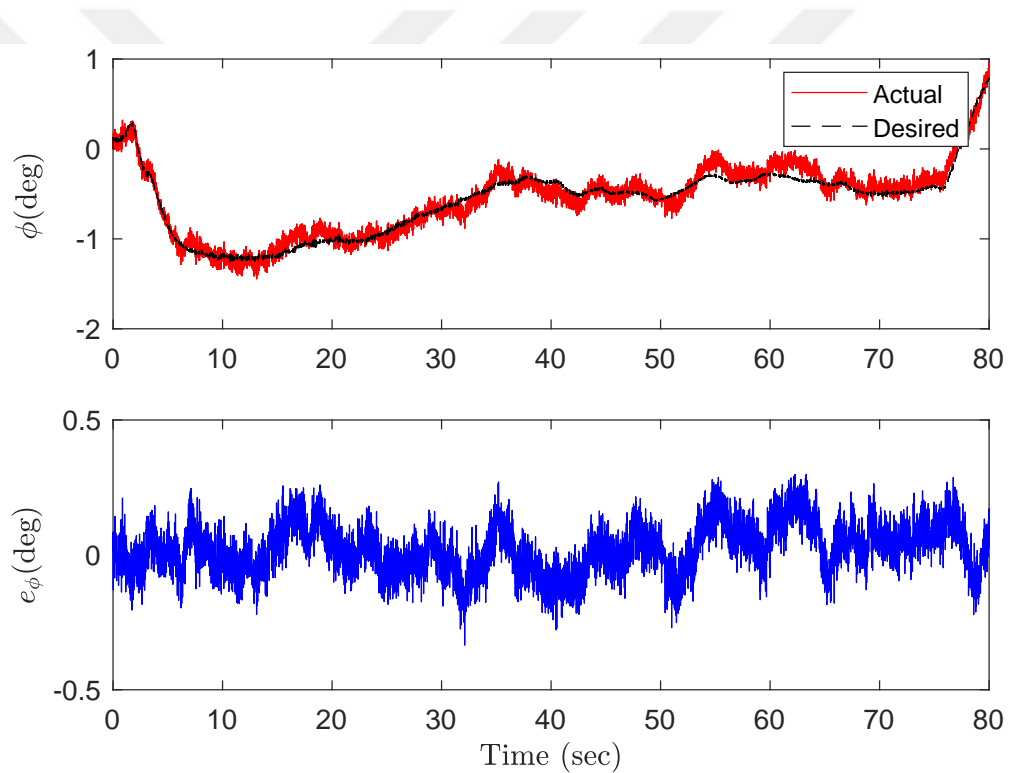


FIGURE 6.7: Roll angle ( $\phi$ ) (top), tracking error (bottom) vs Time

Based on the tracking performances in Table 6.2, the attitude tracking of the quadrotor is quite accurate and precise with RMSE in the range of  $0.051^\circ$ – $0.144^\circ$ . For the manipulator end-effector, RMSE values are in the range of  $0.158^\circ$ – $0.467^\circ$ .

Worst-case attitude errors are  $0.461^\circ$  and  $1.579^\circ$  for the quadrotor and the manipulator, respectively. It is clear that the inner loop controller is quite robust in achieving the desired performance.

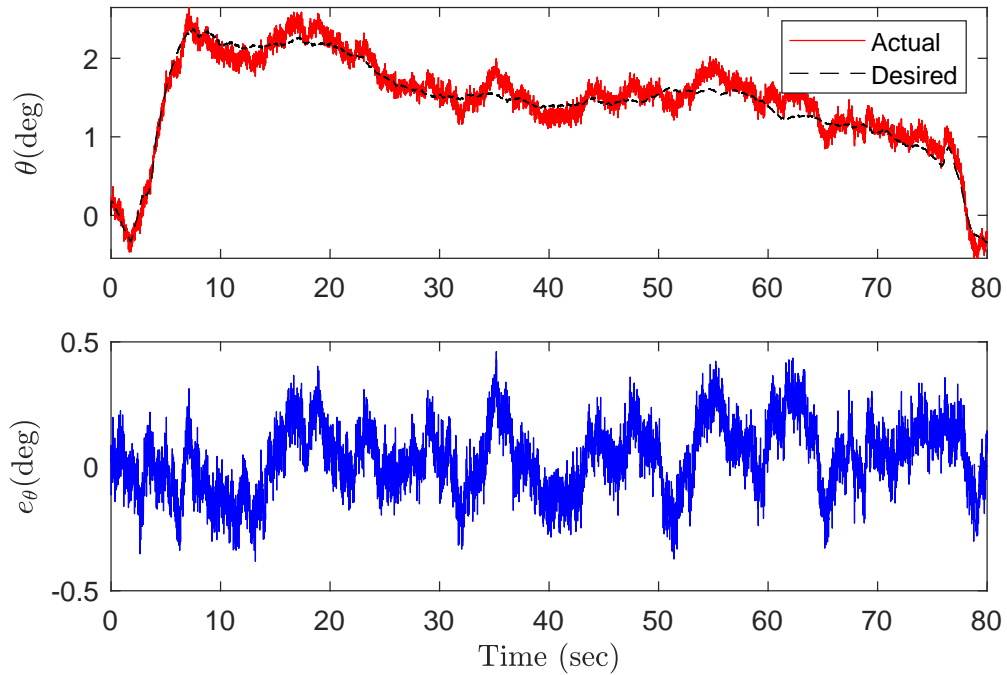


FIGURE 6.8: Pitch angle ( $\theta$ ) (top), tracking error (bottom) vs Time

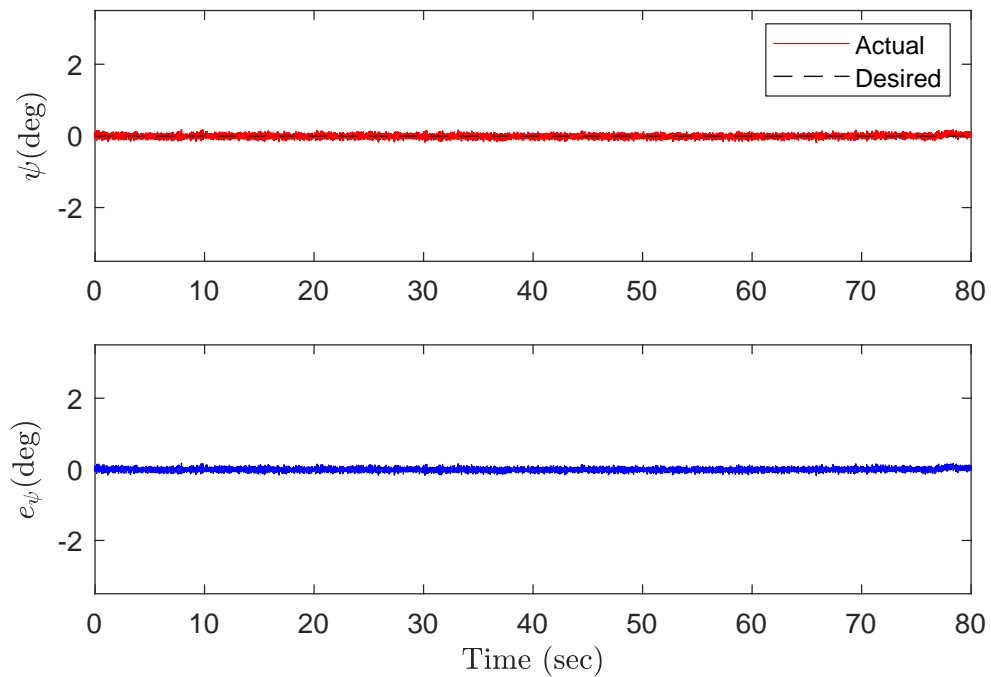


FIGURE 6.9: Yaw angle ( $\psi$ ) (top), tracking error (bottom) vs Time

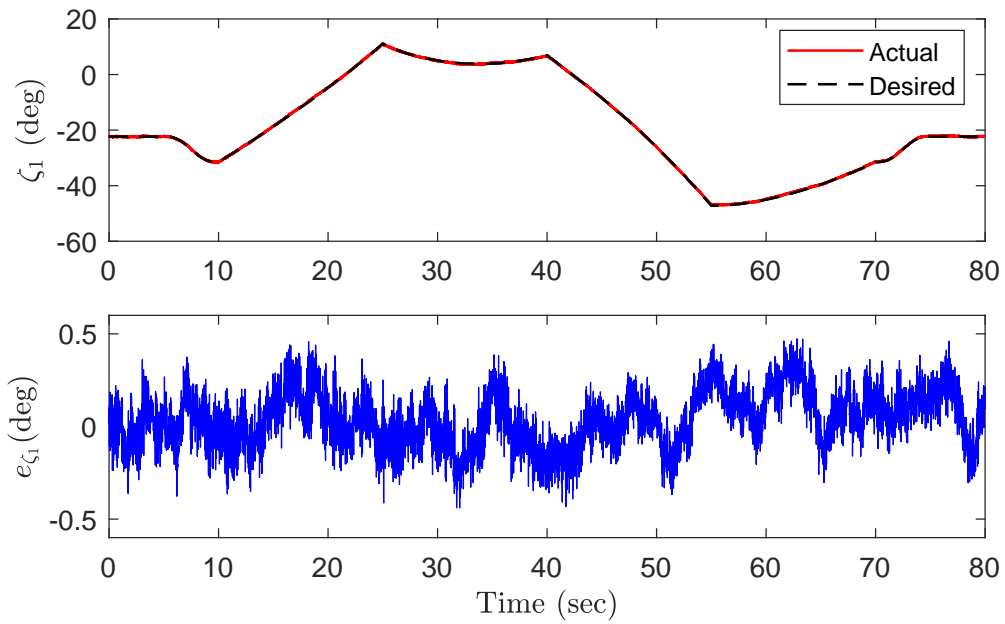


FIGURE 6.10:  $\zeta_1$  tracking of the arm (top), tracking error (bottom) vs Time

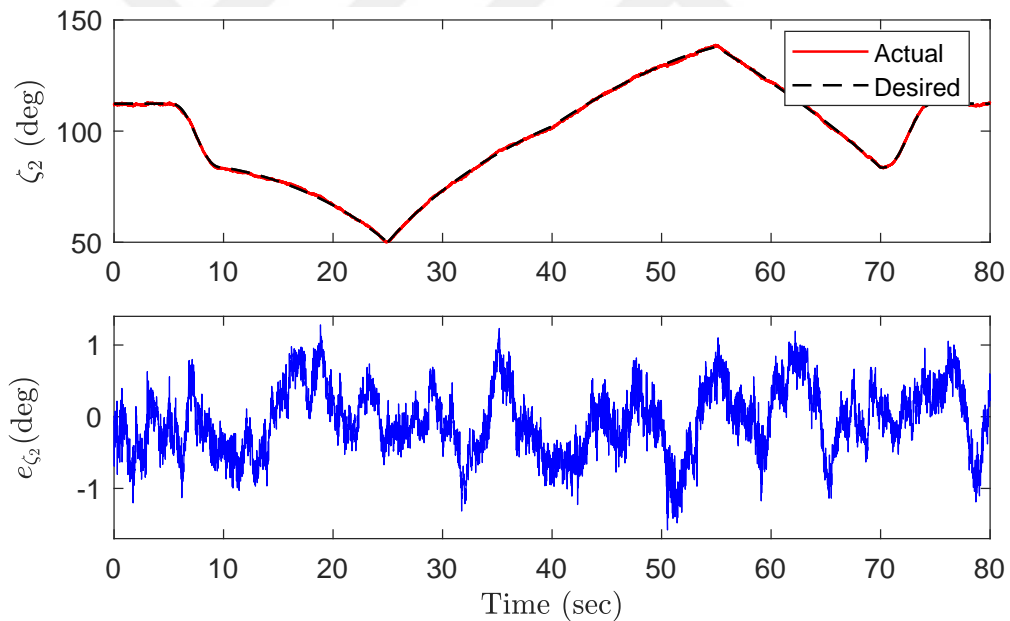


FIGURE 6.11:  $\zeta_2$  tracking of the arm (top), tracking error (bottom) vs Time

Control inputs of the AMS are shown in Fig. 6.12. As time flows, the 20% uncertainty in the mass of the system is estimated, and then U1 converges to the actual system weight of 27 N. Additionally, the wind disturbances cause chattering on the control input signals. However, the magnitude of the control efforts are not significantly high thus not burdening the actuators.

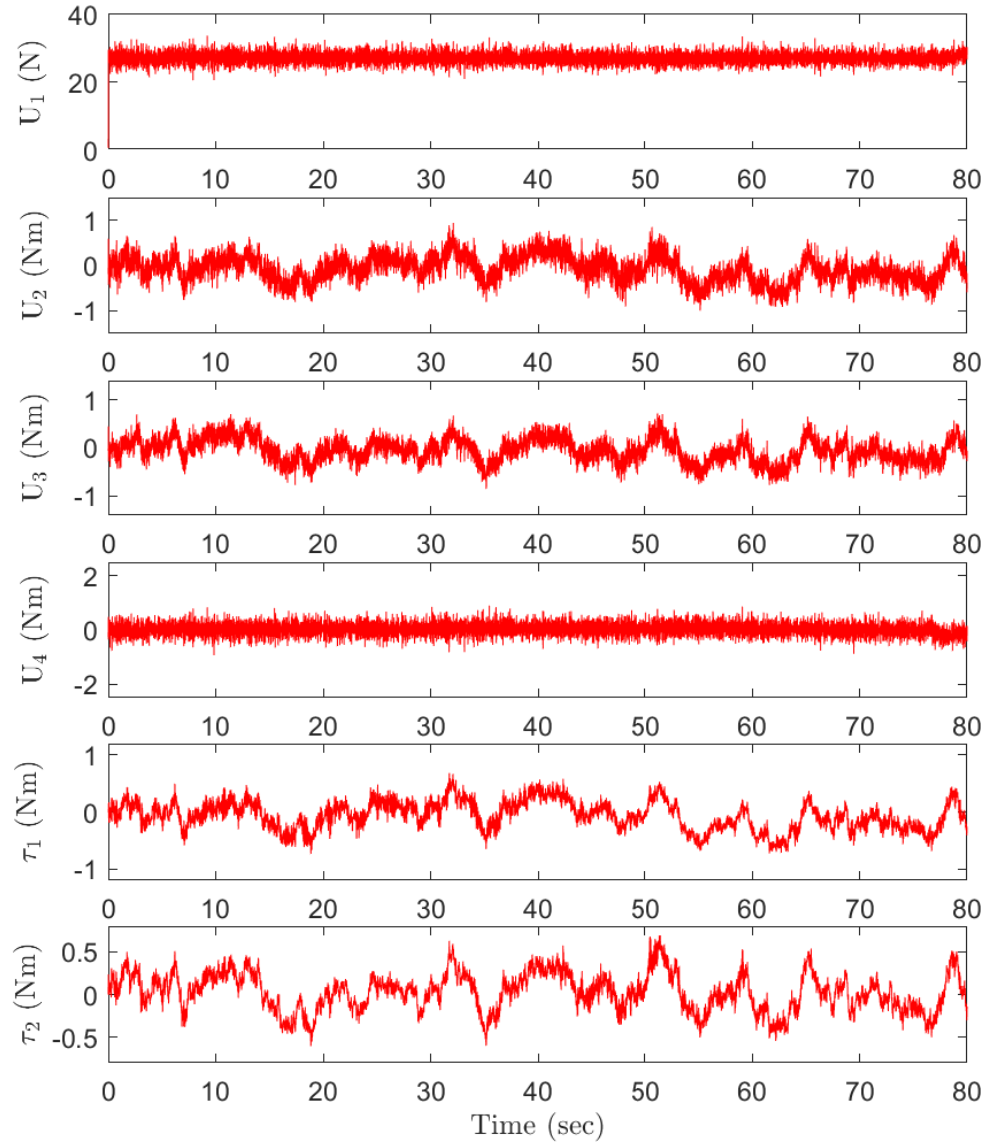


FIGURE 6.12: Control inputs

TABLE 6.2: Tracking errors of the AMS for the task of rectangle drawing

Criterion	RMS Errors	Max Errors	Criterion	RMS Errors	Max Errors
$e_X(m)$	0.001	0.003	$e_\phi(deg)$	0.096	0.335
$e_Y(m)$	0.002	0.003	$e_\theta(deg)$	0.144	0.461
$e_Z(m)$	0.030	0.124	$e_\psi(deg)$	0.051	0.180
$e_{X_e}(m)$	0.001	0.003	$e_{\zeta_1}(deg)$	0.158	0.473
$e_{Y_e}(m)$	0.001	0.005	$e_{\zeta_2}(deg)$	0.467	1.579
$e_{Z_e}(m)$	0.030	0.126			

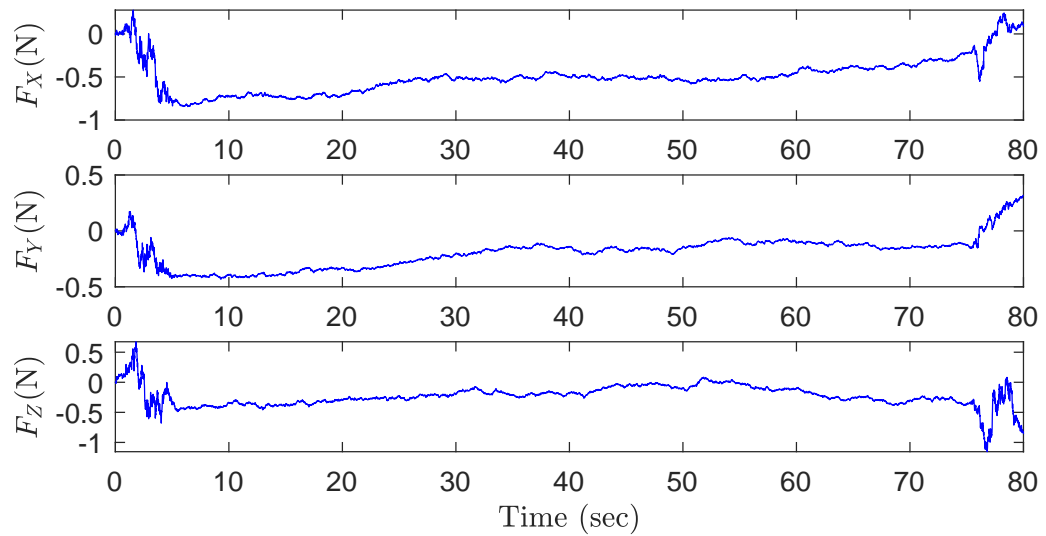


FIGURE 6.13: Wind forces during the rectangle drawing task of the arm

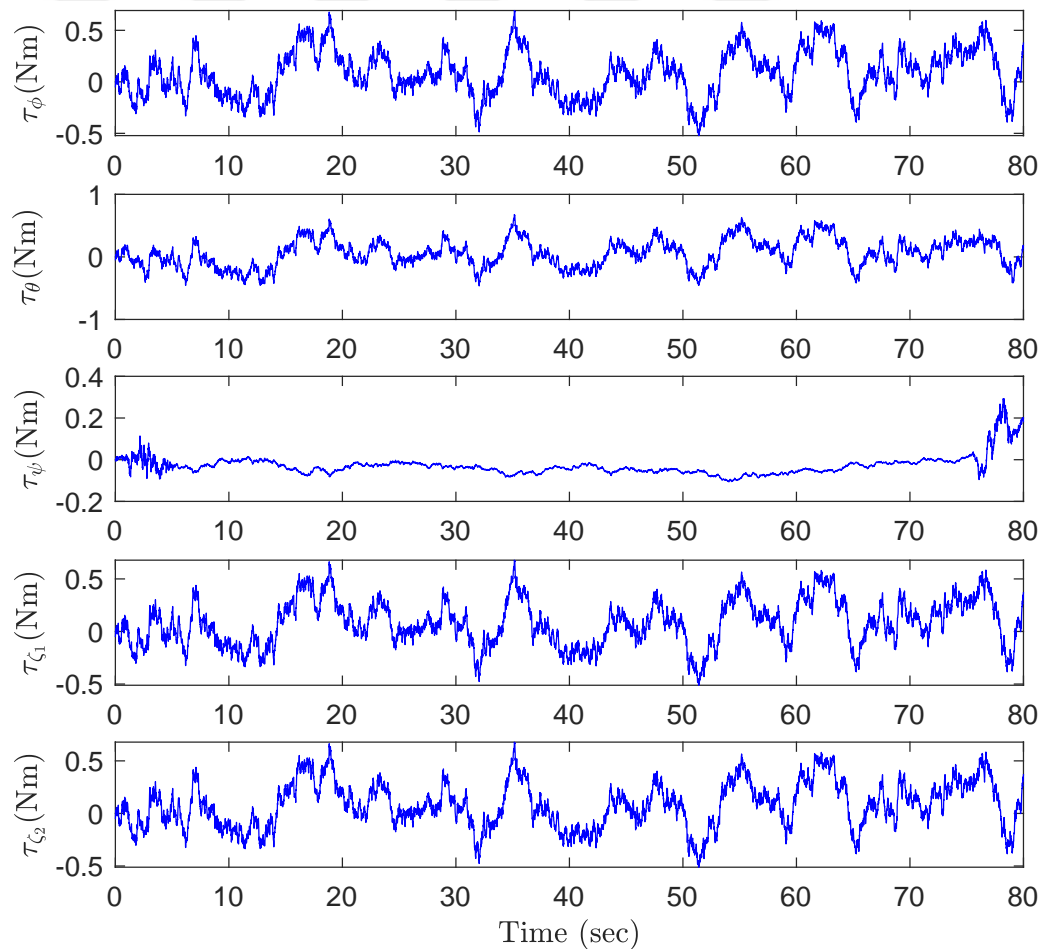


FIGURE 6.14: Wind moments during the rectangle drawing task of the arm

### 6.1.2 Drawing a Circular Shape

In this scenario, the quadrotor hovers at a certain altitude, then the end-effector of the manipulator draws a circle. Fig. 6.15 visualizes the flight scenario which was constructed in MATLAB Virtual Reality (VR) environment.

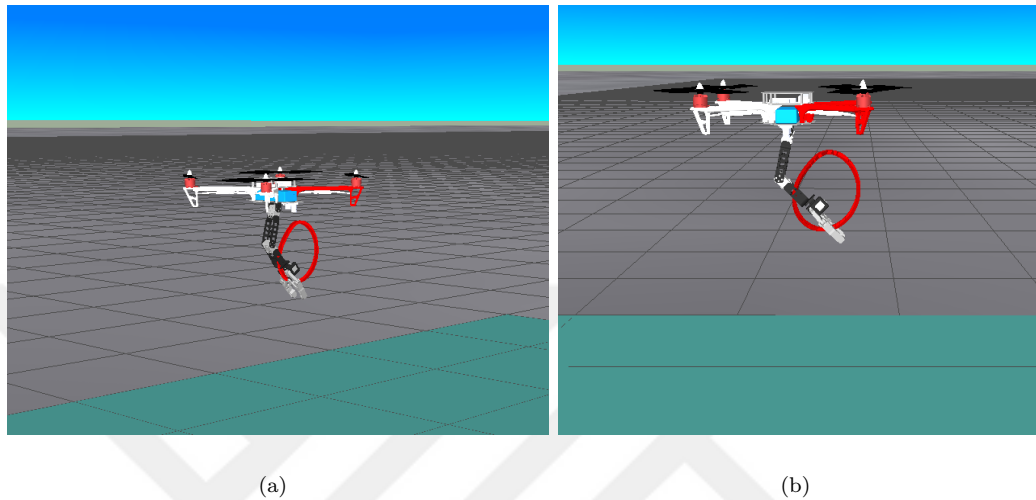


FIGURE 6.15: The flight mode visualization from different views

The trajectory of the end-effector of the manipulator for this scenario is shown in Fig. 6.16. Cartesian position plots for the quadrotor have been depicted in Figs. 6.17–6.19, where the quadrotor shows a stable hovering at the desired altitude under wind disturbances varying from  $-3\text{N}$  to  $1\text{N}$ .

According to the tracking errors given in Table 6.3, the position tracking of the quadrotor has RMSE values in the range of  $0.001\text{m}$  to  $0.034\text{m}$ . As before, the difference between tracking performances of the quadrotor and the manipulator end-effector is not significant. Worst-case position errors are around  $0.1\text{m}$  for both the quadrotor and the manipulator.

Attitude angles of the quadrotor and the manipulator joint angles have been depicted in Figs. 6.20–6.24, where both the quadrotor and the manipulator follow their desired trajectories smoothly under wind disturbances varying from  $-0.5\text{Nm}$  to  $1\text{Nm}$ .

Note that the wind profiles applied for this scenario are shown in Figs 6.26-6.27.

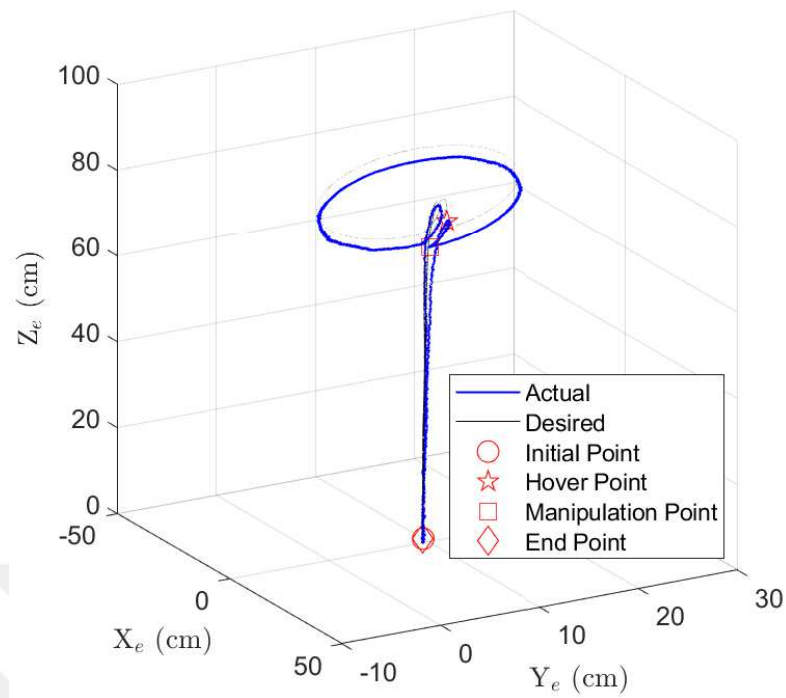


FIGURE 6.16: Trajectory of the end-effector

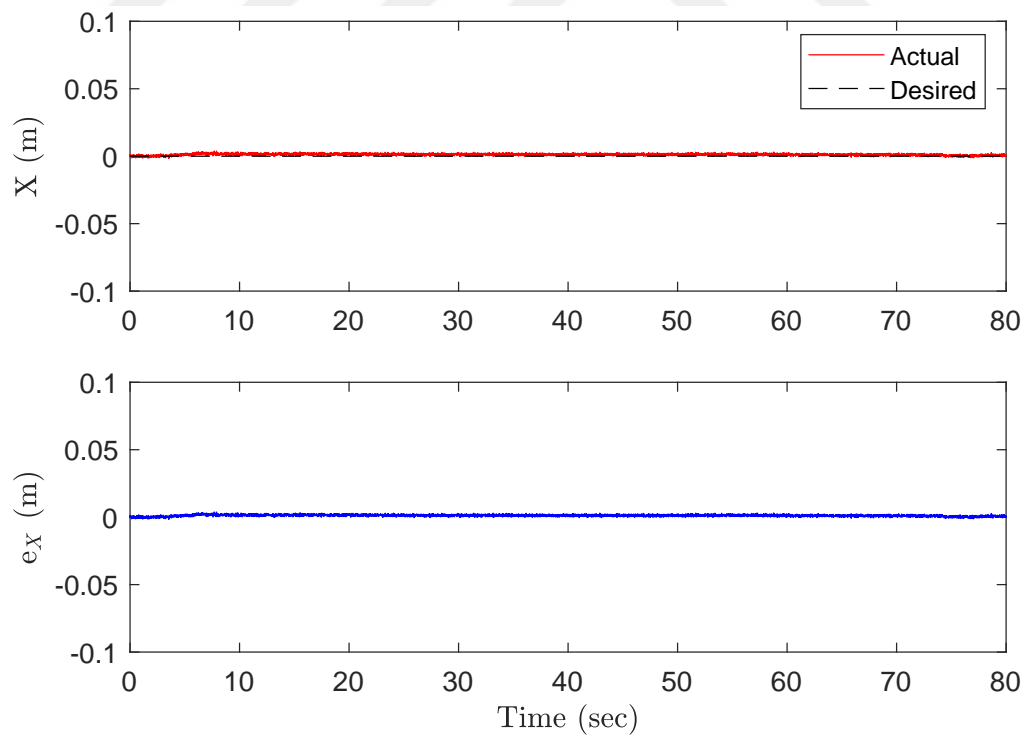


FIGURE 6.17: X position of the quadrotor (top), position error (bottom) vs Time



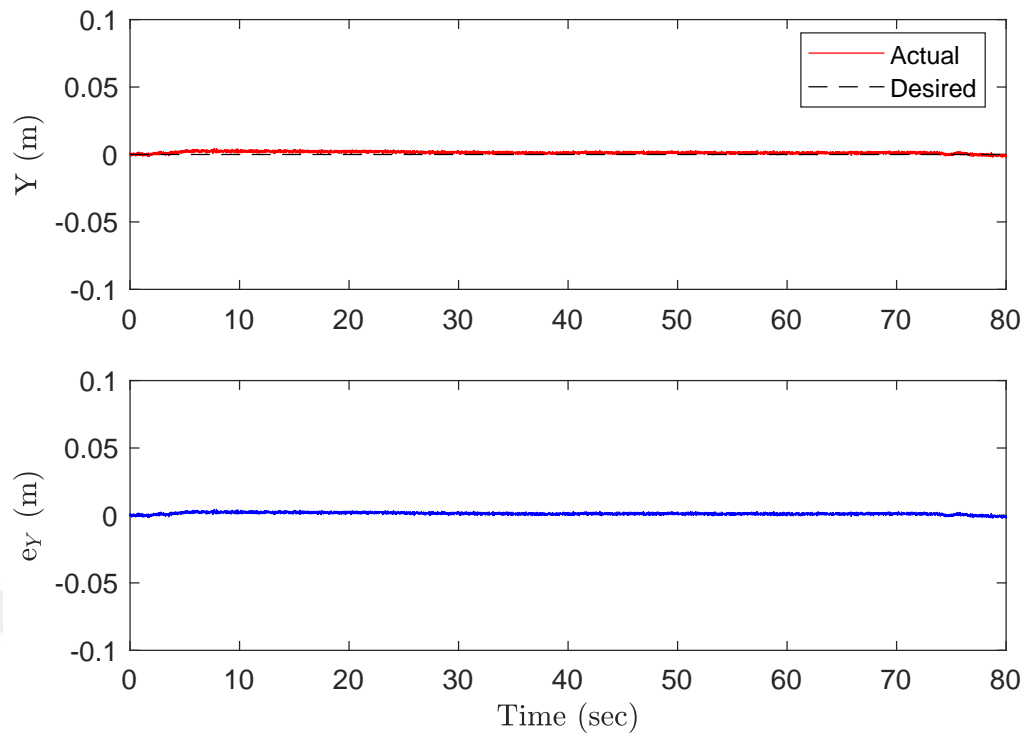


FIGURE 6.18: Y position of the quadrotor (top), position error (bottom) vs Time

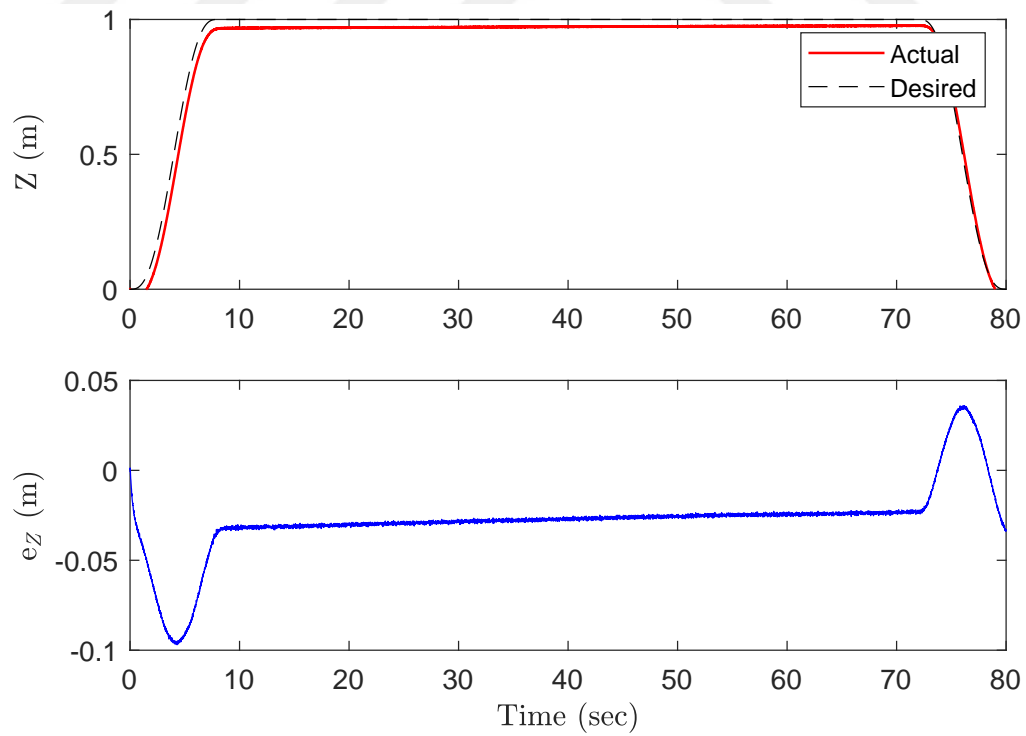
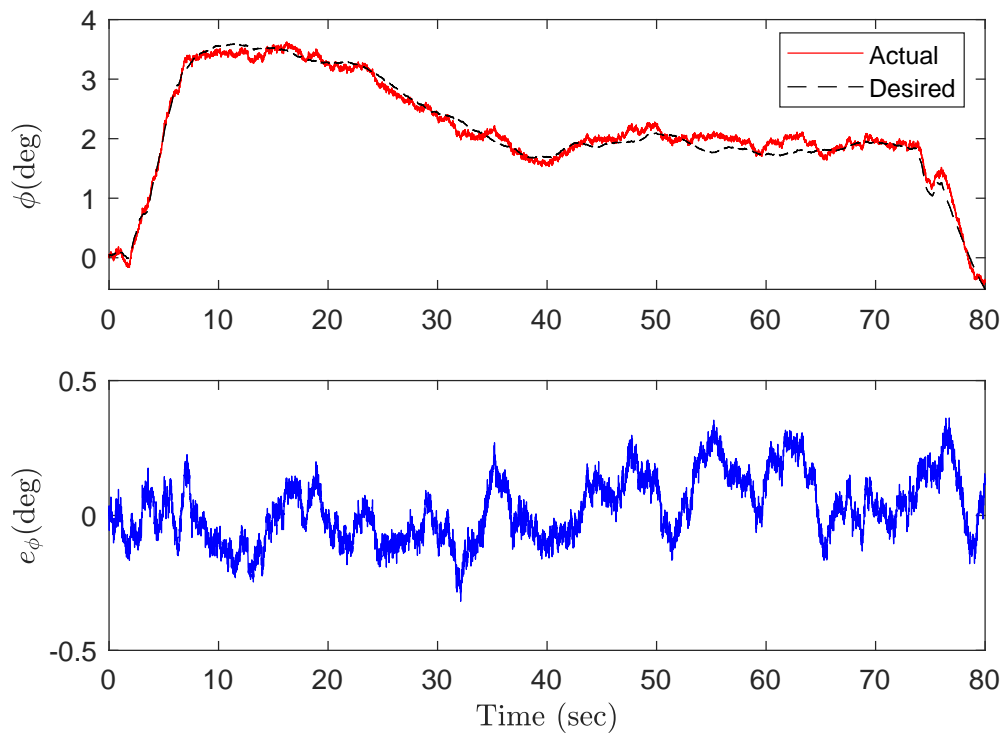
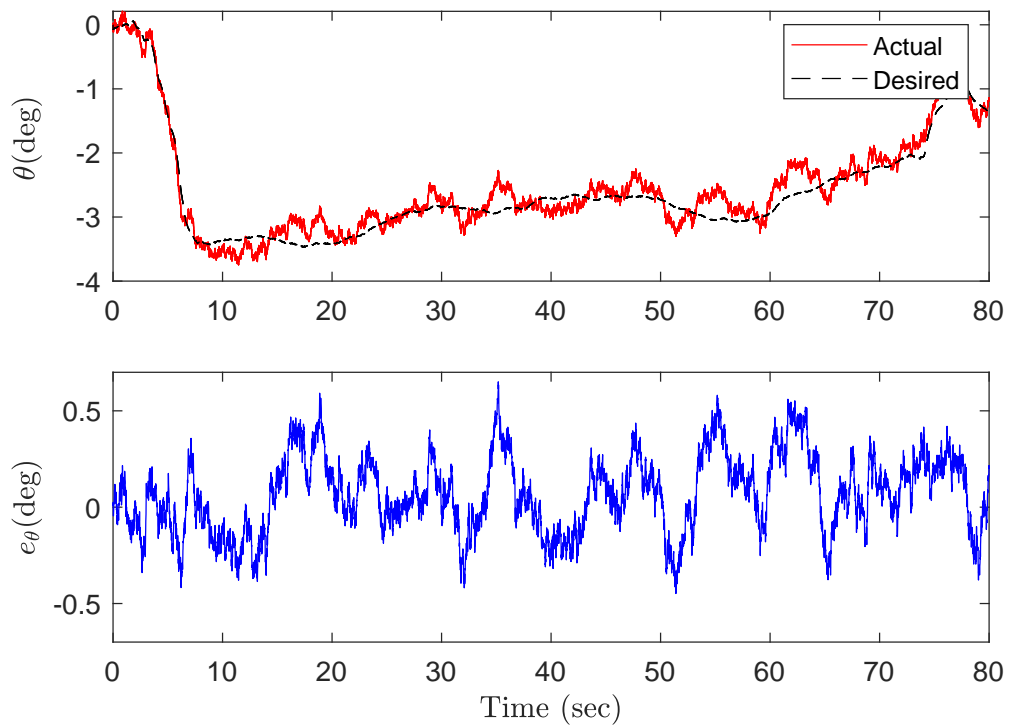
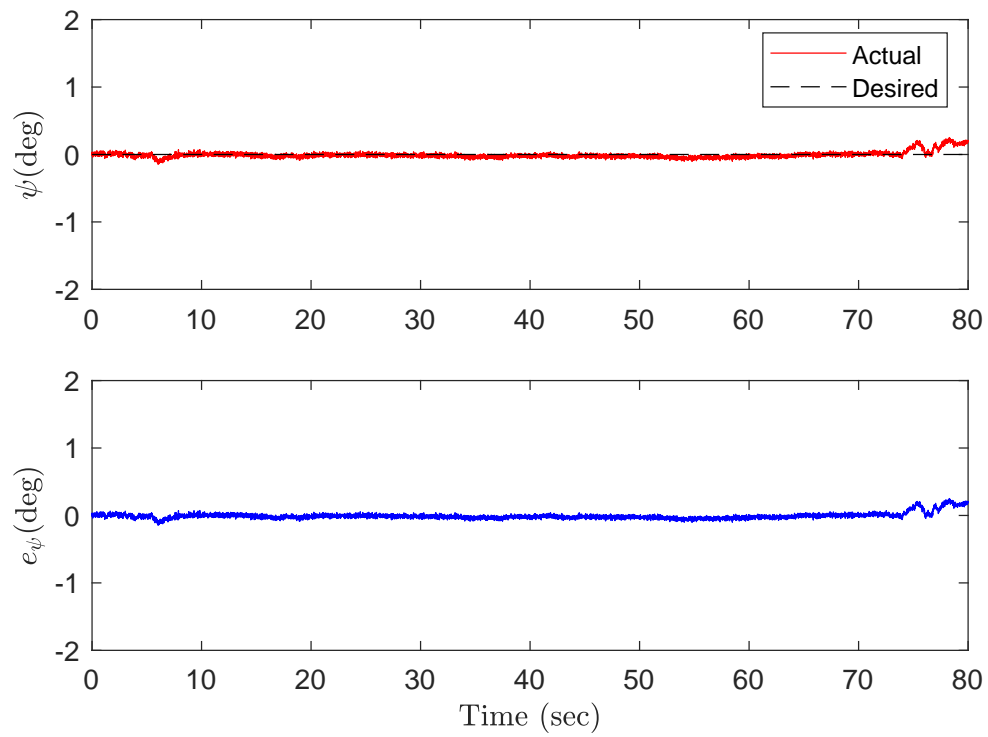
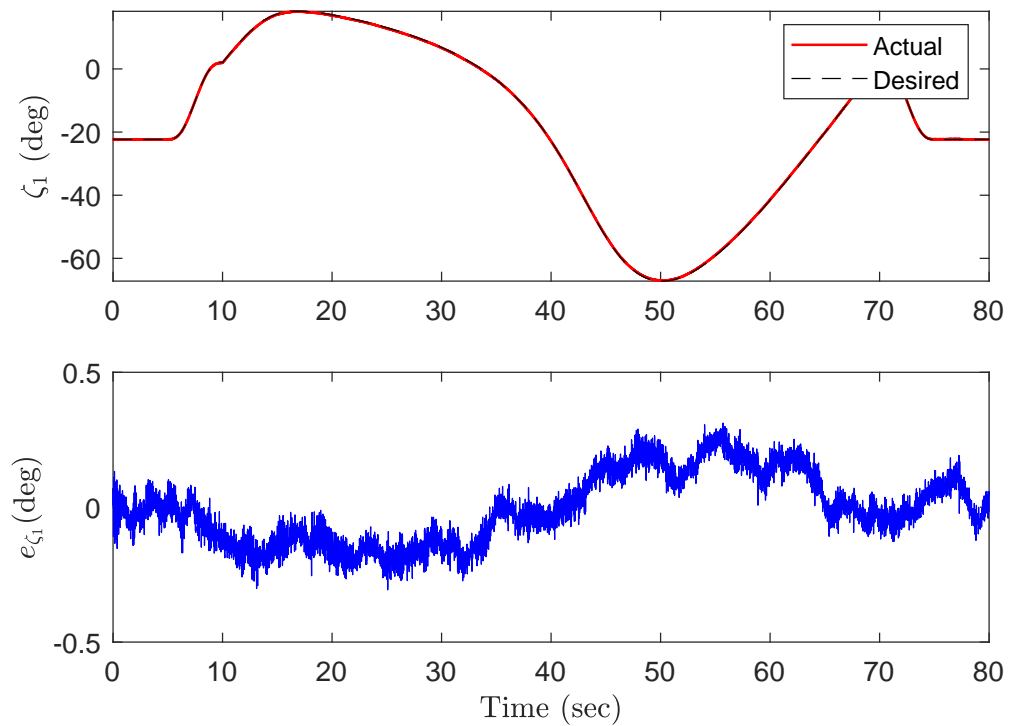


FIGURE 6.19: Z position of the quadrotor (top), position error (bottom) vs Time

FIGURE 6.20: Roll angle ( $\phi$ ) (top), tracking error (bottom) vs TimeFIGURE 6.21: Pitch angle ( $\theta$ ) (top), tracking error (bottom) vs Time

FIGURE 6.22: Yaw angle ( $\psi$ ) (top), tracking error (bottom) vs TimeFIGURE 6.23:  $\zeta_1$  tracking of the arm (top), tracking error (bottom) vs Time

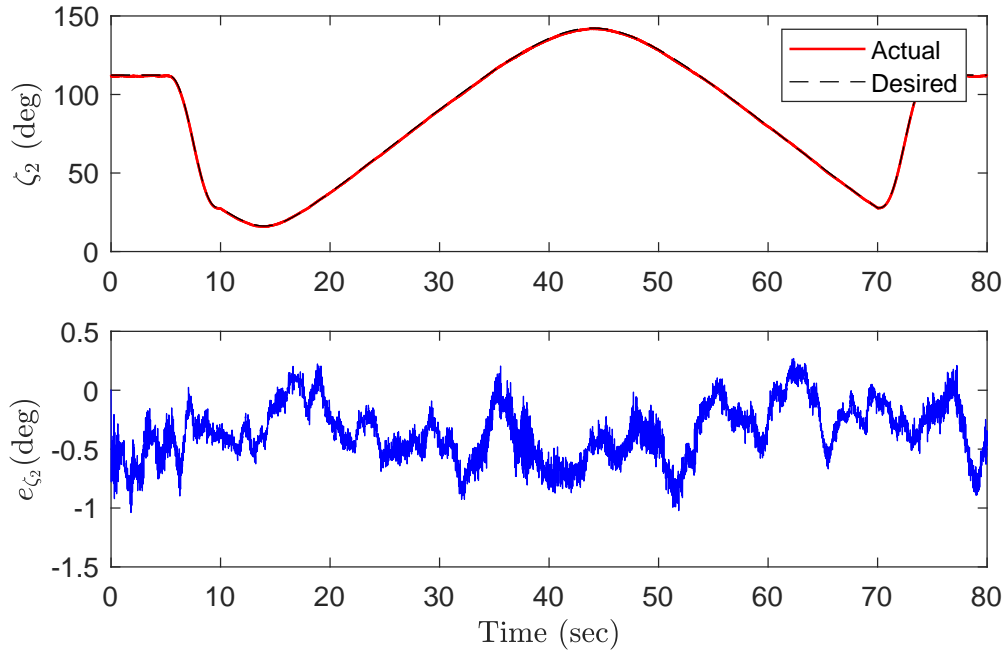


FIGURE 6.24:  $\zeta_2$  tracking of the arm (top), tracking error (bottom) vs Time

Based on the tracking errors in Table 6.3, the attitude tracking of the quadrotor is very accurate and precise with RMSE in the range of  $0.049^\circ$ - $0.210^\circ$ . For the manipulator end-effector, RMSE values are in the range of  $0.131^\circ$ - $0.427^\circ$ . Worst-case attitude errors are  $0.651^\circ$  and  $1.038^\circ$  for the quadrotor and the manipulator, respectively. It is clear that the inner loop nonlinear adaptive controller is quite successful in following the desired trajectory.

TABLE 6.3: Tracking errors of the AMS for the task of circle drawing

<b>Criterion</b>	<b>RMS</b>	<b>Max</b>	<b>Criterion</b>	<b>RMS</b>	<b>Max</b>
	<b>Errors</b>	<b>Errors</b>		<b>Errors</b>	<b>Errors</b>
$e_X(m)$	0.001	0.004	$e_\phi(deg)$	0.122	0.361
$e_Y(m)$	0.002	0.005	$e_\theta(deg)$	0.210	0.651
$e_Z(m)$	0.034	0.097	$e_\psi(deg)$	0.049	0.251
$e_{Xe}(m)$	0.001	0.004	$e_{\zeta_1}(deg)$	0.131	0.312
$e_{Ye}(m)$	0.002	0.005	$e_{\zeta_2}(deg)$	0.427	1.038
$e_{Ze}(m)$	0.035	0.099			

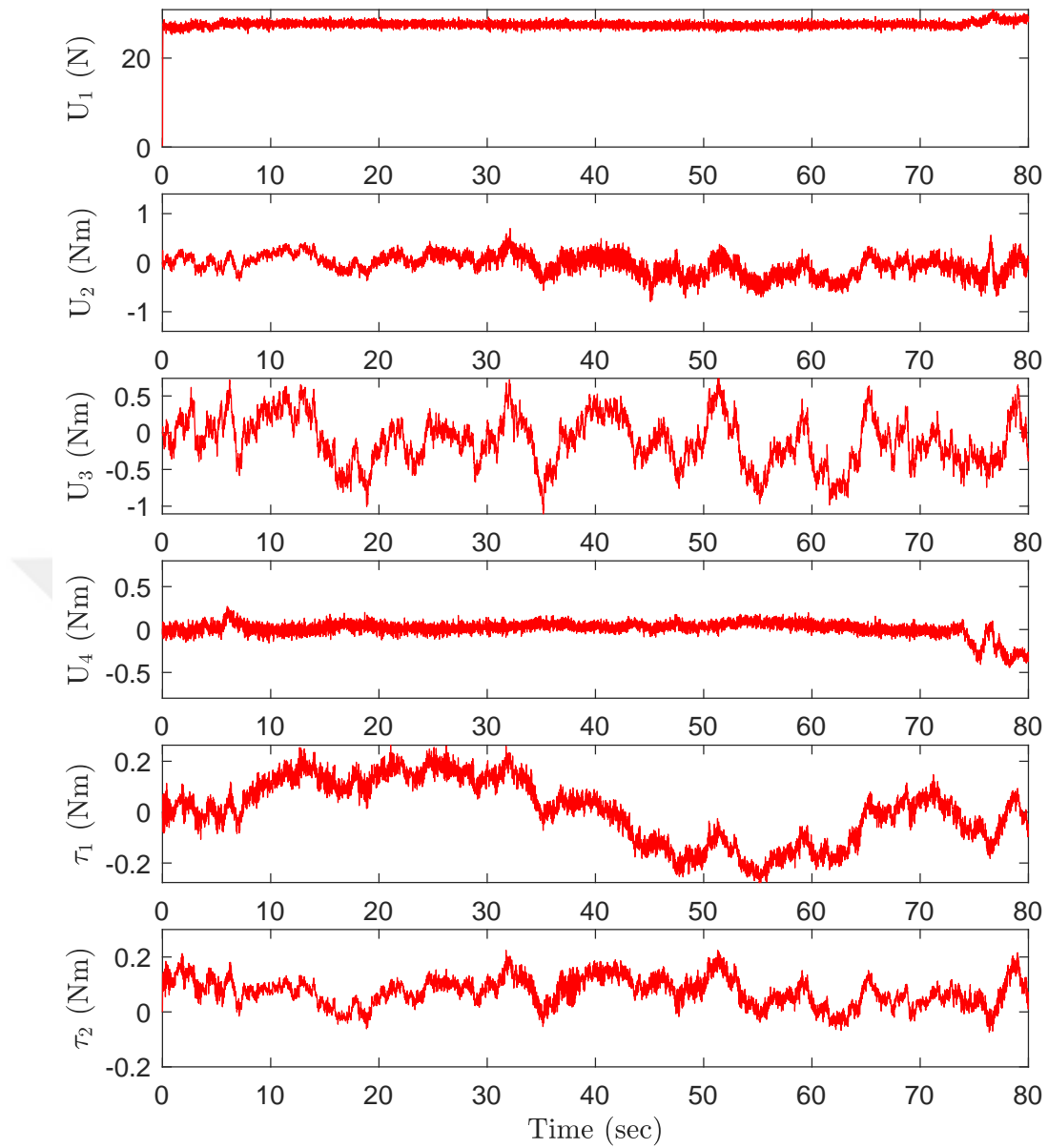


FIGURE 6.25: Control inputs

Required control efforts to complete the operation have been provided in Fig. 6.25. In this figure, the thrust force  $U_1$  converges to 27 N during the flight. This indicates that the 20% uncertainty in the mass of the system is estimated and it converged to the actual system weight. Additionally, the magnitudes of the desired control efforts are found reasonable.

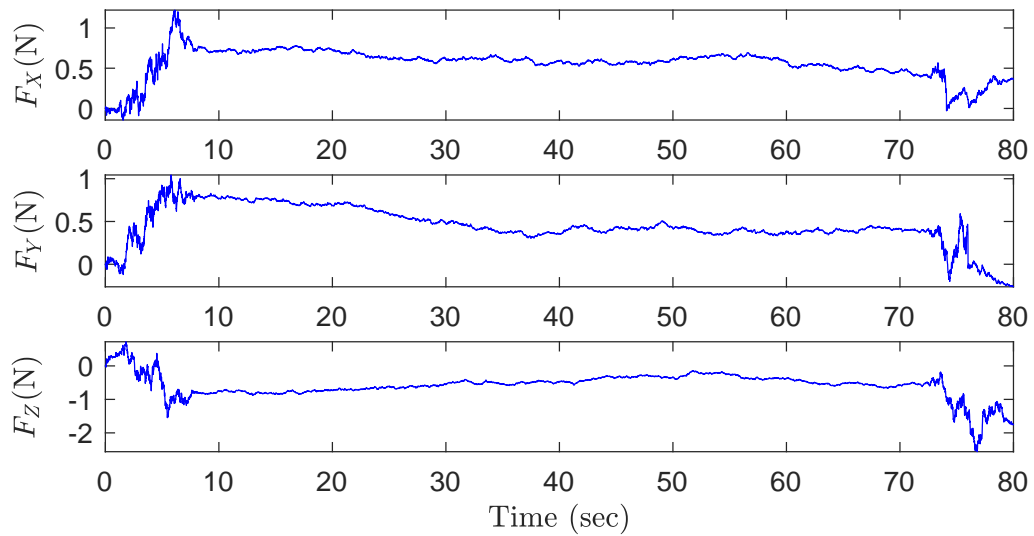


FIGURE 6.26: Wind forces during the circle drawing task of the arm

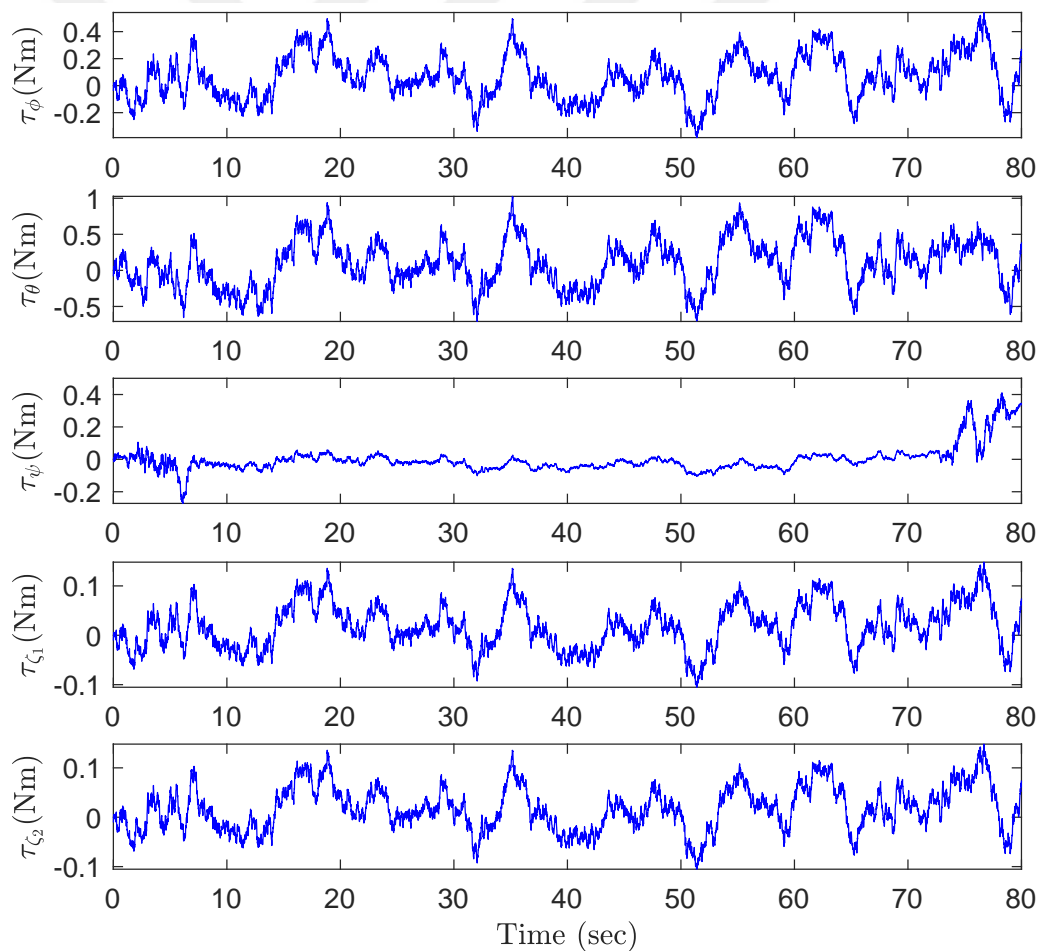


FIGURE 6.27: Wind moments during the circle drawing task of the arm

## 6.2 Motion of the Quadrotor with the Robotic Arm in a Fixed Position

Another free motion scenario of the AMS is that the joint angles of the manipulator are fixed and the quadrotor follows a circular path in  $YZ$  plane after reaching a certain altitude. The flight scenario was visualized in MATLAB Virtual Reality (VR) platform shown in Fig. 6.28.

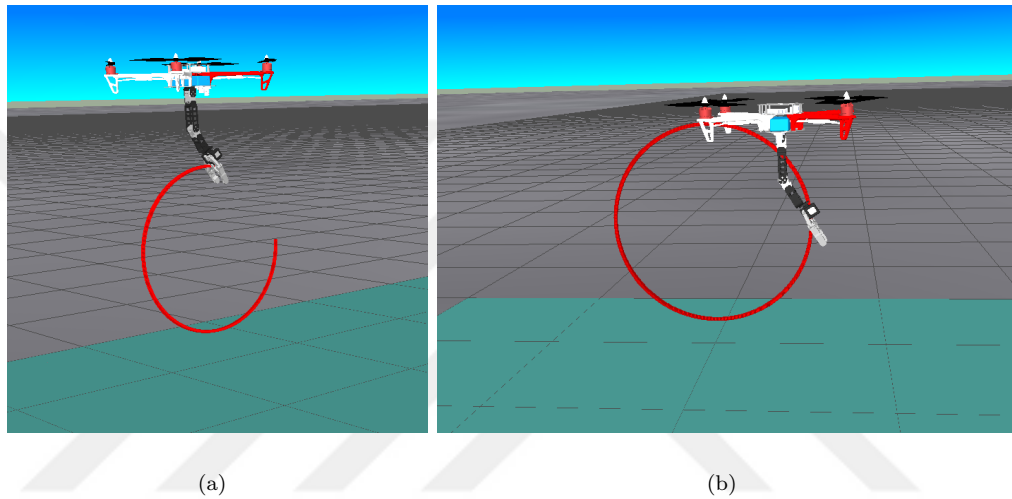


FIGURE 6.28: The flight mode visualization from different views

Cartesian position plots in Figs. 6.29–6.31 introduce that the quadrotor follows the desired trajectory smoothly under external disturbances varying from  $-1N$  to  $2N$ . According to the tracking errors given in Table 6.4, the position tracking error of the quadrotor has RMSE values in the range of  $0.002m$  to  $0.023m$ . As before, the difference between tracking performances of the quadrotor and the manipulator end-effector is not significant. Worst-case position errors are around  $0.1m$  for both the quadrotor and the manipulator.

Attitude angles of the quadrotor and manipulator joint angles have been depicted in Figs. 6.32–6.36, where both the quadrotor and the manipulator follow their desired trajectories smoothly under external disturbances varying from  $-1Nm$  to  $1Nm$ .

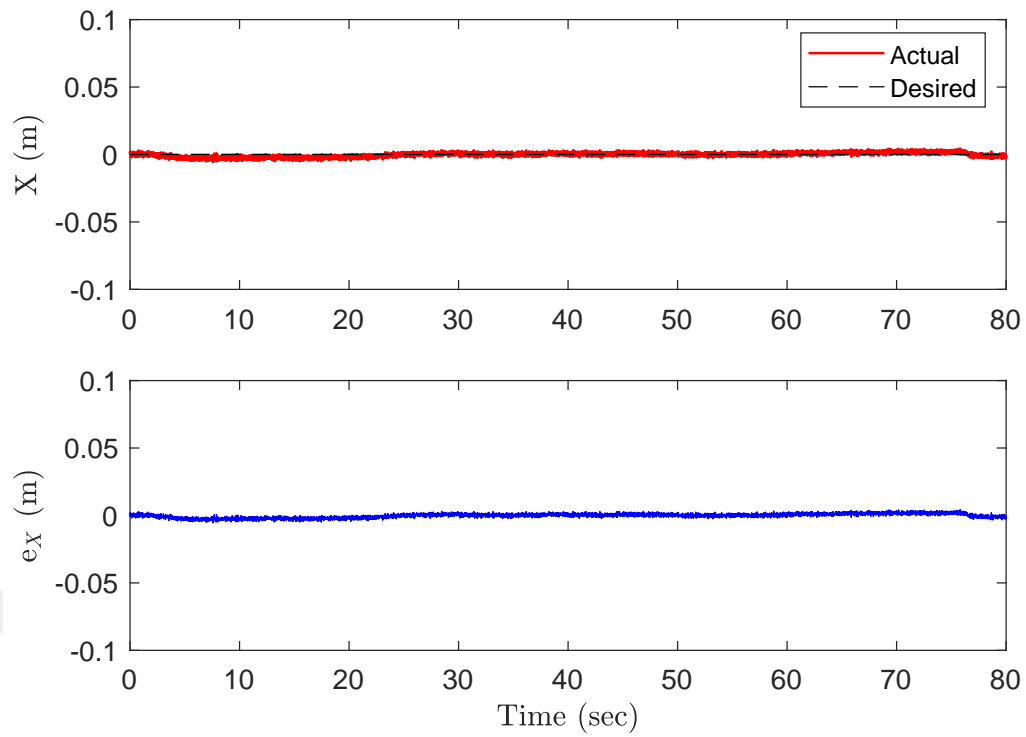


FIGURE 6.29: X position of the quadrotor (top), position error (bottom) vs Time

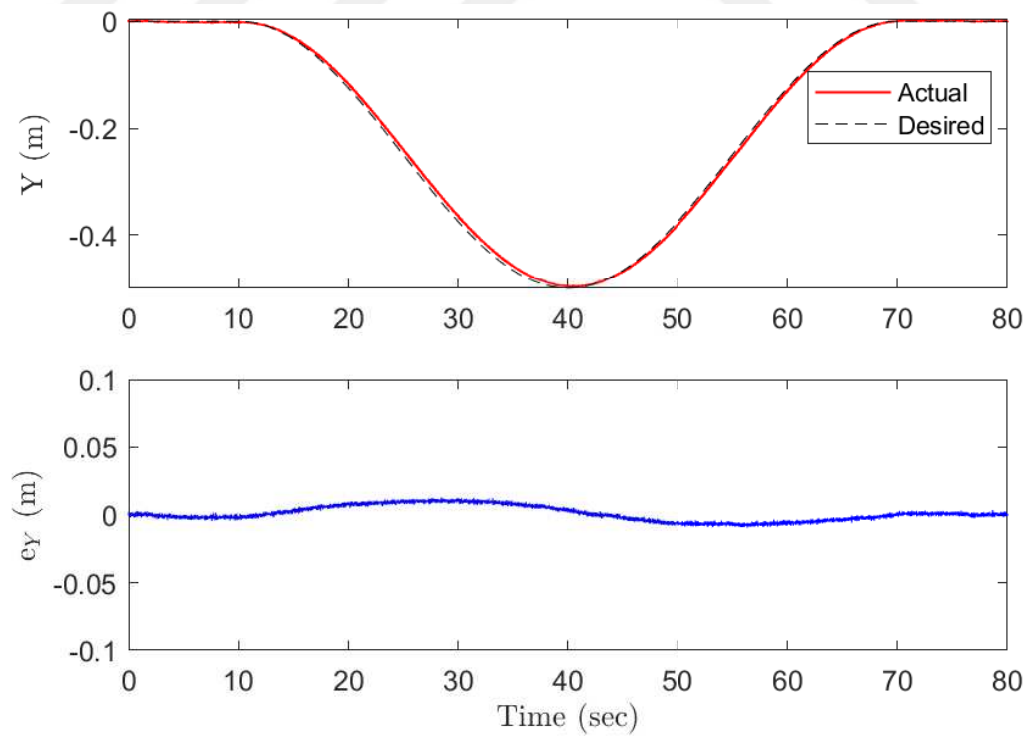


FIGURE 6.30: Y position of the quadrotor (top), position error (bottom) vs Time



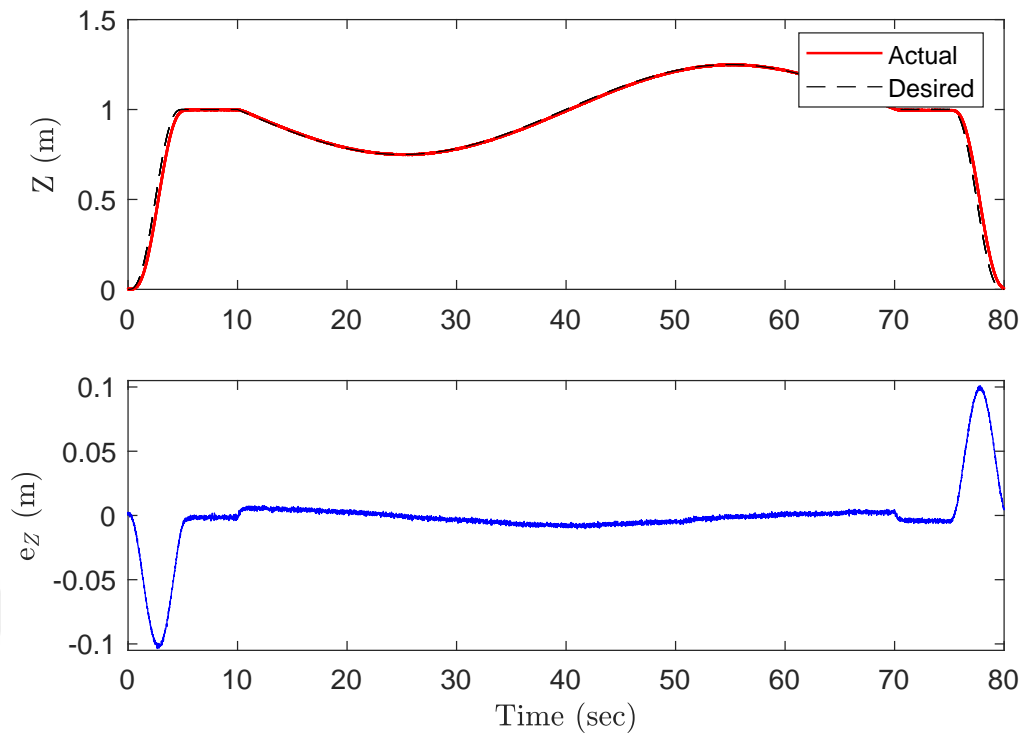


FIGURE 6.31: Z position of the quadrotor (top), position error (bottom) vs Time

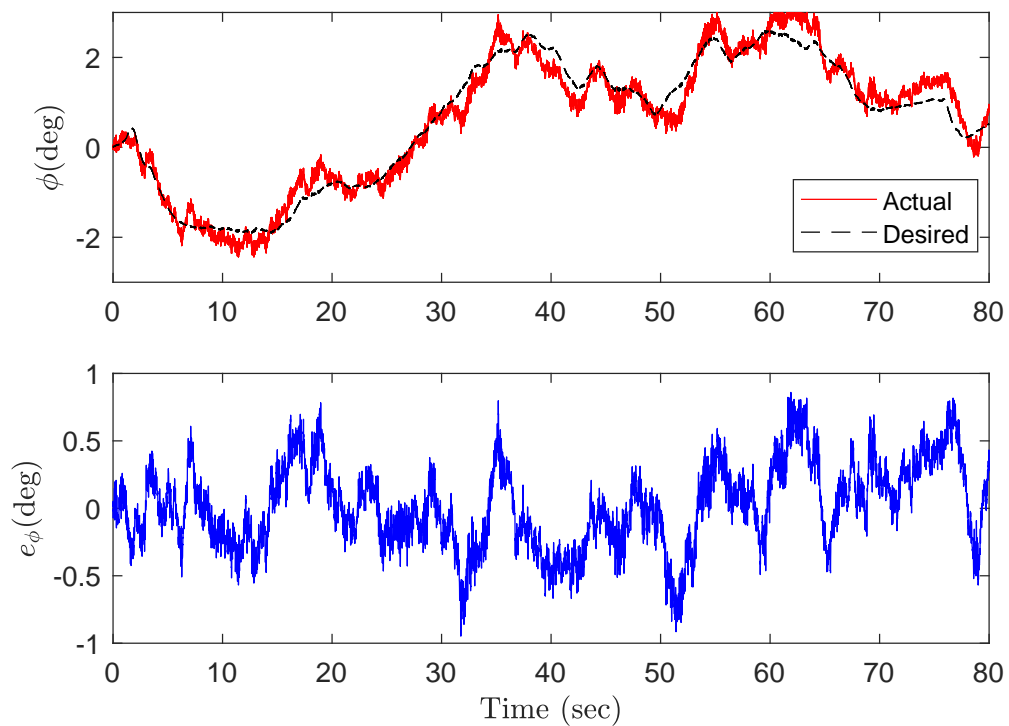
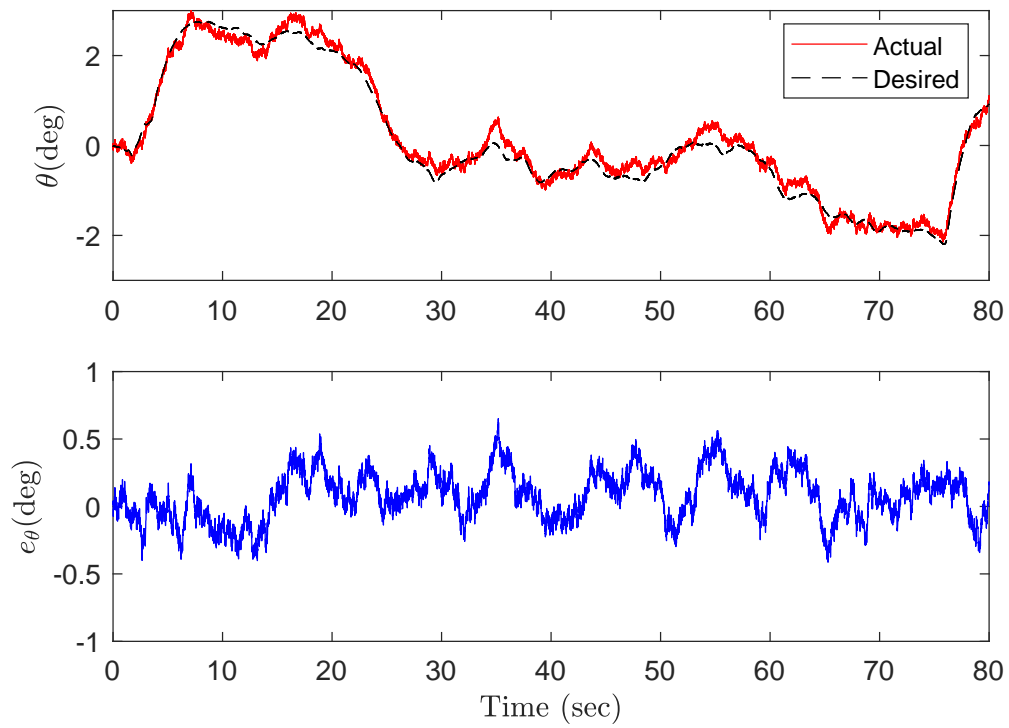
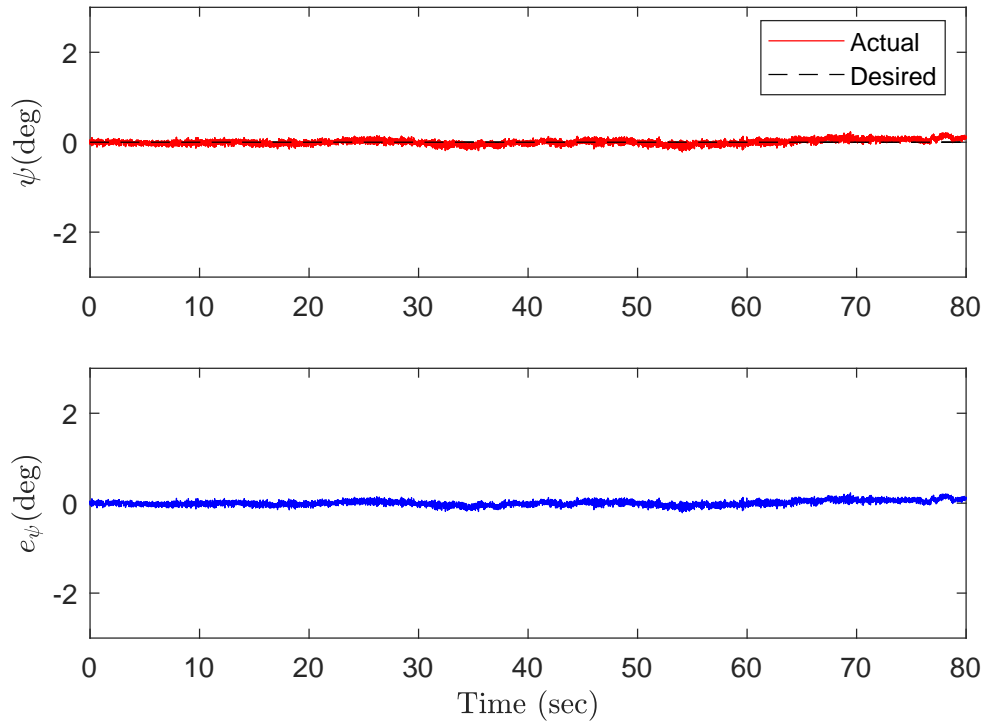
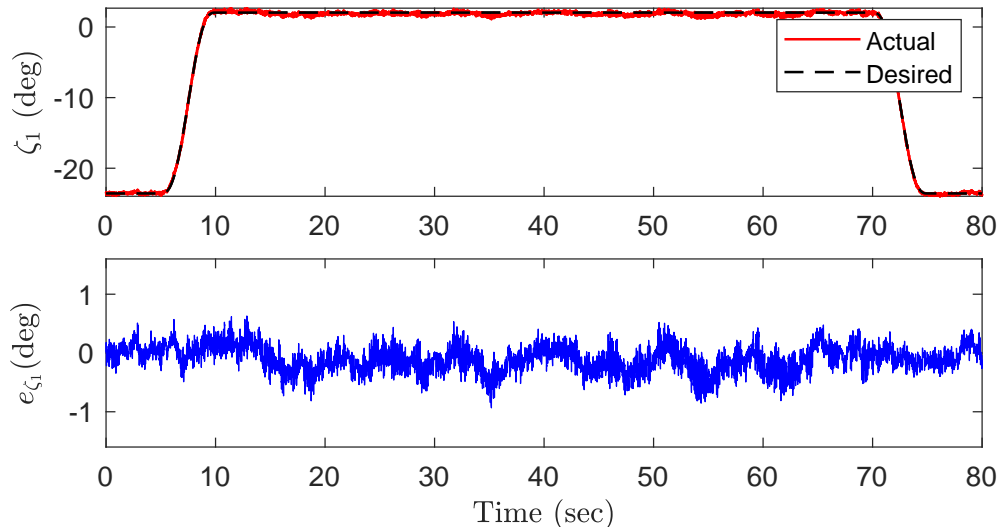
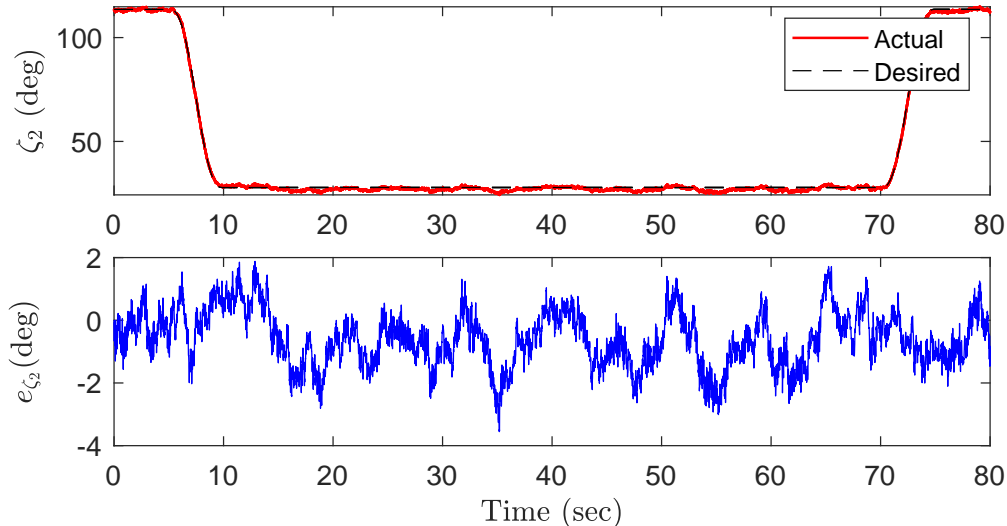


FIGURE 6.32: Roll angle ( $\phi$ ) (top), tracking error (bottom) vs Time

FIGURE 6.33: Pitch angle ( $\theta$ ) (top), tracking error (bottom) vs TimeFIGURE 6.34: Yaw angle ( $\psi$ ) (top), tracking error (bottom) vs Time

FIGURE 6.35:  $\zeta_1$  tracking of the arm (top), tracking error (bottom) vs TimeFIGURE 6.36:  $\zeta_2$  tracking of the arm (top), tracking error (bottom) vs Time

Based on tracking errors provided in Table 6.4, the attitude tracking of the quadrotor is very accurate with RMSE in the range of  $0.060^\circ$ - $0.311^\circ$ . For the manipulator end-effector, RMSE values are in the range of  $0.244^\circ$ - $1.059^\circ$ . The inner loop nonlinear adaptive controller successfully rejects the disturbances acting on the system. Worst-case attitude errors are  $0.948^\circ$  and  $3.554^\circ$  for the quadrotor and the manipulator, respectively.

Control inputs to make the AMS follow its desired trajectory have been provided in Fig. 6.37.

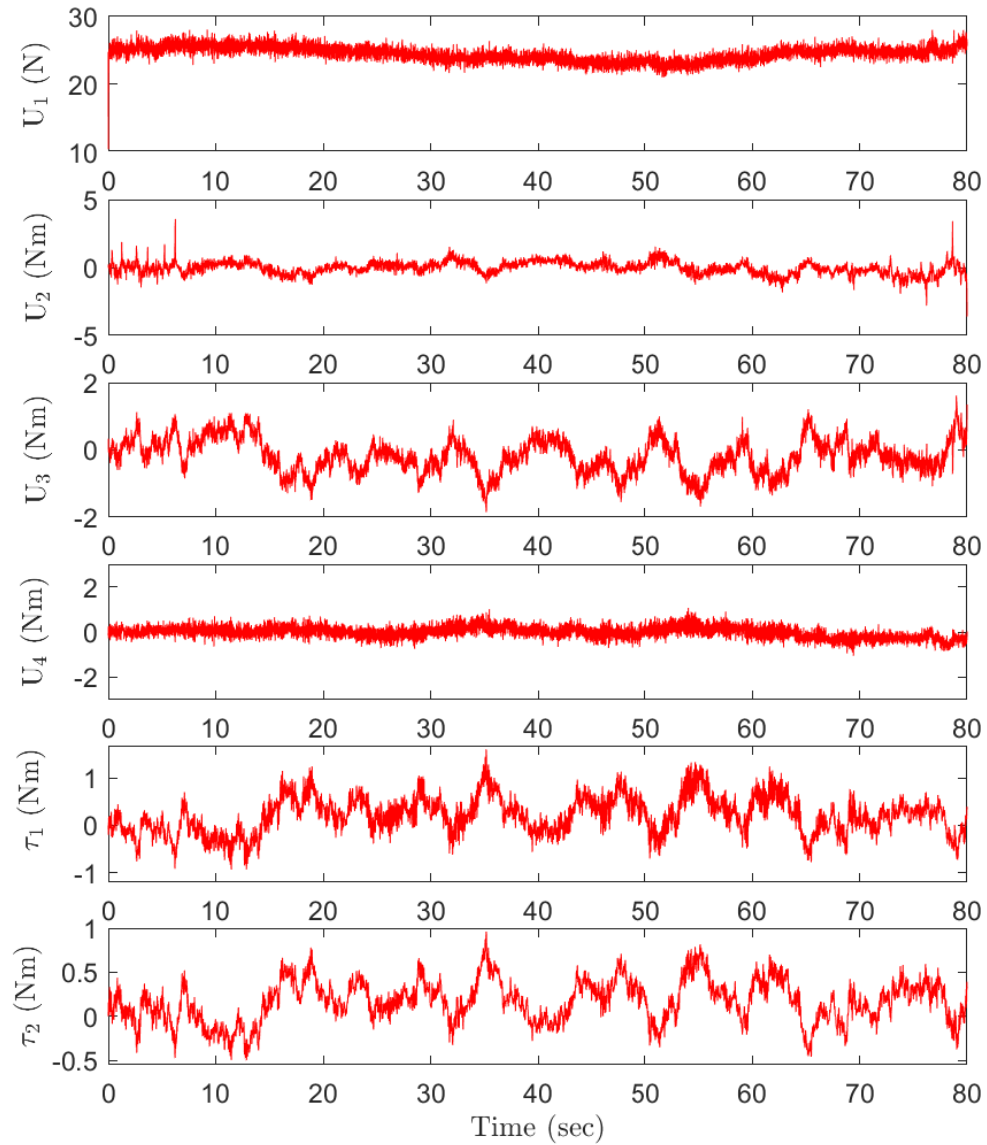


FIGURE 6.37: Control inputs

TABLE 6.4: Tracking errors of the AMS for the scenario

Criterion	RMS Errors	Max Errors	Criterion	RMS Errors	Max Errors
$e_X(m)$	0.002	0.006	$e_\phi(deg)$	0.311	0.948
$e_Y(m)$	0.006	0.013	$e_\theta(deg)$	0.197	0.651
$e_Z(m)$	0.023	0.104	$e_\psi(deg)$	0.060	0.230
$e_{X_e}(m)$	0.002	0.006	$e_{\zeta_1}(deg)$	0.244	0.933
$e_{Y_e}(m)$	0.006	0.016	$e_{\zeta_2}(deg)$	1.059	3.554
$e_{Z_e}(m)$	0.023	0.103			

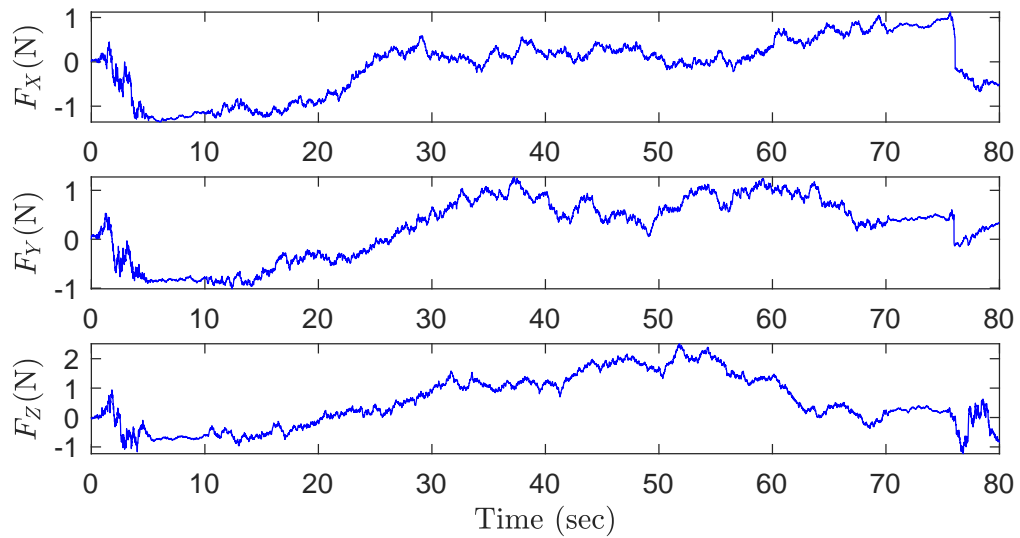


FIGURE 6.38: Wind forces during the circle drawing task of the quadrotor

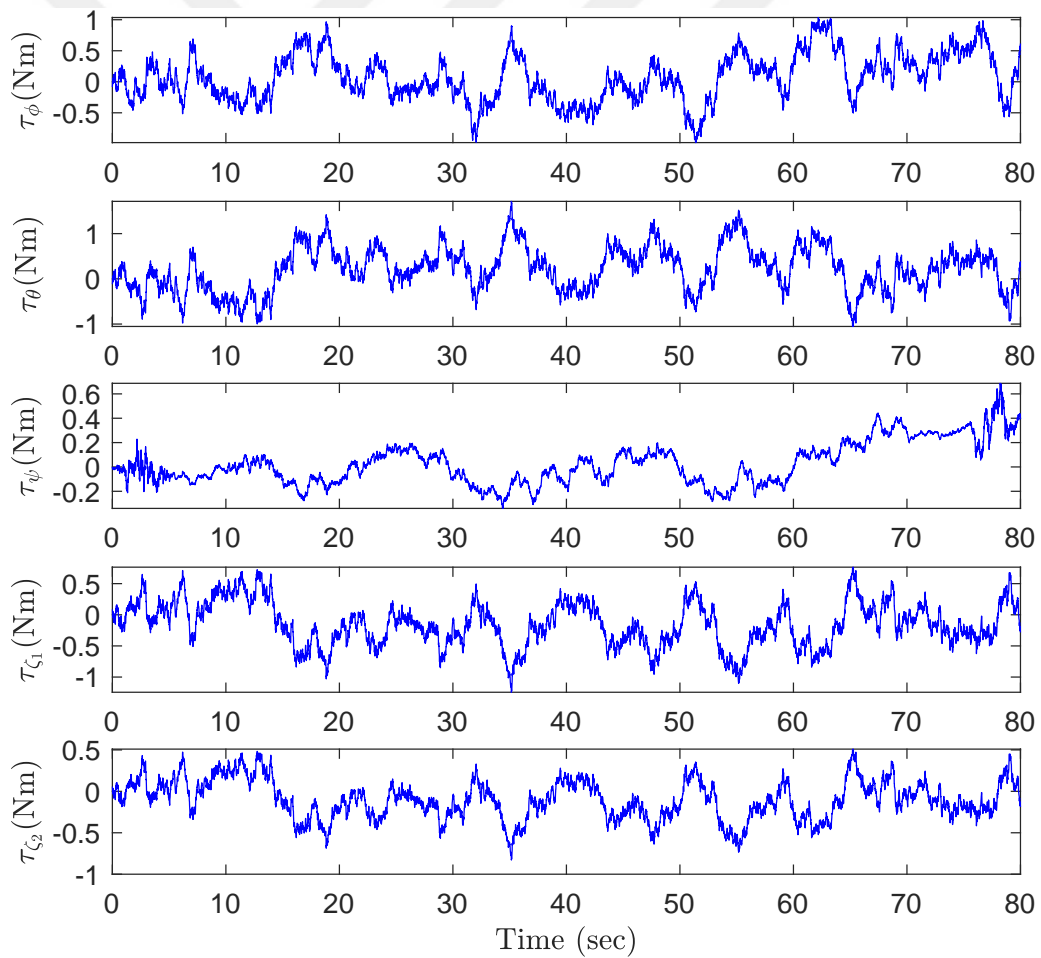


FIGURE 6.39: Wind moments during the circle drawing task of the quadrotor

### 6.3 A Manipulation Scenario Under Varying Disturbances

Let us consider a realistic scenario where an object is stuck in a position and is required to be pulled out. Furthermore, the controller is expected to compensate for not only the interaction forces and moments, but also reject the disturbing effects of wind forces. Under these conditions, the AMS should locate itself in front of the target and should start pulling the object. During the interaction with the object, the AMS should maintain its position at a fixed altitude. Once the object is pulled off, the AMS should retain its stability. Different from the previous ones, the challenge in this task is the compensation of the sudden changes in the interaction forces and moments. Note that this scenario utilizes Eqn. (4.59) as the dynamics model of the AMS.

Cartesian position plots for this scenario have been shown in Figs. 6.40–6.42, where the quadrotor shows a stable hovering at the desired altitude under the interaction forces (in Fig. 6.49) and the disturbing effect of the wind forces (in Fig. 6.50). Based on the tracking errors given in Table 6.5, the position tracking of the quadrotor is quite accurate with RMSE in the range of 0.018m-0.028m. In Table 6.5,  $e_{Xe}$ ,  $e_{Ye}$ , and  $e_{Ze}$  denote the positional errors for the end-effector of the manipulator. The tracking performance of the manipulator end-effector is similar to the quadrotor. Worst-case position errors are also very small, i.e around 0.12m, for both the quadrotor and the manipulator.

Attitude angles of the AMS have been depicted in Figs. 6.43–6.47, where both the quadrotor and the manipulator follow their desired trajectories smoothly under the interaction moments (in Fig. 6.49) and the disturbing effect of the wind moments (in Fig. 6.51). According to Table 6.5, the attitude tracking of the quadrotor is quite accurate with RMSE ranging from  $0.023^\circ$  to  $0.243^\circ$ . For the manipulator end-effector, RMSE values are in the range of  $0.177^\circ$ - $1.496^\circ$ . It is clear that the inner loop nonlinear adaptive controller is successful in rejecting the disturbances acting on the system. Worst-case attitude errors are  $0.873^\circ$  and  $3.860^\circ$  for the

quadrotor and the manipulator, respectively.

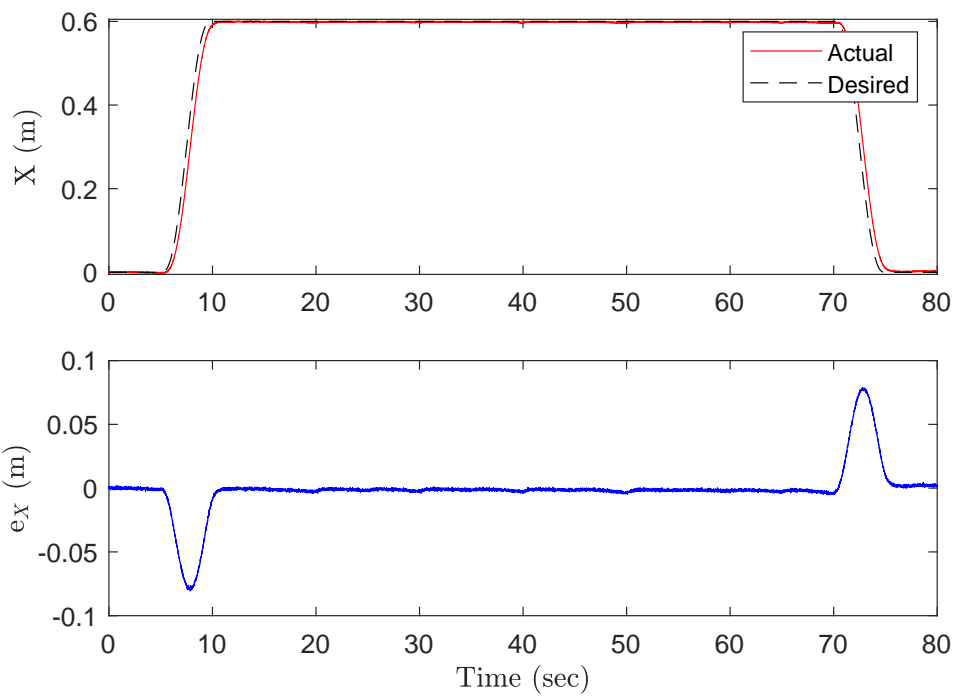


FIGURE 6.40: X position of the quadrotor (top), position error (bottom) vs Time

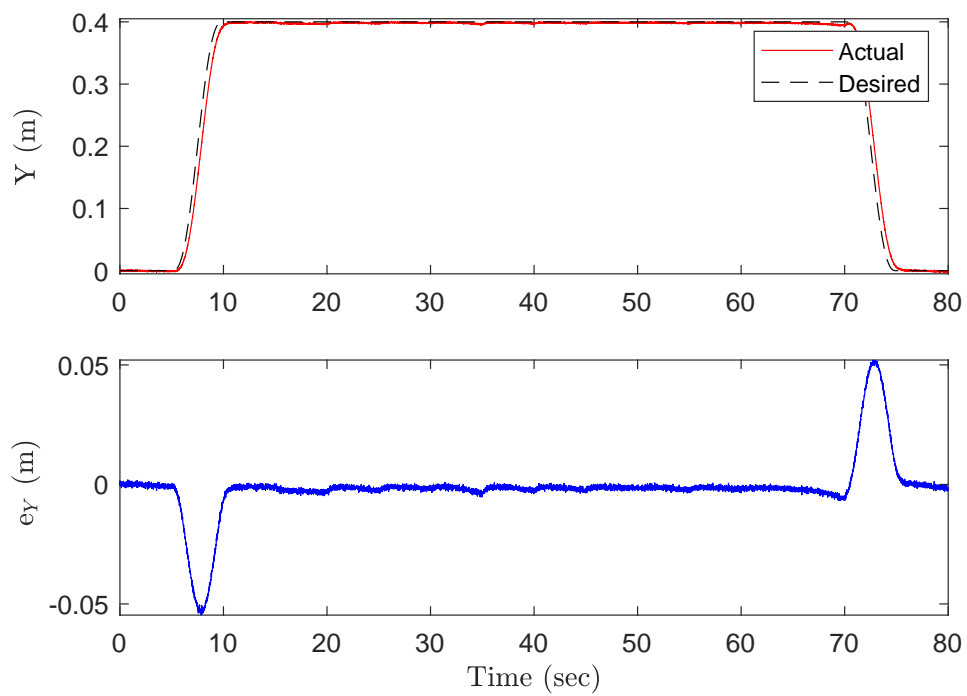


FIGURE 6.41: Y position of the quadrotor (top), position error (bottom) vs Time

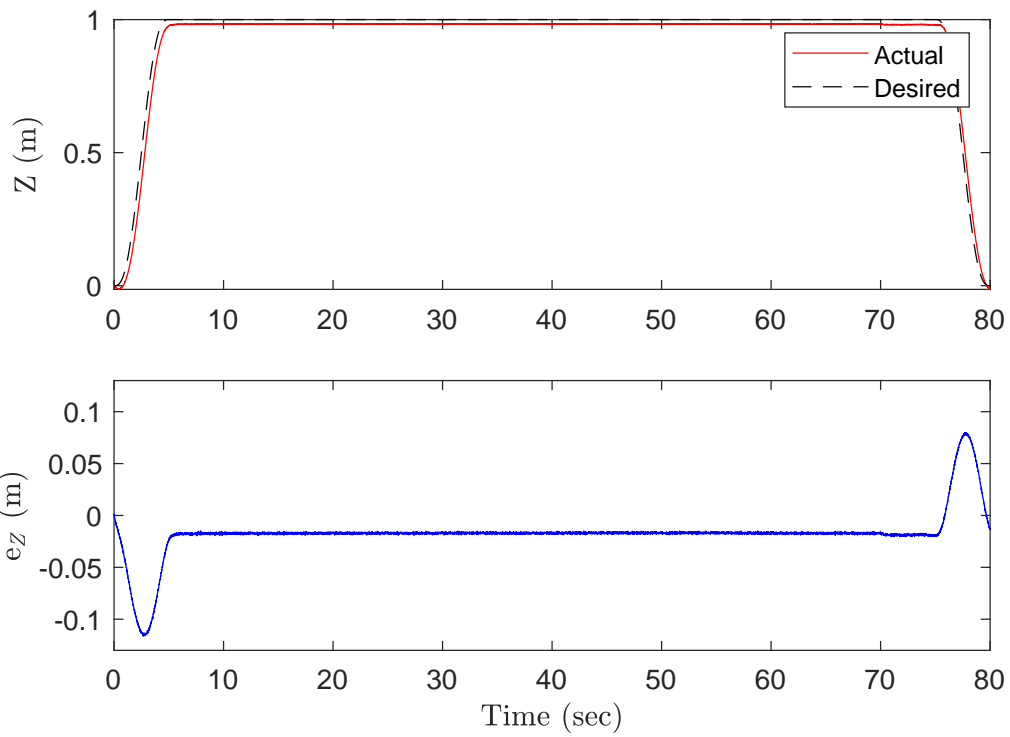


FIGURE 6.42: Z position of the quadrotor (top), position error (bottom) vs Time

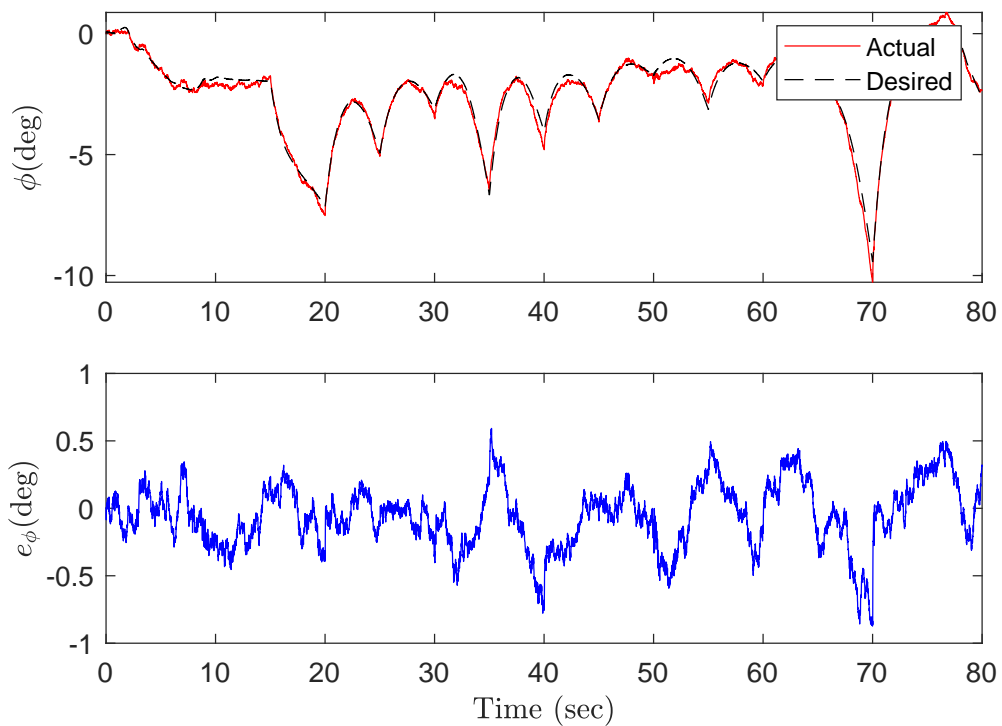
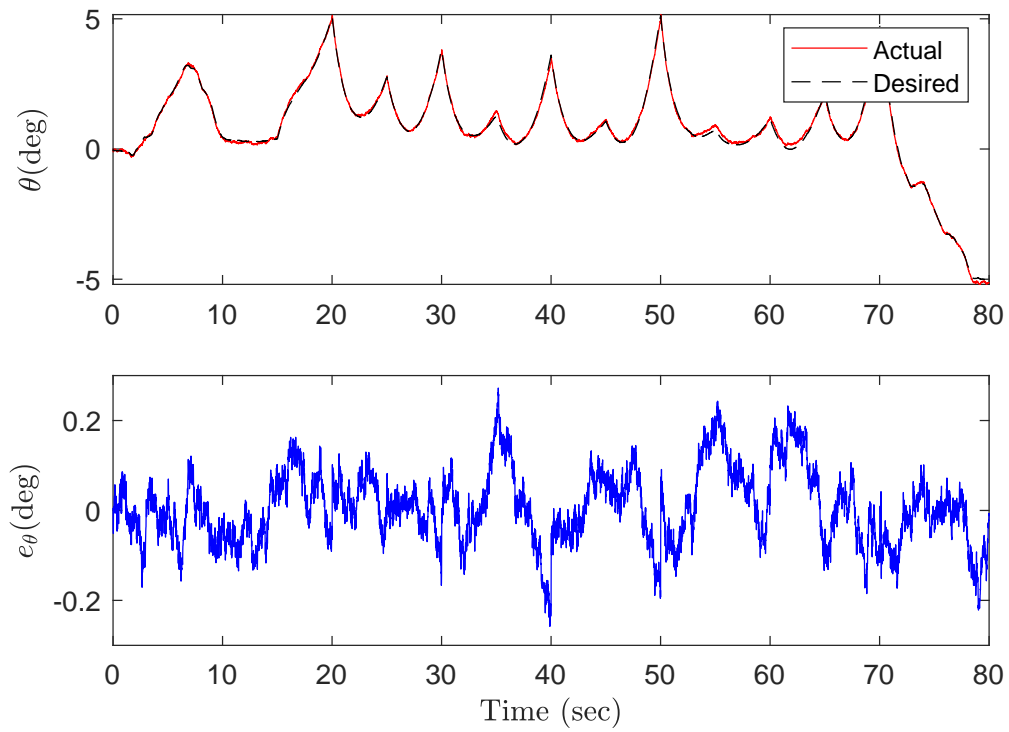
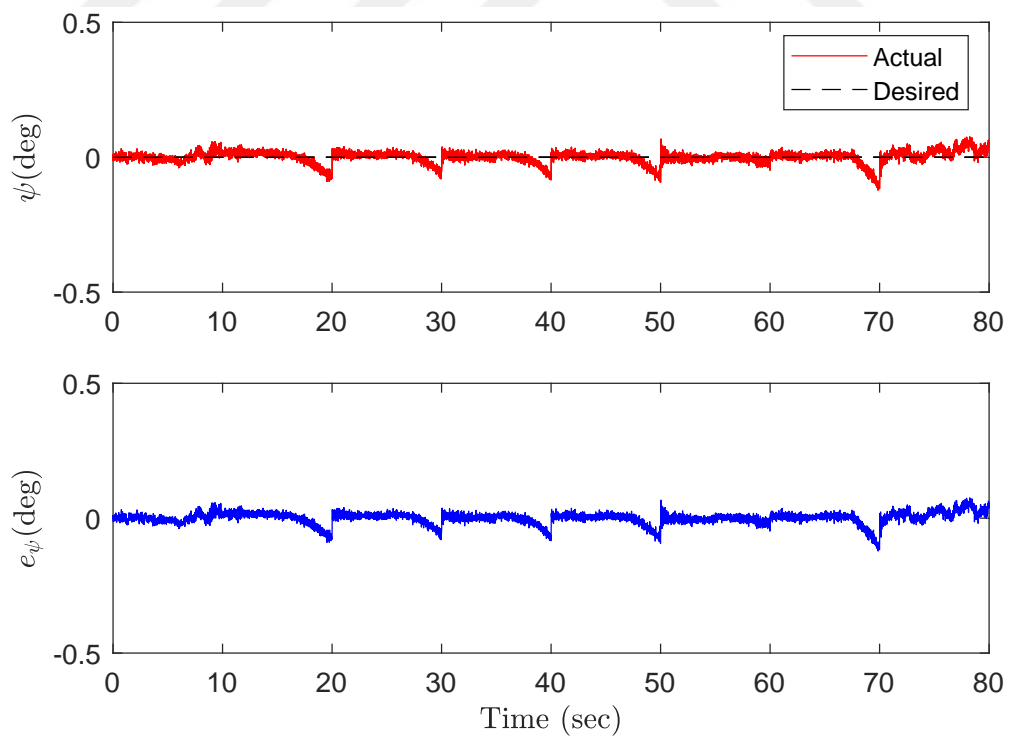
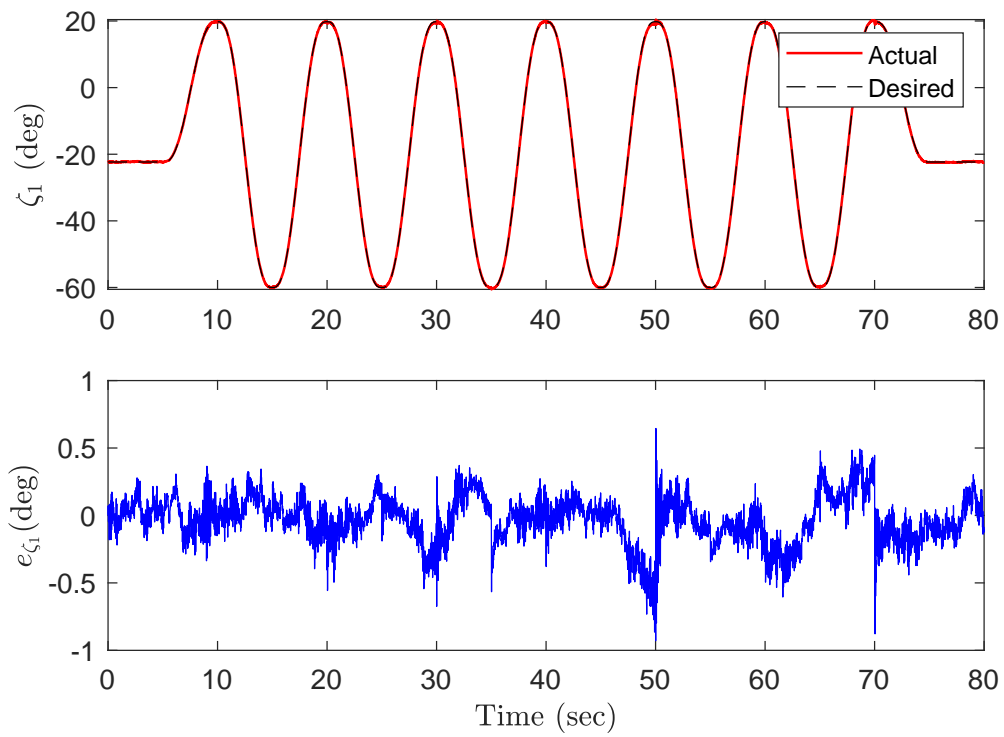
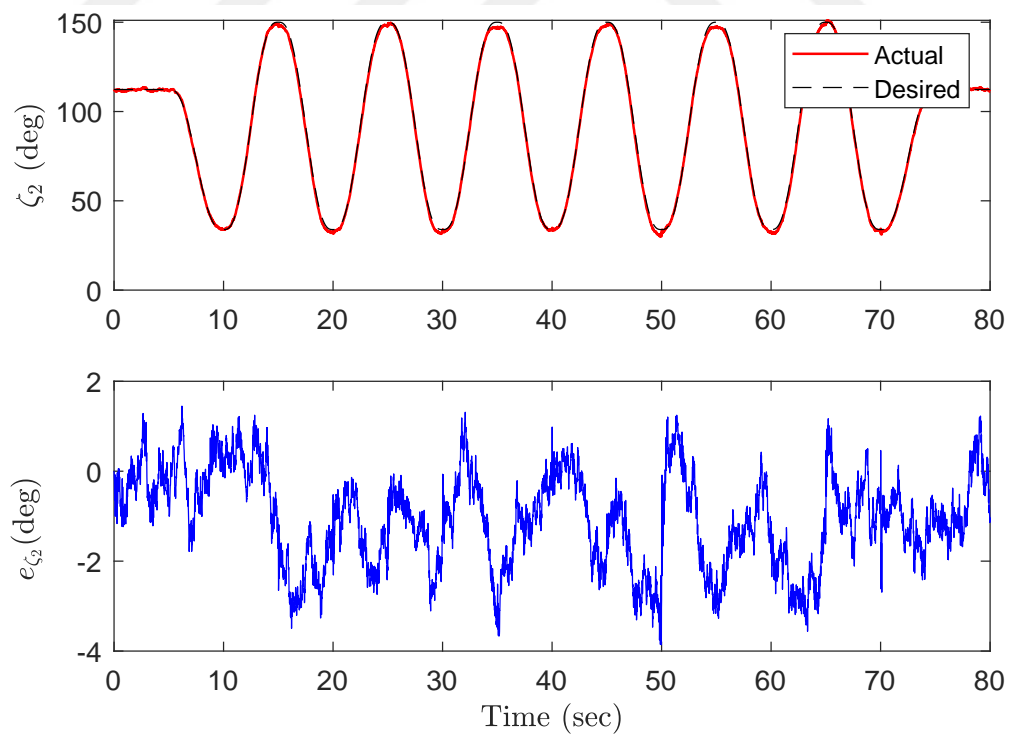


FIGURE 6.43: Roll angle ( $\phi$ ) (top), tracking error (bottom) vs Time



FIGURE 6.44: Pitch angle ( $\theta$ ) (top), tracking error (bottom) vs TimeFIGURE 6.45: Yaw angle ( $\psi$ ) (top), tracking error (bottom) vs Time

FIGURE 6.46:  $\zeta_1$  tracking of the arm (top), tracking error (bottom) vs TimeFIGURE 6.47:  $\zeta_2$  tracking of the arm (top), tracking error (bottom) vs Time

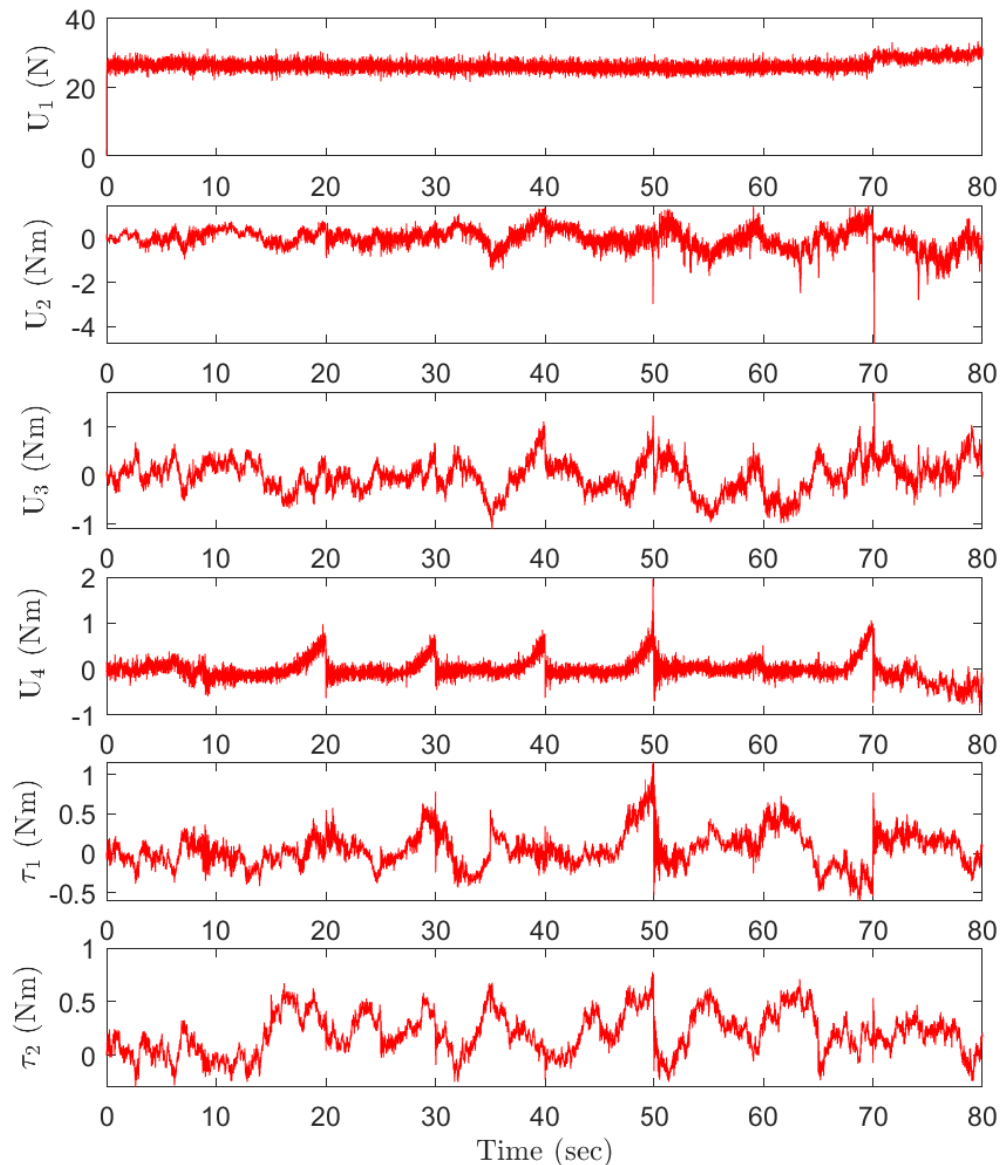


FIGURE 6.48: Control inputs

The interaction forces and moments in Fig. 6.49 indicate that the AMS attempts to pull off the object several times at  $t=15-70$  sec. Finally, at  $t=70$  sec the AMS pulled the object from where it stuck. After the operation, the total weight of the system is changed. Control inputs in Fig. 6.48 show the response of the outer and inner loop controllers to compensate for the abrupt change in the interaction forces and moments at that time instant.

During the operation, the disturbing effects of the wind forces were varying from  $-2\text{N}$  to  $3\text{N}$  (Fig. 6.50), and wind moments were varying from  $-1\text{Nm}$  to  $1\text{Nm}$  (Fig. 6.51).

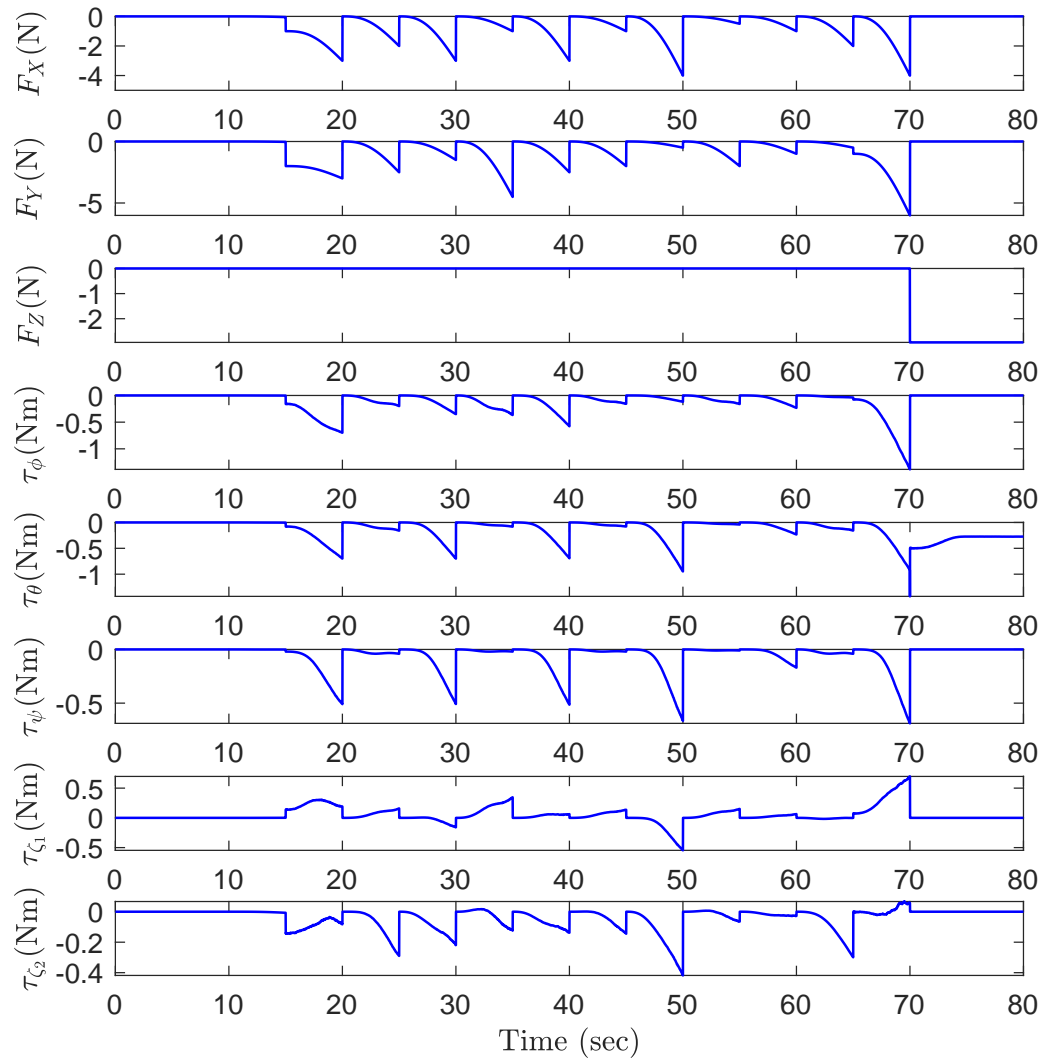


FIGURE 6.49: Interaction forces and moments during the manipulation task

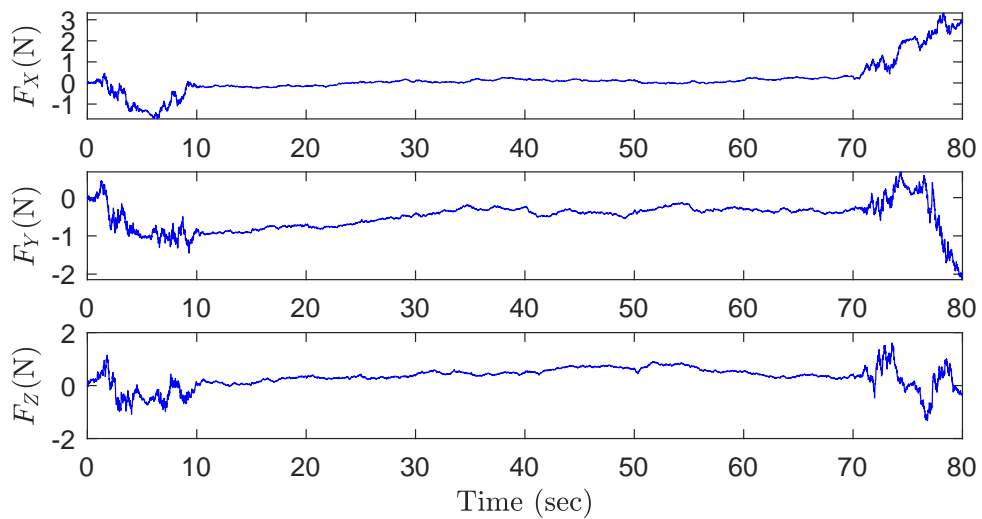


FIGURE 6.50: Wind forces during the manipulation task

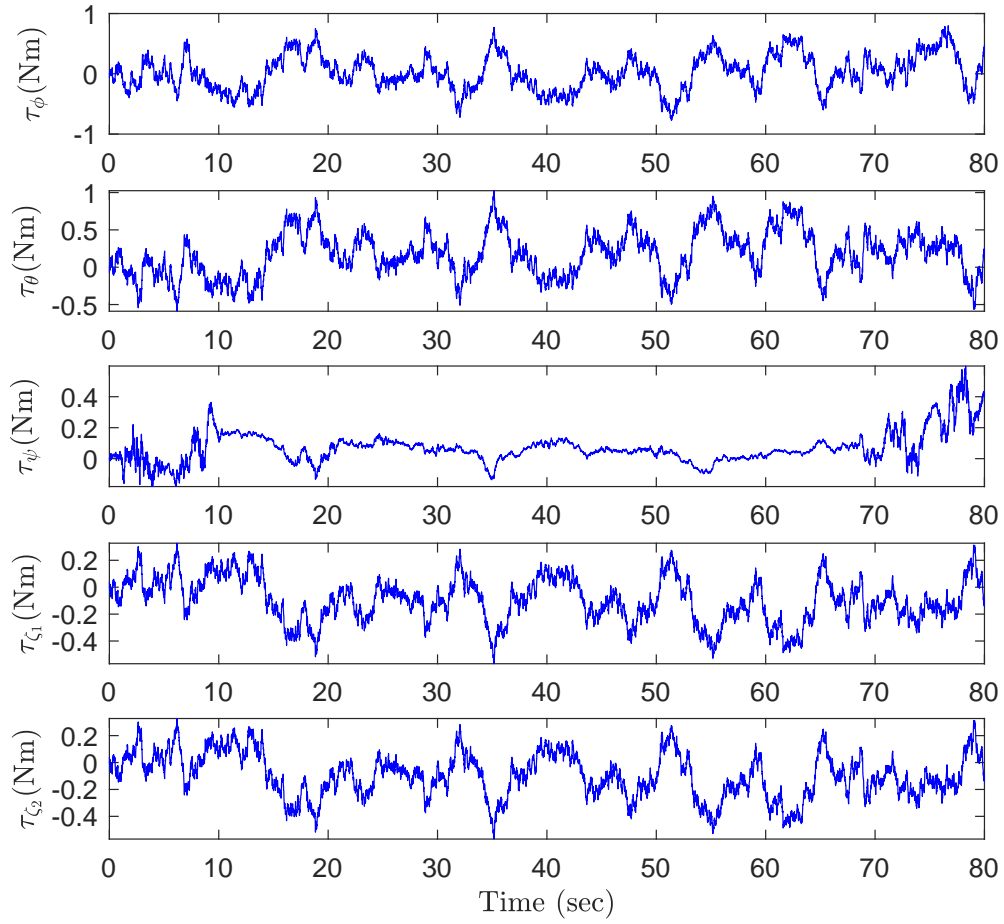


FIGURE 6.51: Wind moments during the manipulation task

TABLE 6.5: Tracking errors of the AMS for the task of pulling object

<b>Criterion</b>	<b>RMS</b>	<b>Max</b>	<b>Criterion</b>	<b>RMS</b>	<b>Max</b>
	<b>Errors</b>	<b>Errors</b>		<b>Errors</b>	<b>Errors</b>
$e_X(m)$	0.018	0.081	$e_\phi(deg)$	0.243	0.873
$e_Y(m)$	0.012	0.055	$e_\theta(deg)$	0.082	0.272
$e_Z(m)$	0.028	0.116	$e_\psi(deg)$	0.023	0.122
$e_{X_e}(m)$	0.018	0.081	$e_{\zeta_1}(deg)$	0.177	0.929
$e_{Y_e}(m)$	0.012	0.056	$e_{\zeta_2}(deg)$	1.496	3.860
$e_{Z_e}(m)$	0.030	0.115			

# Chapter 7

## Conclusion and Future Works

In this thesis, an aerial manipulation system (AMS) consisting of a quadrotor with a 2-DOF manipulator was designed and constructed. The entire mathematical model of the system that incorporates the coupling between the quadrotor and robotic arm, and the physical interaction with the environment was derived through the Euler-Lagrange formulation. Based on this mathematical model, a nonlinear adaptive control framework was developed. It was applied on a high fidelity AMS model which includes mass and inertia uncertainties, wind disturbances, and measurement noises. In order to control the positional dynamics of the AMS in the presence of mass uncertainty and reaction forces, model reference adaptive control (MRAC) was utilized. Using the command signals generated by the MRAC and making small angle approximations, desired attitude angles were calculated analytically for the low-level controller. Attitude dynamics of the quadrotor and 2-DOF manipulator dynamics were combined as a 5-DOF fully actuated system. Nonlinear adaptive control was implemented for this 5-DOF rotational dynamics where uncertainties in inertias were considered.

Performance of the proposed method was validated through simulations where various cases have been taken into account. These cases include: (i) rectangular shape drawing and (ii) circular shape drawing with the robotic arm during hovering, (iii) trajectory tracking of the quadrotor, when the joint angles of the manipulator are fixed, and (iv) a manipulation scenario for pulling a stuck object where

AMS was exposed to sudden changes in the interaction forces and moments along with the disturbing effects of the wind forces and moments. In these scenarios, the position controller achieved RMSE values of 0.001m–0.030m, 0.001m–0.034m, 0.002m–0.023m, and 0.018m–0.028m, respectively. These small tracking errors indicate that MRAC is very effective in self-tuning the position controller gains to assure the system stability despite the uncertainty in the mass, and varying conditions of aforementioned motion scenarios. For the attitude and joint tracking, the RMSE values are  $0.051^\circ$ – $0.467^\circ$ ,  $0.049^\circ$ – $0.427^\circ$ ,  $0.060^\circ$ – $1.059^\circ$ , and  $0.023^\circ$ – $1.496^\circ$ , respectively. These relatively small errors show the quite promising performance of the nonlinear adaptive controller in handling the inertia changes and rejecting the undesirable external moments due to wind and/or interaction with the environment. Besides, the generated control efforts for both controllers were found to be within reasonable physical limits as expected.

As future work, the model will be extended by taking actuator dynamics and the center of mass changes into account. The proposed control system will also be tested on an actual experimental setup.

# Bibliography

- [1] “Turkish Aerospace Industry (TAI) ANKA.” <https://www.tai.com.tr/fotograf-galerisi/anka>, 2019. Accessed: 01 July 2019.
- [2] “DJI Mavic Air – Foldable 4K Drone.” <https://www.dji.com/mavic-air>, 2019. Accessed: 01 July 2019.
- [3] E. Çetinsoy, S. Dikyar, C. Haçer, K. Oner, E. Sirimoglu, M. Unel, and M. Aksit, “Design and construction of a novel quad tilt-wing UAV,” *Mechatronics*, vol. 22, no. 6, pp. 723–745, 2012.
- [4] A. Suarez, A. E. Jimenez-Cano, V. M. Vega, G. Heredia, A. Rodriguez-Castaño, and A. Ollero, “Design of a lightweight dual arm system for aerial manipulation,” *Mechatronics*, vol. 50, pp. 30–44, 2018.
- [5] J. Slotine and W. Li, *Applied Nonlinear Control*. Prentice-Hall, 1991.
- [6] “Niryo One – Robotics for Everyone – Gripper 2.” <https://niryo.com/product/niryo-one-gripper-2/>, 2019. Accessed: 01 July 2019.
- [7] M. Ben-Ari and F. Mondada, *Elements of robotics*, ch. Robots and Their Applications, pp. 1–20. Springer, 2018.
- [8] R. Kelly, V. S. Davila, and J. A. L. Perez, *Control of robot manipulators in joint space*. Springer Science and Business Media, 2006.
- [9] E. Guizzo, “How google’s self-driving car works,” IEEE Spectrum Online, 2011.



- [10] M. Raibert, K. Blankespoor, G. Nelson, and R. Playter, “Bigdog, the rough-terrain quadruped robot,” *IFAC Proceedings Volumes*, vol. 41, no. 2, pp. 10822–10825, 2008.
- [11] R. Hull and R. Bourne, “Radio control of model aircraft,” 1937.
- [12] F. Gudaitis, “The first days of radio control,” 1994.
- [13] H. A. Almurib, P. T. Nathan, and T. N. Kumar, “Control and path planning of quadrotor aerial vehicles for search and rescue,” in *SICE Annual Conference 2011*, pp. 700–705, IEEE, 2011.
- [14] R. W. Beard, T. W. McLain, D. B. Nelson, D. Kingston, and D. Johanson, “Decentralized cooperative aerial surveillance using fixed-wing miniature uavs,” *Proceedings of the IEEE*, vol. 94, no. 7, pp. 1306–1324, 2006.
- [15] H. Li, B. Wang, L. Liu, G. Tian, T. Zheng, and J. Zhang, “The design and application of smartcopter: An unmanned helicopter based robot for transmission line inspection,” in *2013 Chinese Automation Congress*, pp. 697–702, IEEE, 2013.
- [16] F. G. Costa, J. Ueyama, T. Braun, G. Pessin, F. S. Osório, and P. A. Vargas, “The use of unmanned aerial vehicles and wireless sensor network in agricultural applications,” in *2012 IEEE International Geoscience and Remote Sensing Symposium*, pp. 5045–5048, IEEE, 2012.
- [17] D. W. Casbeer, D. B. Kingston, R. W. Beard, and T. W. McLain, “Cooperative forest fire surveillance using a team of small unmanned air vehicles,” *International Journal of Systems Science*, vol. 37, no. 6, pp. 351–360, 2006.
- [18] M. Weyrer, M. Brandstötter, and M. Husty, “Singularity avoidance control of a non-holonomic mobile manipulator for intuitive hand guidance,” *Robotics*, vol. 8, no. 1, p. 14, 2019.
- [19] D. Floreano and R. J. Wood, “Science, technology and the future of small autonomous drones,” *Nature*, vol. 521, no. 7553, p. 460, 2015.

- [20] E. Çetinsoy, *Design, construction and flight control of a quad tilt-wing unmanned aerial vehicle*. 2010. Doctoral dissertation, Sabanci University.
- [21] J. Valasek, K. Gunnam, J. Kimmett, J. L. Junkins, D. Hughes, and M. D. Tandale, “Vision-based sensor and navigation system for autonomous air refueling,” *Journal of Guidance, Control, and Dynamics*, vol. 28, no. 5, pp. 979–989, 2005.
- [22] K. Kondak, F. Huber, M. Schwarzbach, M. Laiacker, D. Sommer, M. Bejar, and A. Ollero, “Aerial manipulation robot composed of an autonomous helicopter and a 7 degrees of freedom industrial manipulator,” in *2014 IEEE international conference on robotics and automation (ICRA)*, pp. 2107–2112, IEEE, 2014.
- [23] Y. Zhang, C. Xiang, B. Xu, Y. Wang, and X. Wang, “Design and implementation of a novel aerial manipulator with tandem ducted fans,” in *2018 IEEE/RSJ International Conference on Intelligent Robots and Systems (IROS)*, pp. 4210–4217, IEEE, 2018.
- [24] R. Mahony, R. W. Beard, and V. Kumar, *Modeling and Control of Aerial Robots*, pp. 1307–1334. 2016.
- [25] C. Papachristos, K. Alexis, and A. Tzes, “Efficient force exertion for aerial robotic manipulation: Exploiting the thrust-vectoring authority of a tri-tiltrotor uav,” in *2014 IEEE International Conference on Robotics and Automation (ICRA)*, pp. 4500–4505, 2014.
- [26] A. Oosedo, S. Abiko, S. Narasaki, A. Kuno, A. Konno, and M. Uchiyama, “Flight control systems of a quad tilt rotor unmanned aerial vehicle for a large attitude change,” in *2015 IEEE International Conference on Robotics and Automation (ICRA)*, pp. 2326–2331, 2015.
- [27] K. Bodie, M. Brunner, M. Pantic, S. Walser, P. Pfändler, U. Angst, R. Siegwart, and J. Nieto, “An omnidirectional aerial manipulation platform for contact-based inspection,” 2019.

- [28] D. Mellinger, M. Shomin, and V. Kumar, “Control of quadrotors for robust perching and landing,” in *Proceedings of the International Powered Lift Conference*, pp. 205–225, 2010.
- [29] V. Ghadiok, J. Goldin, and W. Ren, “Autonomous indoor aerial gripping using a quadrotor,” in *2011 IEEE/RSJ International Conference on Intelligent Robots and Systems*, pp. 4645–4651, IEEE, 2011.
- [30] P. E. Pounds and A. Dollar, “Hovering stability of helicopters with elastic constraints,” in *ASME 2010 Dynamic Systems and Control Conference*, pp. 781–788, American Society of Mechanical Engineers, 2010.
- [31] H. B. Khamseh, F. Janabi-Sharifi, and A. Abdessameud, “Aerial manipulation—a literature survey,” *Robotics and Autonomous Systems*, vol. 107, pp. 221–235, 2018.
- [32] B. Yang, Y. He, J. Han, and G. Liu, “Rotor-flying manipulator: modeling, analysis, and control,” *Mathematical Problems in Engineering*, vol. 2014, 2014.
- [33] M. Orsag, C. Korpela, S. Bogdan, and P. Oh, “Valve turning using a dual-arm aerial manipulator,” in *2014 international conference on unmanned aircraft systems (ICUAS)*, pp. 836–841, IEEE, 2014.
- [34] S. Kim, S. Choi, and H. J. Kim, “Aerial manipulation using a quadrotor with a two dof robotic arm,” in *2013 IEEE/RSJ International Conference on Intelligent Robots and Systems (IROS)*, pp. 4990–4995, Nov 2013.
- [35] S. Kannan, M. A. Olivares-Mendez, and H. Voos, “Modeling and control of aerial manipulation vehicle with visual sensor,” *IFAC Proceedings Volumes*, vol. 46, no. 30, pp. 303–309, 2013.
- [36] G. Heredia, A. Jimenez-Cano, I. Sanchez, D. Llorente, V. Vega, J. Braga, J. Acosta, and A. Ollero, “Control of a multicopter outdoor aerial manipulator,” in *2014 IEEE/RSJ International Conference on Intelligent Robots and Systems*, pp. 3417–3422, IEEE, 2014.

- [37] F. Ruggiero, M. A. Trujillo, R. Cano, H. Ascorbe, A. Viguria, C. Pérez, V. Lippiello, A. Ollero, and B. Siciliano, “A multilayer control for multi-rotor uavs equipped with a servo robot arm,” in *2015 IEEE international conference on robotics and automation (ICRA)*, pp. 4014–4020, IEEE, 2015.
- [38] C. M. Korpela, T. W. Danko, and P. Y. Oh, “Designing a system for mobile manipulation from an unmanned aerial vehicle,” in *2011 IEEE Conference on Technologies for Practical Robot Applications*, pp. 109–114, IEEE, 2011.
- [39] C. D. Bellicoso, L. R. Buonocore, V. Lippiello, and B. Siciliano, “Design, modeling and control of a 5-dof light-weight robot arm for aerial manipulation,” in *2015 23rd Mediterranean Conference on Control and Automation (MED)*, pp. 853–858, IEEE, 2015.
- [40] R. Rossi, A. Santamaria-Navarro, J. Andrade-Cetto, and P. Rocco, “Trajectory generation for unmanned aerial manipulators through quadratic programming,” *IEEE Robotics and Automation Letters*, vol. 2, no. 2, pp. 389–396, 2016.
- [41] V. Lippiello, J. Cacace, A. Santamaria-Navarro, J. Andrade-Cetto, M. A. Trujillo, Y. R. Esteves, and A. Viguria, “Hybrid visual servoing with hierarchical task composition for aerial manipulation,” *IEEE Robotics and Automation Letters*, vol. 1, no. 1, pp. 259–266, 2015.
- [42] T. W. Danko and P. Y. Oh, “A hyper-redundant manipulator for mobile manipulating unmanned aerial vehicles,” in *2013 International Conference on Unmanned Aircraft Systems (ICUAS)*, pp. 974–981, IEEE, 2013.
- [43] T. W. Danko and P. Y. Oh, “Design and control of a hyper-redundant manipulator for mobile manipulating unmanned aerial vehicles,” *Journal of Intelligent and Robotic Systems*, vol. 73, no. 1-4, pp. 709–723, 2014.
- [44] A. Y. Mersha, S. Stramigioli, and R. Carloni, “Exploiting the dynamics of a robotic manipulator for control of uavs,” in *2014 IEEE International Conference on Robotics and Automation (ICRA)*, pp. 1741–1746, IEEE, 2014.

- [45] F. Forte, R. Naldi, A. Macchelli, and L. Marconi, "Impedance control of an aerial manipulator," in *2012 American Control Conference (ACC)*, pp. 3839–3844, IEEE, 2012.
- [46] M. Orsag, C. M. Korpela, S. Bogdan, and P. Y. Oh, "Hybrid adaptive control for aerial manipulation," *Journal of intelligent and robotic systems*, vol. 73, no. 1-4, pp. 693–707, 2014.
- [47] G. Arleo, F. Caccavale, G. Muscio, and F. Pierri, "Control of quadrotor aerial vehicles equipped with a robotic arm," in *21St mediterranean conference on control and automation*, pp. 1174–1180, IEEE, 2013.
- [48] A. Jimenez-Cano, J. Martin, G. Heredia, A. Ollero, and R. Cano, "Control of an aerial robot with multi-link arm for assembly tasks," in *2013 IEEE International Conference on Robotics and Automation*, pp. 4916–4921, IEEE, 2013.
- [49] N. Michael, J. Fink, and V. Kumar, "Cooperative manipulation and transportation with aerial robots," *Autonomous Robots*, vol. 30, no. 1, pp. 73–86, 2011.
- [50] J. Fink, N. Michael, S. Kim, and V. Kumar, "Planning and control for cooperative manipulation and transportation with aerial robots," *The International Journal of Robotics Research*, vol. 30, no. 3, pp. 324–334, 2011.
- [51] L. Gentili, R. Naldi, and L. Marconi, "Modeling and control of vtol uavs interacting with the environment," in *2008 47th IEEE Conference on Decision and Control*, pp. 1231–1236, IEEE, 2008.
- [52] S. Bellens, J. De Schutter, and H. Bruyninckx, "A hybrid pose/wrench control framework for quadrotor helicopters," in *2012 IEEE International Conference on Robotics and Automation*, pp. 2269–2274, IEEE, 2012.
- [53] A. Y. Mersha, S. Stramigioli, and R. Carloni, "Variable impedance control for aerial interaction," in *2014 IEEE/RSJ International Conference on Intelligent Robots and Systems*, pp. 3435–3440, IEEE, 2014.

- [54] K. Alexis, G. Darivianakis, M. Burri, and R. Siegwart, “Aerial robotic contact-based inspection: planning and control,” *Autonomous Robots*, vol. 40, no. 4, pp. 631–655, 2016.
- [55] H. Tsukagoshi, M. Watanabe, T. Hamada, D. Ashlih, and R. Iizuka, “Aerial manipulator with perching and door-opening capability,” in *2015 IEEE International Conference on Robotics and Automation (ICRA)*, pp. 4663–4668, IEEE, 2015.
- [56] G. Gioioso, M. Ryll, D. Prattichizzo, H. H. Bühlhoff, and A. Franchi, “Turning a near-hovering controlled quadrotor into a 3d force effector,” in *2014 IEEE International Conference on Robotics and Automation (ICRA)*, pp. 6278–6284, IEEE, 2014.
- [57] H.-N. Nguyen and D. Lee, “Hybrid force/motion control and internal dynamics of quadrotors for tool operation,” in *2013 IEEE/RSJ International Conference on Intelligent Robots and Systems*, pp. 3458–3464, IEEE, 2013.
- [58] C. Papachristos, K. Alexis, and A. Tzes, “Efficient force exertion for aerial robotic manipulation: Exploiting the thrust-vectoring authority of a tri-tiltrotor uav,” in *2014 IEEE international conference on robotics and automation (ICRA)*, pp. 4500–4505, IEEE, 2014.
- [59] M. Fumagalli, R. Naldi, A. Macchelli, F. Forte, A. Q. Keemink, S. Stramigioli, R. Carloni, and L. Marconi, “Developing an aerial manipulator prototype: Physical interaction with the environment,” *IEEE robotics and automation magazine*, vol. 21, no. 3, pp. 41–50, 2014.
- [60] H.-N. Nguyen, C. Ha, and D. Lee, “Mechanics, control and internal dynamics of quadrotor tool operation,” *Automatica*, vol. 61, pp. 289–301, 2015.
- [61] G. Darivianakis, K. Alexis, M. Burri, and R. Siegwart, “Hybrid predictive control for aerial robotic physical interaction towards inspection operations,” in *2014 IEEE international conference on robotics and automation (ICRA)*, pp. 53–58, IEEE, 2014.

- [62] O. Shakernia, Y. Ma, T. J. Koo, and S. Sastry, “Landing an unmanned air vehicle: Vision based motion estimation and nonlinear control,” *Asian journal of control*, vol. 1, no. 3, pp. 128–145, 1999.
- [63] C. S. Sharp, O. Shakernia, and S. S. Sastry, “A vision system for landing an unmanned aerial vehicle,” in *Proceedings 2001 ICRA. IEEE International Conference on Robotics and Automation (Cat. No. 01CH37164)*, vol. 2, pp. 1720–1727, Ieee, 2001.
- [64] O. Shakernia, R. Vidal, C. S. Sharp, Y. Ma, and S. Sastry, “Multiple view motion estimation and control for landing an unmanned aerial vehicle,” in *Proceedings 2002 IEEE International Conference on Robotics and Automation (Cat. No. 02CH37292)*, vol. 3, pp. 2793–2798, IEEE, 2002.
- [65] F. Augugliaro, S. Lupashin, M. Hamer, C. Male, M. Hehn, M. W. Mueller, J. S. Willmann, F. Gramazio, M. Kohler, and R. D’Andrea, “The flight assembled architecture installation: Cooperative construction with flying machines,” *IEEE Control Systems Magazine*, vol. 34, no. 4, pp. 46–64, 2014.
- [66] Q. Lindsey, D. Mellinger, and V. Kumar, “Construction of cubic structures with quadrotor teams,” *Proc. Robotics: Science and Systems VII*, 2011.
- [67] Q. Lindsey and V. Kumar, “Distributed construction of truss structures,” in *Algorithmic Foundations of Robotics X*, pp. 209–225, Springer, 2013.
- [68] J. Kimmet, J. Valasek, and J. Junkins, “Autonomous aerial refueling utilizing a vision based navigation system,” in *AIAA Guidance, Navigation, and Control Conference and Exhibit*, p. 4469, 2002.
- [69] J. Kimmet, J. Valasek, and J. L. Junkins, “Vision based controller for autonomous aerial refueling,” in *Proceedings of the International Conference on Control Applications*, vol. 2, pp. 1138–1143, IEEE, 2002.
- [70] N. Macmillan, “Flight refuelling: Its development and current use,” *Royal United Services Institution. Journal*, vol. 100, no. 597, pp. 39–46, 1955.

- [71] C. Latimer-Needham, “Flight refuelling,” *The Aeronautical Journal*, vol. 70, no. 662, pp. 335–339, 1966.
- [72] L. Pollini, G. Campa, F. Giulietti, and M. Innocenti, “Virtual simulation setup for uavs aerial refuelling,” in *AIAA Modeling and Simulation Technologies Conference and Exhibit*, p. 5682, 2003.
- [73] L. Pollini, M. Innocenti, and R. Mati, “Vision algorithms for formation flight and aerial refueling with optimal marker labeling,” in *AIAA Modeling and Simulation Technologies Conference and Exhibit*, p. 6010, 2005.
- [74] M. Fravolini, A. Ficola, M. Napolitano, G. Campa, and M. Perhinschi, “Development of modelling and control tools for aerial refueling for uavs,” in *AIAA Guidance, Navigation, and Control Conference and Exhibit*, p. 5798, 2003.
- [75] D. B. Wilson, A. H. Göktoğan, and S. Sukkarieh, “Experimental validation of a drogue estimation algorithm for autonomous aerial refueling,” in *2015 IEEE International Conference on Robotics and Automation (ICRA)*, pp. 5318–5323, IEEE, 2015.
- [76] D. Mellinger, Q. Lindsey, M. Shomin, and V. Kumar, “Design, modeling, estimation and control for aerial grasping and manipulation,” in *2011 IEEE/RSJ International Conference on Intelligent Robots and Systems*, pp. 2668–2673, IEEE, 2011.
- [77] C. Korpela, M. Orsag, M. Pekala, and P. Oh, “Dynamic stability of a mobile manipulating unmanned aerial vehicle,” in *2013 IEEE International Conference on Robotics and Automation*, pp. 4922–4927, IEEE, 2013.
- [78] M. Orsag, C. Korpela, M. Pekala, and P. Oh, “Stability control in aerial manipulation,” in *2013 American Control Conference*, pp. 5581–5586, IEEE, 2013.



- [79] A. Das, K. Subbarao, and F. Lewis, “Dynamic inversion with zero-dynamics stabilisation for quadrotor control,” *IET Control Theory Applications*, vol. 3, pp. 303–314, March 2009.
- [80] M. W. Achtelik, S. Lynen, M. Chli, and R. Siegwart, “Inversion based direct position control and trajectory following for micro aerial vehicles,” in *2013 IEEE/RSJ International Conference on Intelligent Robots and Systems*, pp. 2933–2939, IEEE, 2013.
- [81] P. Mukherjee and S. Waslander, “Direct adaptive feedback linearization for quadrotor control,” in *AIAA Guidance, Navigation, and Control Conference*, p. 4917, 2012.
- [82] Z. T. Dydek, A. M. Annaswamy, and E. Lavretsky, “Adaptive control of quadrotor uavs: A design trade study with flight evaluations,” *IEEE Transactions on control systems technology*, vol. 21, no. 4, pp. 1400–1406, 2012.
- [83] H. J. Kim and D. H. Shim, “A flight control system for aerial robots: algorithms and experiments,” *Control engineering practice*, vol. 11, no. 12, pp. 1389–1400, 2003.
- [84] X. Heng, D. Cabecinhas, R. Cunha, C. Silvestre, and X. Qingsong, “A trajectory tracking lqr controller for a quadrotor: Design and experimental evaluation,” in *TENCON 2015-2015 IEEE Region 10 Conference*, pp. 1–7, IEEE, 2015.
- [85] D. C. Tosun, Y. Işık, and H. Korul, “Lqr control of a quadrotor helicopter,” in *Proceedings of the International Conference on Pure Mathematics*, pp. 247–252, 2015.
- [86] I. D. Cowling, O. A. Yakimenko, J. F. Whidborne, and A. K. Cooke, “A prototype of an autonomous controller for a quadrotor uav,” in *2007 European Control Conference (ECC)*, pp. 4001–4008, IEEE, 2007.
- [87] A. J.K. Hedrick, *Feedback Linearization, in Control of Nonlinear Dynamic Systems: Theory and Applications*. University of California, Berkeley, 2010.

- [88] A. Y. Mersha, S. Stramigioli, and R. Carloni, “Exploiting the dynamics of a robotic manipulator for control of uavs,” in *2014 IEEE International Conference on Robotics and Automation (ICRA)*, pp. 1741–1746, May 2014.
- [89] M. Ryll, D. Bicego, and A. Franchi, “A truly redundant aerial manipulator exploiting a multi-directional thrust base,” *IFAC-PapersOnLine*, vol. 51, no. 22, pp. 138–143, 2018.
- [90] A. Caballero, M. Bejar, A. Rodriguez-Castaño, and A. Ollero, “Motion planning with dynamics awareness for long reach manipulation in aerial robotic systems with two arms,” *International Journal of Advanced Robotic Systems*, vol. 15, no. 3, 2018.
- [91] K. Kondak, M. Bernard, N. Meyer, and G. Hommel, “Autonomously flying vtol-robots: Modeling and control,” in *Proceedings 2007 IEEE International Conference on Robotics and Automation*, pp. 736–741, April 2007.
- [92] I. D. Landau, R. Lozano, M. M’Saad, and A. Karimi, *Adaptive control: algorithms, analysis and applications*. Springer Science and Business Media, 2011.
- [93] R. Riccardo Zanella, “Decoupled controllers for mobile manipulation with aerial robots: Design, implementation and test,” 2016.
- [94] Y. Zhu and S. Zhu, “Adaptive sliding mode control based on uncertainty and disturbance estimator,” *Mathematical Problems in Engineering*, vol. 2014, 2014.
- [95] H. Lee, S. Kim, and H. J. Kim, “Control of an aerial manipulator using on-line parameter estimator for an unknown payload,” in *2015 IEEE International Conference on Automation Science and Engineering (CASE)*, pp. 316–321, IEEE, 2015.
- [96] I. A. Raptis and K. P. Valavanis, *Fundamentals of Backstepping Control, in Linear and nonlinear control of small-scale unmanned helicopters*, vol. 45. Springer Science and Business Media, 2010.

- 
- [97] M. Kobilarov, “Nonlinear trajectory control of multi-body aerial manipulators,” *Journal of Intelligent and Robotic Systems*, vol. 73, no. 1-4, pp. 679–692, 2014.
- [98] S. Mokhtatab, J. Y. Mak, J. V. Valappil, and D. A. Wood, *Handbook of liquefied natural gas*. Gulf Professional Publishing, 2013.
- [99] M. Spong, S. Hutchinson, and M. Vidyasagar, *Robot Modeling and Control*. Wiley, 2005.
- [100] L. Tsai, *Robot Analysis: The Mechanics of Serial and Parallel Manipulators*. Wiley, 1999.
- [101] M. Orsag, C. Korpela, P. Oh, S. Bogdan, and A. Ollero, *Aerial Manipulation*. Springer International Publishing, 2017.
- [102] E. Lavretsky, “Adaptive control: Introduction, overview, and applications,” in *Lecture notes from IEEE Robust and Adaptive Control Workshop*, 2008.
- [103] Y. Yildiz, M. Unel, and A. E. Demirel, “Nonlinear hierarchical control of a quad tilt-wing UAV: An adaptive control approach,” *International Journal of Adaptive Control and Signal Processing*, vol. 31, no. 9, pp. 1245–1264, 2017.